2020

Process control for WAAM using computer vision

Shiyu Zhang

UNIVERSITY
OF WOLLONGONG
AUSTRALIA

Process control for WAAM using computer vision

By

Shiyu Zhang

Supervisors:

A / Professor Stephen Pan, Professor Huijun Li & Dr. Dominic Cuiuri

This thesis is presented as part of the requirement for the conferral of the degree:

MASTER OF PHILOSOPHY

(Mechatronics)

UNIVERSITY OF WOLLONGONG

FACULTY OF ENGINEERING AND INFORMATION SCIENCES

December 2020

ACKNOWLEGEMENTS

I would like to especially thank A / Professor Stephen Pan for his valuable supervision, the highly valued feedback and very close assistance during the course of undertaking the experimental part of this study. As well as Dr. Dominic Cuiuri and Chunyang Xia for helping me with my experiments and programming, and Professor Huijun Li for his supervision and advice on the process of my project. I would also like to thank the academic and technical staff of the school for other contributions in providing practical resources. These laid a solid foundation for this study.

In addition, I would also like to thank my friends and family for always providing the necessary personal support.

ABSTRACT

This study is mainly about the vision system and control algorithm programming for wire arc additive manufacturing (WAAM). Arc additive manufacturing technology is formed by the principle of heat source cladding produced by welders using molten inert gas shielded welding (MIG), tungsten inert gas shielded welding (TIG) and layered plasma welding power supply (PA). It has high deposition efficiency, short manufacturing cycle, low cost, and easy maintenance.

Although WAAM has very good uses in various fields, the inability to control the adding process in real time has led to defects in the weld and reduced quality. Therefore, it is necessary to develop the real-time feedback through computer vision and algorithms for WAAM to ensure that the thickness and the width of each layer during the addition process are the same.

In order to ensure that the algorithm can achieve stable control during welding, Simulink programming environment is used to establish a dynamic model according to the width and wire feeding speed of the welding machine. At the same time, in order to better identify and filter the collected data, this study uses an identification algorithm - particle swarm genetic hybrid algorithm (PSO-GA). The simulation results show that the use of difference equation, fuzzy PID control and adaptive control algorithms can achieve good real-time welding control and fit the desired trajectory.

However, in the actual additive welding process, although fuzzy PID can control the first layer of welds in real time, it cannot effectively control the second layer of welds, and problems such as collapse still occur.

In the future, through the adjustment of fuzzy PID parameters and the practical application of adaptive control, it is expected to realize accurate real-time control of additive manufacturing.

NOMENCLATURE

AM	Additive manufacturing
CAD	Computer-Aided Design
CCD	Charge-coupled Device
CMT	Cold Metal Transfer
e	Error
GA	Genetic algorithm
GMAW	Gas Metal Arc Welding
K_D	Differential gain
K_I	Integral gain
K_P	Proportion gain
LabVIEW	Laboratory Virtual Instrument Engineering Workbench
MATLAB	Matrix Laboratory
MIG	Melt-Inert Gas Shielded Welding
PSO	Particle swarm optimization
PSO-GA	Particle swarm genetic hybrid algorithm
TIG	Tungsten Inert Gas Welding
WAAM	Wire Arc Additive Manufacturing

CONTENT

FIGURE LIST

TABLE LIST

CHAPTER 1 INTRODUCTION

1.1 INTRODUCTION OF WAAM

Additive manufacturing (AM), also inferred as three-dimensional printing, freeform molding, or rapid prototyping, is a technology which is been expected to decrease market time and material waste, thus lowering the cost of parts. Additionally, AM increases design freedom by reducing weight and facilitating the manufacture of complex components which is previously made from various subassemblies. Due to its ability to manufacture complex geometries such as honeycomb structures and lattice structures, AM not only saves time, but also has broad prospects for freeform manufacturing and repair. The basic AM system includes motion systems, materials and thermal sources.

WAAM (wire arc additive manufacturing), a combination of wire as a feedstock and arcs as a source of thermal energy, has been used in AM applications. WAAM hardware now uses standard off-the-shelf welding equipment: a welding power supplier, torch and wire feed system. Then a robotic system or a computer numerically controlled gantry would be the provider of the motion.

1.2 BACKGROUND

The arc additive manufacturing technology is a thermal source generated by three parts: a welder using a plasma welding power source (PA), a melt-inert gas shielded welding (MIG), and a tungsten inert gas welding (TIG), combined using a layer-by-layer cladding principle. (Globalrobots.com., 2020) Through the program-controlled addition of wire material, the advanced digital manufacturing technology of metal parts is gradually formed from the line-face-body following

the design of the three-dimensional digital model. It not only has high deposition efficiency, high utilization rate of wire followed by short manufacturing cycle, low cost, fewer restrictions on part size and less difficulties in repairing parts, but also has the ability to in-situ composite manufacturing as well as forming large-size parts.

Comparing with the traditional casting and forging process, arc additive manufacturing technology does not need a model. Additionally, this technology not only has a short overall manufacturing cycle, but also has a high degree of flexibility, and the ability to realize digital, intelligent and parallel manufacturing. It has a short response time and is especially suitable for small batches and varieties manufacture. WAAM technology is superior to the casting technology in the fabrication of materials and mechanical properties due to less raw materials used than that of casting technology, especially precious metal materials. Compared with the AM technology using laser and electron beam as the heat source, it has the advantages of high deposition rate, low manufacturing cost and less manufacturing technology requirements, meaning that it is insensitive to metal materials and can be formed into materials with high laser reflectivity, such as aluminum alloys and copper alloys.

Due to the fact that this technology is able to manufacturing large metal parts in a high deposition rate and material utilization rate while at the same time maintain a low equipment cost, it is increasingly concerned by scientific research and industrial manufacturing.

The additive manufacturing process is based on high-temperature liquid metal transfer, which means that as the deposited layer increases, the heat accumulation of the workpiece becomes more serious and overheat will occur in the molten pool. The geometric accuracy and surface quality of the final product are affected by the difficulties in controlling morphology and size of the deposited layer. Therefore, real-time control should be accomplished during the amplitude modulation process.

WAAM, integrating electromagnetic, chemical, and thermodynamic processes, is a complex process. Due to the lack in systematic testing methods, it is hard to evaluate the quality of the component in which some have prone to trachoma inside, not to mention other defects. Additionally, WAAM technology, in terms of control, lacks online monitoring and diagnosis, and it is inaccessible to adjust the additive in real time during the welding additive process.

1.3 AIM & OBJECTIVE

1.3.1. Aim

The aim of this study is to develop the process control method for WAAM using computer vision to ensure that the geometry structure of each layer is the same during the additive process, and improve the accuracy of the welding control.

1.3.2. Objectives

The objectives of the thesis are listed below:

- Conduct a literature review related to relevant processes and how these control processes influence the weld geometry based on the vision system.

- Develop an image acquisition system, which combines CCD camera and WAAM control system, to obtain the images of the welding pools under different wire feeding speed.
- Analyze the various welding pools in different size and shape by MATLAB through the image.
- Obtain a relationship between the welding current and the geometry of the welding pool by collecting data and filter these data by recognition algorithm.
- Build a suitable control algorithm with corresponding parameters through a simulation model that is based on the relationship between weld bead width which includes measured width and physical width, and the wire feed speed.
- Deploy an experiment to validate whether the algorithm is effective for attaining the welding geometry and controlling the weld of the next layer.

1.4 METHODOLOGY

This study, firstly, will summarize the application and algorithm of WAAM. Relevant journals will be explored to provide the necessary basis for addressing this issue. The information gathered will be presented topically to build a knowledge basement that is critical to the development of visual based control systems. Broad questions will be raised about the working process of WAAM and its applications: how to form stable welding pools and how to modify them; and how additive manufacturing is being used and what might happen in the future.

Then the hardware construction will be introduced. The hardware includes a camera and ABB robotic welding arm. The camera will be mounted on the ABB robotic welding arm. The following processes will be completed here: camera

positioning; choosing the filters that work best for the camera and how to capture images on the PC. A scanner will also be placed to determine the stability of the pool. Experiments are expected to determine the ideal configuration.

The weld information captured by the camera will be combined with the wire feeding speed. Software will also be developed to collect real-time data from the system. Through a series of tests, the relationship between weld geometry parameters, weld pool width (visual data) and wire feeding speed will be determined. The width data will be identified with the algorithm, and be used for simulation control. The simulation model can avoid the delay of the system, identify and predict the weld size in real time and control it in real time.

According to the parameters obtained from the simulation model, the experimental data will be modified to realize real-time control of the weld bead.

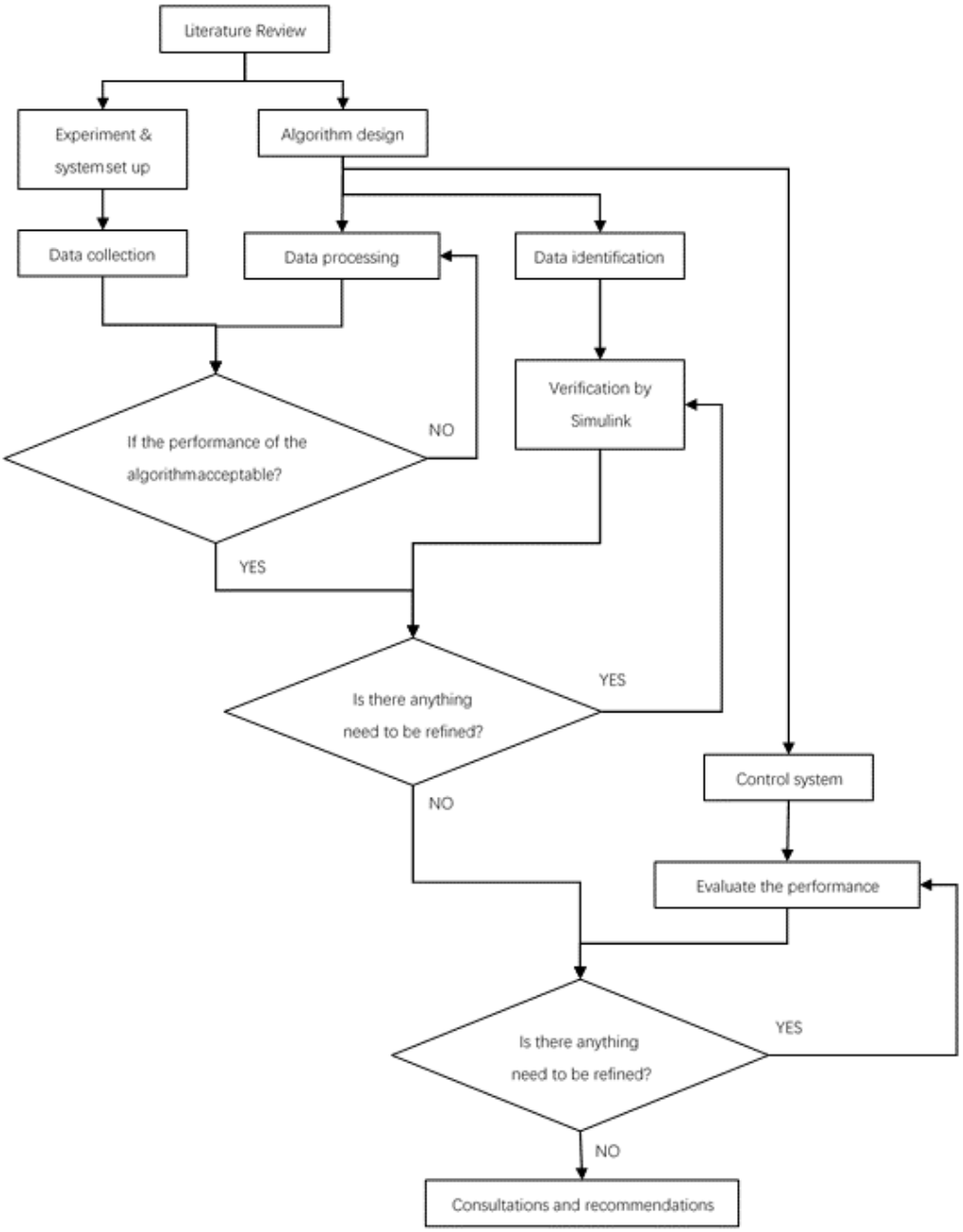

Figure 1 Flow chart of methodology

1.5 REPORT STRUCTURE

The dissertation contains eight chapters. These chapters reflect the processes during the research.

The first chapter is the introduction. This chapter introduces the purpose of this research and provides a systematic overview of the entire progress report.

Chapter 2 is the literature review. The knowledge of WAAM, especially the TIG and MIG welding which have been used in the project is included in this chapter. Also, the welding material are selected and analyzed. This literate review demonstrates the principal of separation technology and related experiments in recent decades. At the same time, it points out the difficulties faced by this study, as well as the control methods and algorithms to be used.

Chapter 3 introduces the design of hardware and software. For different WAAM welding methods, what hardware and software will be used, and how they are selected and matched.

Chapter 4 mainly describes the data collection methods and the data processing methods. The relationship between the width of the molten pool and the feeding speed of the additive is established to achieve real-time control. Then the data obtained from the experiment is analyzed.

The identification algorithm, particle swarm genetic hybrid algorithm, is been developed and used to analyze the experiment data in chapter 5. Through the identification of the data, the available experimental data can be screened out, which provides a basis for the determination of the control algorithm parameters later.

In chapter 6, the dynamic model of control algorithm is built with Simulink. Control algorithms include common difference equations and fuzzy PID that can eliminate delay. The adaptive control processed by Smith predictor and RBF neural network is also simulated.

Chapter 7 analyze the results of the experiment. A comparative experiment was carried out between the controlled weld and the uncontrolled weld, and the effectiveness of the control algorithm was verified by analyzing the experimental data.

The chapter 8 is the conclusion of this study. This chapter analyzes the achievements in the experiment process and the problems that still need improvement. Finally, a prospect for the future work is given.

CHAPTER 2 LITERATURE REVIEW

This chapter will detail the existing literature on additive manufacturing and related processes. The advantages and disadvantages are determined for the additive manufacturing method. Then the monitoring methods of TIG welding, MIG welding and the formation of welds will be introduced to assist these two kinds of welding method to be emphatically understood. The reason to choose aluminium as a welding material is analyzed with considering the advantages and disadvantages. Furthermore, the comparison between different control strategy is stated to offer a global impression of four control strategies. Finally, the research gap and a summary are determined.

2.1 ADDITIVE MANUFACTURING

Additive Manufacturing (AM), also called as rapid prototyping (RP), is a kind of trending processing method that allows staffs to transfer their imagination to realism directly from the three-dimensional (3D) model through stack material layer by layer. As opposed to the traditional reduced manufacturing, the advantages of the AM are significant. (L.E. Weiss et al., 1992) The budget for prototype is relatively lower because the raw material will not be wasted; The duration for a RP process only cost a few days, but several weeks or even months will be taken through conventional manufacture methods. Moreover, the capability to produce complex model is easier, especially for those who includes small internal structures. (P. Acquaviva et al., 1997)

AM could take a wide range of materials as the raw material. These materials are always in the form of filaments, wire, etc., and both the plastic and the metal could be used during the fabrication process. However, nowadays, the AM is mainly

consuming non-metallic materials, such as plastic and photocurable resins and widely used in the aerospace and bioengineering fields. (L.E. Weiss et al., 1992) For example, the AM helps patients to suffer less open surgery than those without the assistant of the AM. (Adrian Wong et al., 2019) There are two main reasons that the AM are only applied in such a small range of the fields and material. Firstly, although the AM could allow the staffs to create the extremely complex shapes, it is only a cost-effective manufacture method for lower production volumes. (Banks J, 2013) Secondly, the inaccuracy and poor surface of the finished parts requires the post-processing, such as machining, heat-treatment, be applied. Main benefits and challenges for applying metal in AM are shown in Table 1.

Benefits	Challenges
Multifunctional optimization	Limited AM method
Property customization	Poor finished surface quality
Lower material waste	High cost
Fewer assembly process required	

Table 1 Main benefits and challenges for applying metal in AM

2.2 WIRE ARC ADDITIVE MANUFACTURING

2.2.1. Welding process

Wire arc additive manufacturing (WAAM) is a kind of AM method that allow staffs to produce the metal productions in low cost and short duration. There are several reasons that WAAM could be an ideal method to produce the final metal components. Firstly, the deposition efficiency of WAAM is much higher than laser-based AM. The deposition rate of AM based on laser or electron beam is only about 2-10g/min which indicates WAAM is more suitable for fabricate large and complex components.(Ngo TD et al., 2018) Secondly, the budgets for WAAM equipment and material is relatively low compared with

others. Many of the producers are using the welding system during production process, and WAAM does not require to change their production system totally. Further porosity, especially for metals with an oxide film, such as titanium alloys, can separate fine needle martensite from the inner particles under rapid cooling conditions, resulting in a significant improve in yield strength and plasticity.

Nevertheless, compared to other AM methods, people pay less attention to WAAM due to a few reasons. Firstly, the residual stress will influence the mechanical properties because of the high heat introduced in the process. (Feng Z, 2005) Secondly, a low accuracy about ±2mm will present (Ding D et al., 2015) and the welding trajectories will be shown in the final part due to lack of the valid and reliable process monitoring system, and this will cause the low repeatability and quality of the productions.

Hence, ensuring the repeatability and quality of the added production parts is a basic requirement for meeting certification limits and the stringent requirements of leading industries such as aerospace and medical. For example, if the repeatability is high enough, the trajectory of each layer will in a good stability, and this will decrease the surface roughness, and increase the accuracy of the final part. To solve this problem, many recent special projects, roadmaps, and studies have pointed out that the development of process

monitoring methods are based on field induction while new feedback control strategies are priority areas of research.

According to the National Institute of Standards and Technology (NIST) Metal AM (Bourell, Leu & Rosen, 2009), AM's closed-loop control system was identified as a significant measurement and technical challenge for equipment performance and monitor process. It is critical to ensure that parts are in compliance with norms and capabilities which are used to identify certify parts and processes. A number of factors makes achieving high quality and repeatability of metal AM components a challenging task.

The relationship between AM process parameters and process/part characteristics should be established due to the fact that once the correlation is established, the AM process will be able to perform sensing and real-time control, reducing changes in the AM process which ensure the required component quality. Then the variability of part quality is reduced by a robust process.

By cutting a 3D geometrical model to a simple 2.5-dimensional layer instead of conventional removal processes that form part (Karunakaran, K. P. et al., 2010), an additional process called rapid manufacturing is achieved. Using this technology, significant reduction in production costs and time from the initial

concept to the end product can be achieved, which went on saving material (Mughal, M.P. et al., 2006). Additionally, industrial waste and energy consumption can be reduced by using only the amount of material required. In addition, due to the fact that it does not require specially designed fixtures or tools, the flexibility of the moulding process increases while the cost of manufacturing extraordinary tools reduces (Morrow, W. R. et al., 2007).

Rapid manufacturing based on GMAW demonstrates new promises because of its high density, simple device, high productivity and outstanding bond strength of components (Mughal, M. P. et al) as the demand for building metal tools continues to increase. Typically, the GMAW-based rapid manufacturing process is consists of few programs: the creation of 3D models for the parts, the slice of each layer into required thickness, the design of the weld path and parameters of each layer, and the stacking of the deposited beads. However, multilayer deposition is formed in the processes of GMAW-based rapid manufacturing.

With a constant thermal energy input, the deposited weld pool easily flows as the deposited beads increase. The shape of each weld bead is not easy to control due to severe thermal energy build-up, especially at the weld pool and the boundary of the part. In addition, at high temperatures, cavities and bubbles may generate in the molten pool due to strong metallurgical reactions (Zhang,

Y. et al., 2003).

Two methods of rapid prototyping (RP) systems were used in Zhang's research (Zhang, Y. et al., 2003). One method uses a grid to create an image of continuous or overlapping line segment, as shown in Figure 2(a). Another method plans the rough sketch of the image with a motion vector where the raster is filled, as shown by the arrow in Figure 2(c). Thus, showing the basic relationship between precision and speed.

It is essential to use vector motion to fill the rough sketch of the image due to the fact that the width of the RP-based weld line segment (weld bead) is larger than that of other methods, otherwise, the surface error will become worse. The rough sketch of the image is later filling with a motion vector while the inner portion will be filled using a raster method. However, the grating filling method in the system differs greatly from the initial RP method because each welding path has ignition and an end process.

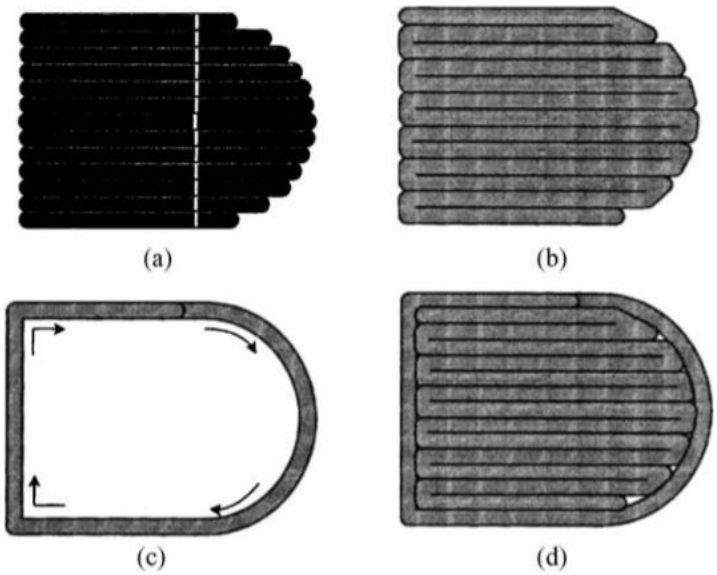

Figure 2 Images the layer: (a) laser filled with raster, (b) welding filled with raster, (c) outline filled with vector, and (d) welding RP (Zhang, Y. et al., 2003)

Experiments show that comparing with the rest of the channel, additional procedures were needed to maintain the accuracy and quality of the beginning and end of each weld bead. Findings show that weld bead joints reduce accuracy, so the number of weld beads and the joints between them must be minimized to increase speed and accuracy. Thus, welding precision cannot be changed effectively by only altering the path planning, making developing a new imaging algorithm that satisfies all these requirements very essential.

Experiments using the new imaging method have shown that the controllability of heat input, integration and precision has improved significantly. Nevertheless, a welding process that use very fine wires and have high droplet transfer stability needs to be developed in order to meet the requirements of practical applications. Research based on the sedimentary

trajectory and posture of the current substrate conditions is also required.

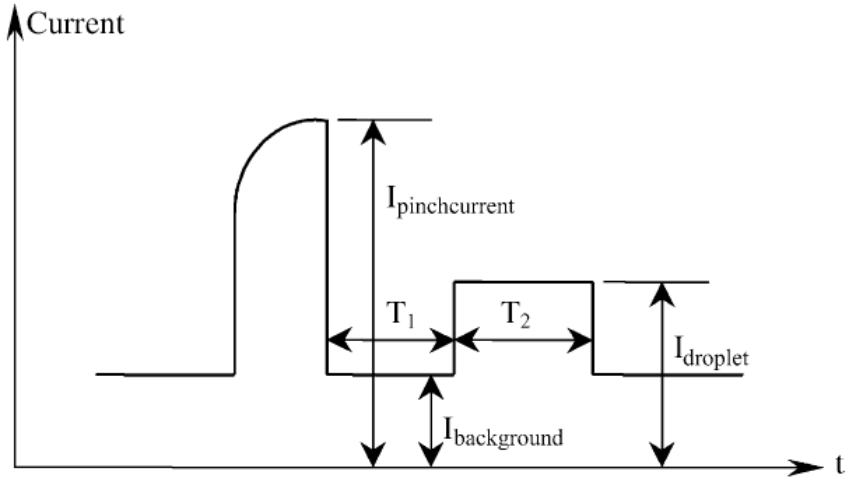

Figure 3 Welding Current of Process (Zhang, Y. et al., 2003)

Adjustment in the thickness of the layer is also needed to obtain geometric accuracy. To achieve this goal, the mass flux needs to be adjustable by precise control on the mass flux to the substrate in order to realize the expected shape deposition. This requires free yet precise control on the size of the droplets so that it stays within a certain range. Additionally, the splash needs to be maintained at a low level in order to maintain the controllability of the mass flow.

Due to reasons listed above, controlling thermal energy input is essential to increasing stability during stratified deposition.

2.2.2. Welding method

TIG and MIG welding are used in this study for the WAAM technology. Although there are some differences between the two welding methods, the vision system developed in this study will be used simultaneously.

Tungsten inert gas shielded welding is a welding method in which arc heat generated between the tungsten electrode and the workpiece, under the protection of inert gas, melts the base material and the filler wire. During the process of welding, in order to obtain a high-quality welding bead the shielding gas is continuously ejected from the nozzle of the welding torch, and a gas protective layer is formed around the arc to block the air, preventing harmful effects on the tungsten electrode, the molten pool.

Unlike TIG welding, to melt the base metal and wire, MIG welding uses meltable wire as electrode and an arc is continuously fed between the wire and the workpiece to be welded as a heat source. The shielding gas-argon gas is continuously delivered to the welding zone through the torch nozzle during the welding process in order to protect the molten pool, the metal base material and the arc in the vicinity from the harmful effects from surrounding air. The welding wire, continuously melted into form of droplets, need to be transferred into the weld pool, where it is fused with molten base metal before condensing to form weld metal.

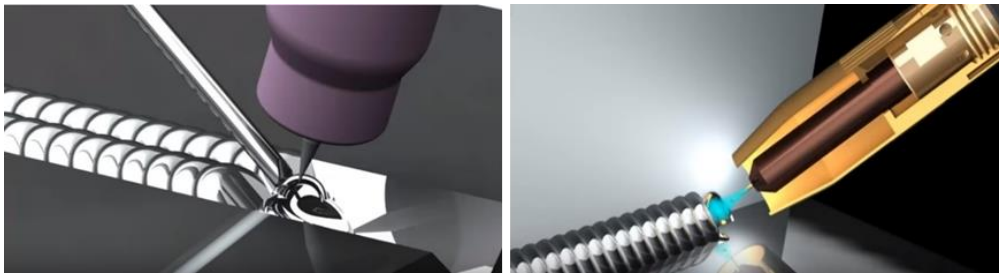

Figure 4 TIG vs. MIG welding schematic (Stoyanov et al., 2017)

2.2.3. Welding material

The weld metal used in this study was aluminum alloy 4043, a silvery white light metal with outstanding plasticity, high electrical and thermal conductivity, together with resistance to oxidation and corrosion, making it quite an ideal metal to be welded. Since aluminum alloys are commonly used as welding materials in industrial production, this paper will also use aluminum alloys as test materials. However, aluminum alloy can also be easily oxidized into a film of Al2O3, which simply causes inclusions in the weld, what's worse, this damages the uniformity and continuity of the metal, causing its mechanical function and corrosion resistance to reduce.

Aluminum alloy 4043 is an aluminum filler metal containing 5% silicon, which is a kind of universal aluminum-silicon alloy welding wire with excellent heat resistance and mechanical properties. The melting point ranges from 1065 to 1170 $°F$. The anodized color is grayish white and the minimum tensile strength is 186 MPa.

First of all, due to its strong oxidizing ability, the oxide on the surface of the weldment must be strictly eliminated before welding and the oxidation needs to be prevented during the process of welding in order to ensure the welding quality. Secondly, using aluminum alloy to weld easily produce pores. The primary cause of pores in the welding process of aluminum alloys is hydrogen dissolved in large quantity in liquid aluminum, a substance that hardly dissolves in solid aluminum. Therefore, when the temperature of the molten pool is cooled and condensed rapidly, hydrogen does not come out, the trapped hydrogen thus went on forming pores. Hydrogen holes are currently difficult to be avoided completely due to the fact that hydrogen has a lot of origins such as in an arc welding atmosphere, aluminum plates, or form moisture in the surrounding air that the appearance of welding wire absorb.

Additionally, the linear expansion coefficient and the crystallization shortening rate of aluminum are about twice as large as that of steel, not to mention that the internal stress of large welding deformation is prone to occur. The occurrence of thermal cracking, causing the weld to be deformed and easier to form cracks, will be promoted in the structure with higher rigidity.

2.3 CONTROL STRATEGY

2.3.1. Difference equation

The difference equation is also known as the recurrence relation in

mathematics. It is an equation that recursively defines a sequence, which means each item of the sequence is defined as a function of the preceding item.

For additive manufacturing, the controlled object is nonlinear, so it is necessary to discretize the differential equation. So, if the differential equation is $d_y + yd_x = 0$, then it will be discretized into Equation 1:

$$k{+}1n{-}y\left({}^{k}/_{n}\right) + y\left({}^{k}/_{n}\right) \times \left({}^{1}/_{n}\right) = 0 \qquad \text{(Equation 1)}$$

Where, $k = 0, 1, 2, \dots, n-1$.

Nonlinear differential equation means it is a differential equation which is not a linear equation in the unknown function and its derivatives.

Due to the existence of unknowns in the nonlinearity and the great effect of unknowns on the system, the most appropriate value should be obtained in the subsequent experiments.

2.3.2. PID control

In order to implement PID control, P control was first tested. P control is the simplest control method for this system, it can achieve fast response, but it is difficult to make it stable.

Then for PD control, when the adjustment deviation changes rapidly, the adjustment amount is adjusted in the shortest time, there is an adjustment static

error, which is applicable to the link with a large lag.

Based on the principle of the PID control, increasing the proportional coefficient K_P will generally speed up the system response. K_P helps to reduce the static error in the static case. But the system will produce a large overshoot when the scale factor becomes too large. The system generates oscillation, resulting in stability reduction. While increasing the integration factor K_I reduces oscillation and overshoot, it increases the system stability and makes the system takes longer time to eliminate static. The system will speed up the response by increasing the differential coefficient K_D. The overshoot of the system reduced and the stability increased, but K_D has an inhibitory effect on the system.

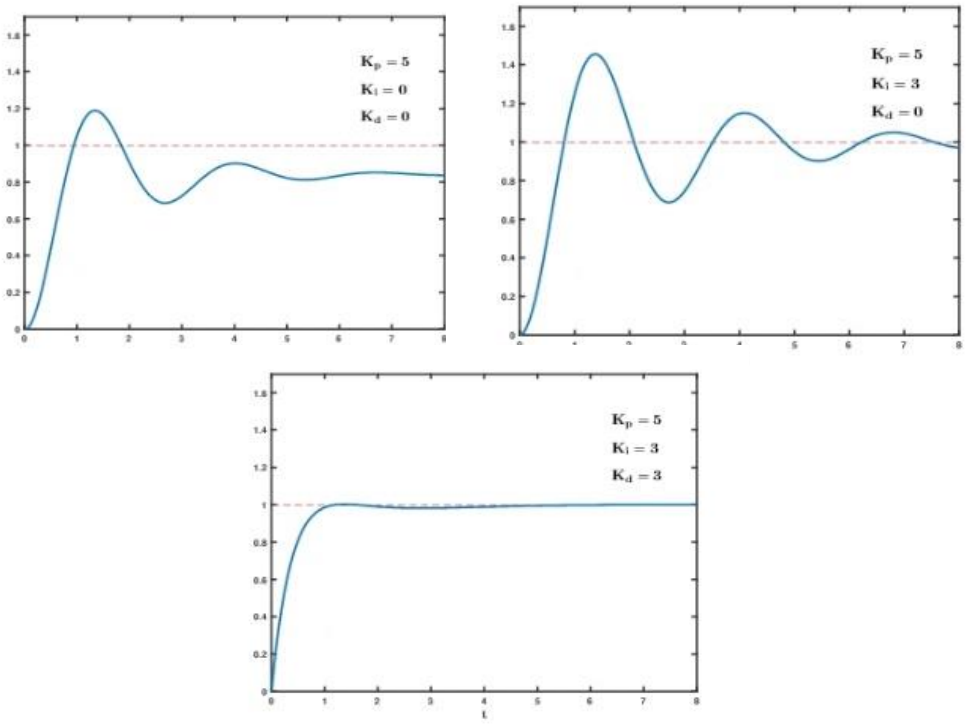

Figure 5 The impact of a change in the PID coefficients
(From left to right: K_P, $K_P + K_I$ & $K_P + K_I + K_D$)

2.3.3. Fuzzy logic

Fuzzy logic is a method of representing and analyzing uncertain and inaccurate information by mimicking the way people think. It is used to deal with the fuzzy phenomenon in order to eliminate the fuzzy. Fuzzy logic can be divided into two types: classical set theory of binary logic and fuzzy set theory of multi-valued logic. In this study, multi-valued logic will be used because it provides the basis and conditions for more accurate logical judgment.

The fuzzy logic can be accomplished effectively by adjusting the membership function and fuzzy rules. Membership functions should meet the following three basic principles: the fuzzy set of membership functions must be convex, the membership functions taken by variables are usually symmetric and

stationary, and the membership functions should avoid inappropriate overlap. Through fuzzy rules, a mathematical model of the relationship between input and output can be established, which can be characterized by a series of transfer functions or by the state space equation of the system.

The fuzzy controller is generally composed of three parts:

1) Input the exact value to know the transformation of fuzzy quantity, that is, "fuzzy"
2) Use fuzzy logic and fuzzy rules for fuzzy reasoning
3) Transformation of fuzzy variables to the exact output, namely "de-fuzzing"

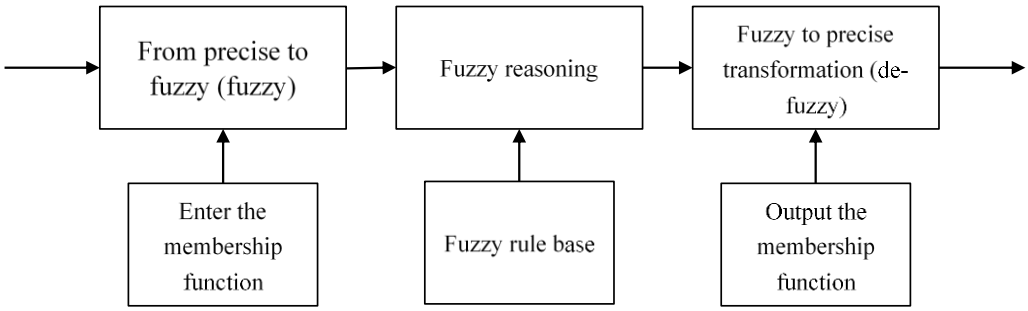

Figure 6 The mode of the fuzzy controller

2.3.4. Adaptive control

Adaptive control is a mathematical model-based control method, much like conventional feedback control. There are two differences: on the one hand, the prior knowledge of the model and disturbance based on adaptive control is relatively small, while on the other hand, the running process of the system needs to be continuous in order to collect the information form the model and

improve the model gradually. In particular, basing on the input and output data of the object, the characteristics of the model can be continually identified. This process is called online recognition of the system, which allows the model become more and more accurate and realistic. In this case, the control system has a certain degree of adaptability.

Adaptive control includes a number of unknown and random factors, which makes the object of adaptive control is an uncertainty system. The definition "uncertainty" here means that the environment describing the controlled object and its mathematical model is not completely certain.

Conventional feedback control system has a typical suppression effect on the changes in the internal properties of the system and the influence of external perturbations. However, because of the fixed controller parameters, when the internal features of the system change or the external perturbations changes significantly, the system performance tends to decline sharply and even turns unstable. Hence, adaptive control is suitable for the object or the perturbation characteristics of a wide change in class of systems, but at the same time requires frequent maintenance of high-performance indicators.

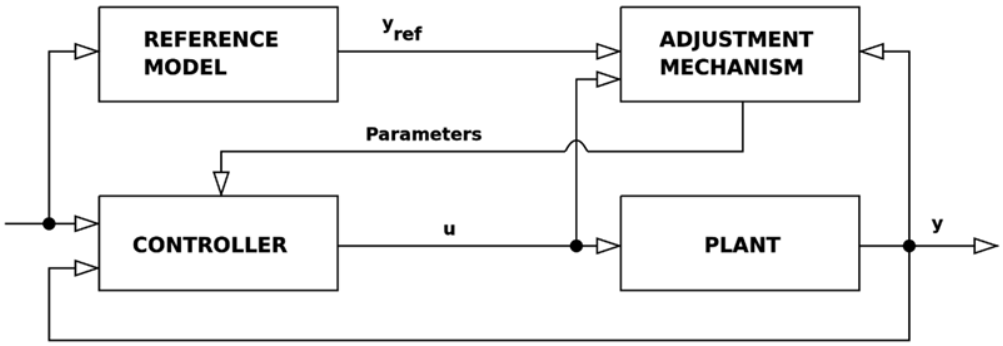

Figure 7 Model Reference Adaptive Control

2.3.5. Comparison among control strategies

A comparison among these four control strategies is presented here. Table 2 gives the comparison summary between the four control methods.

Control Stategy	Complexity	Response Time	Practicality	Stability
Difference Equation	Low	Fast	Easy	Low
PID Control	Medium	Fast	Easy	Medium
Fuzzy Logic	High	Medium	Medium	Medium
Adaptive Control	Relatively High	Medium	Difficult to apply in realistic	High

Table 2 Comparison Among Four Control Strategies

The PID control could be determined as an algorithm evolved from the

difference equation, and add the proportion and integral control to the difference equation. The proportion here offers the ability to increase the sensitivity to the error, so that the steady-state error could be decreased. The integrity will compensate the imperfection of the proportion, which is that the error could not be eliminated. The integrity here accumulates the error and outputs the controlled quantity, and hence the steady-state error will eventually become zero if the duration is long enough. However, at the same time, the integrity subsystem also brings a new problem – oscillation. the oscillation comes from the adjustment during the control under accumulation. This oscillation is restrained by the differential subsystem, and then increase the stability of the whole system.

Fuzzy controller could deal with the non-linear systems, contrasted with the PID control. (Godjevac J., 1993) It could lead a non-linear system to tend to a deterministic system, and a favorable time domain characteristic is presented. However, a significant problem should be mentioned that due to the complex parameters and operations. This causes the system to spend much more computing time than the PID algorithm.

The adaptive control performs as the best choice for controlling the whole system. According to the research achieved by Chaib and Salim (2004), the adaptive control determines the best performance during the testing of car lane

control, which is similar to the welding trajectory control. It offers the smallest error compared among PID, fuzzy and adaptive control methods, and is not affected too much under the circumstance of the environmental intrusion. However, this control algorithm is the most complicated one and is difficult to be implemented in the real life.

2.4 SIMULATION AND POST-PROCESS METHODS

2.4.1. Vision system

Mohammad H. Farshidianfar et al (2003) used Adaptive neuro-fuzzy inference systems (ANFIS) algorithm to control and identify the clad height during the laser cladding process. Actions are controlled based on real-time clad height and scanning speed obtained using CCD camera. D. Hu et al (2002) conducted a research in which a camera with high frame rate of up to 800 frames per second is mounted on the laser nozzle to obtain the infrared image of the molten pool in real time, calculate the size of the molten pool, and achieve closed-loop control.

Xiaoqing Cao and Beshah Ayalew proposed a method for controlling a multiple input multiple output (MIMO) model using a class of laser-aided powder deposition (LAPD) processes. The MIMO model is derived in the form of Hammerstein, in which coupled nonlinear is connected to the linearized dynamic. In this model the inputs consist of scanning speed and laser power while the outputs consist of the temperature of the molten pool and layer height. This work provides reference and inspiration for further

work in AM control even though the control algorithm had not yet been proposed and implemented.

Meysar Zeinali et al. (2018) obtain molten pool height using CCD camera and realize real-time feedback control in laser cladding process. In the process, an adaptive sliding mode control algorithm with uncertainty estimator is suggested and the control of the cladding height is realized. Experiments on the controller ensure its effectiveness.

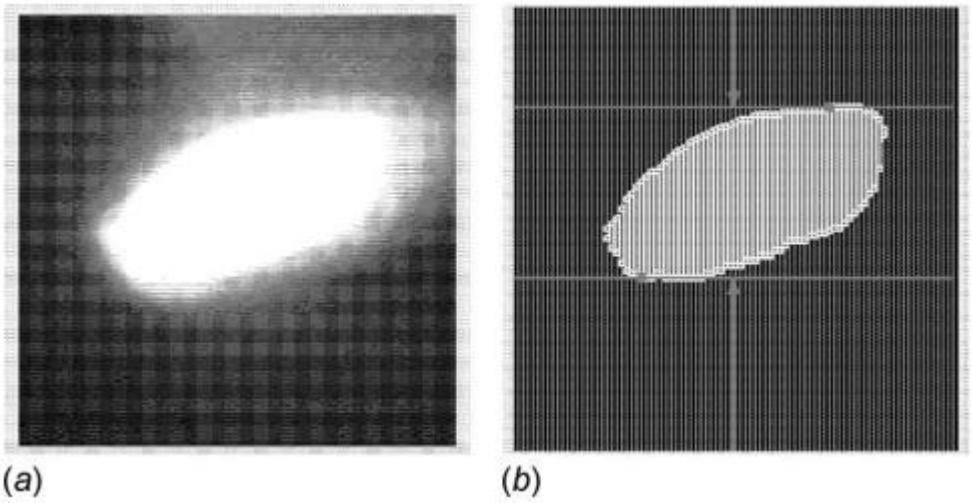

Figure 8 Pool image collected by CCD (Meysar Zeinali et al., 2018)

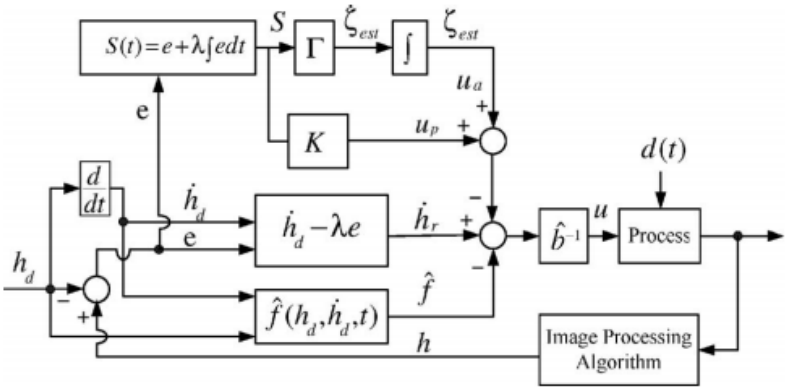

Figure 9 Algorithms and feedback processes (Meysar Zeinali et al., 2018)

Using 3D scan sensor, Almir Heraldic et al (2012) get the height profile. Using the iterative learning control, a feedforward control strategy, and by controlling the feeding rate on the following deposition layer, the deviations of layer height could be maintained constant. Furthermore, a PI controller that modifies the laser power was combined, controlling the bead width.

During laser cladding process, J.T. Hofman et al (2012) acquire the width of the welding pool using a CMOS camera, for which a PI controller was developed to control it. The weld pool size was determined in real time and parameters are transmitted from the camera to the computer, which runs a developed program constructing the digital image of the weld pool, at a frame rate of 200 Hz.

First, a Gaussian shape spread function (PSF) filtered the image in order to remove hot particles and a single bright pixel. Second, the image is transformed into a black and white version using the means of a threshold. Finally, a third step involving the extraction of weld pool width is taken.

Examinations on hundreds of images uncover the fact that the ellipse was essentially a weld pool shape, which is decided by the first and second moments of the region. The width of the weld pool can be calculated from function $w_m = 4 * \sqrt{\frac{\lambda_{min}}{A_m}}$, in which min is the minimum principal torque and A_m is the area of weld pool. By multiplying the scale of the image, the value of the detected bath width is converted from number of pixels into a real unit. In this study, the image processing method is realized in C++.

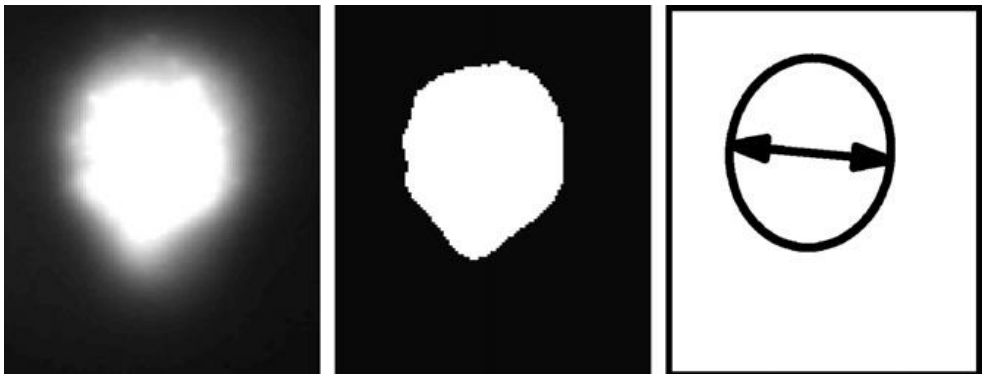

Figure 10 Left: Original Image. Center: Lowpass Filtered and Thresholder Image. Right: Fitted Ellipse (Hofman, J. T. et al., 2012)

2.4.2. Data analysis

Genetic algorithm was first proposed by professor John h. Holland (1975) of Michigan in Adaption in Natural Artificial Systems. In the 1980s, Holland discovered that learning could be achieved through many evolutionary adaptations of the population. Then the first machine learning system based on genetic algorithm was realized.

In 1989, Goldberg expounded the basic principles of genetic algorithm, and summarized the application of genetic algorithm. GA completes biological evolution through crossover and mutation between chromosomes. It is an evolutionary algorithm that is introduced into a mathematical model to solve random problems in actual search. Since its introduction, it has been rapidly developed because it is a practical, efficient, parallel, robust, global search optimization technology.

Genetic algorithms are often used to process traditional statistical and mathematical planning. Metawa et al. (2017) proposed an intelligent model for

organizing bank lending decisions based on genetic algorithms, which reduced the loan screening time by 12-50%, while enabling a significant increase in bank interest rates of 3.9-8.1%. This shows that genetic algorithms are more effective in screening data.

The particle swarm optimization algorithm was first proposed by Eberhart and Kennedy of Purdue University in the United States after being inspired by bird swarm behavior modeling and simulation experiments in 1995. Reynolds (1987) is based on three criteria: keep the distance to the nearest neighbor; move to a known target; move to the center of the group, and simulate the complex group activities of the bird group through CG animation. Because of its concise concept and few parameters, particle swarm optimization is a convenient implementation, fast convergence and efficient group search optimization method, which can effectively optimize various functions, so it has attracted attention in many fields.

Particle swarm optimization algorithms are effective tools for solving all kinds of optimization problems. Wang et al. (2018) combine particle swarm optimization algorithms with adaptive learning strategies to balance the ability to explore and exploit multi-modal problems. The results show that the convergence accuracy and speed of convergence of the PSO algorithm are much better than other algorithms.

Bayesian and k-Nearest Neighbors (k-NN) algorithms are commonly used to identify and classify data. Lakshmi & Nanda Dulal (2019) used identification

algorithms to classify multiple drug molecules and evaluated the two algorithms. The results show that the k-NN method shows higher accuracy and higher precision compared to Bayesian. Moreover, the recall rate and F1-score of k-NN were higher than that of Bayesian.

K-NN can be seen as: there is a bunch of data that is already known to be classified, and then when a new data comes in, the algorithm starts to find the distance to each point in the training data, and then picks the nearest points to the training data to see what type they belong to, and then uses the principle of majority rule to classify the new data.

2.4.3. Dynamic Model

To achieve the stability control, a dynamic model is usually built to obtain stable parameters through self-learning of the model.

Xiong and Zou (2019) designed an active visual sensing system based on camera and auxiliary light source for reverse osmosis monitoring of pulsed MIG suspension welding of aluminum alloy. Based on this, a fuzzy controller is developed to control the reverse welding of aluminum alloy by tuning the welding current in pulse MIG suspension welding.

The weld penetration control structure in their study is the typical Mamdani type single-input single-output fuzzy controller, as shown in Figure 11, where W_g is the required width at the back of weld pool; W_d is the detection width from the computer vision sensing; e is the width deviation; ci is the welding

current increment and ce is the variation in width deviation. With the time t, the width deviation and variations thereof may be given as: $e(t) = W_d(t) - W_g(t)$ & $ce(t) = e(t) - e(t-1)$.

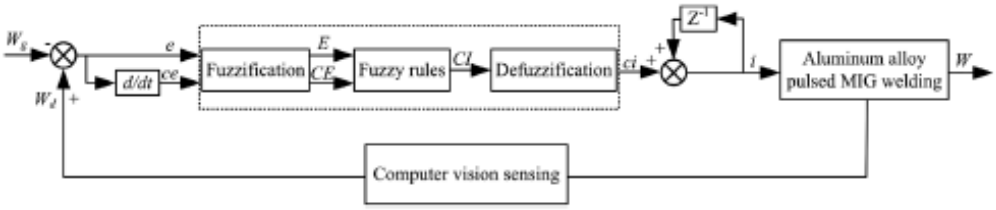

Figure 11 Structure of single-input single-output fuzzy controller for weld penetration rate (Xiong, J. & Zou, SY., 2019)

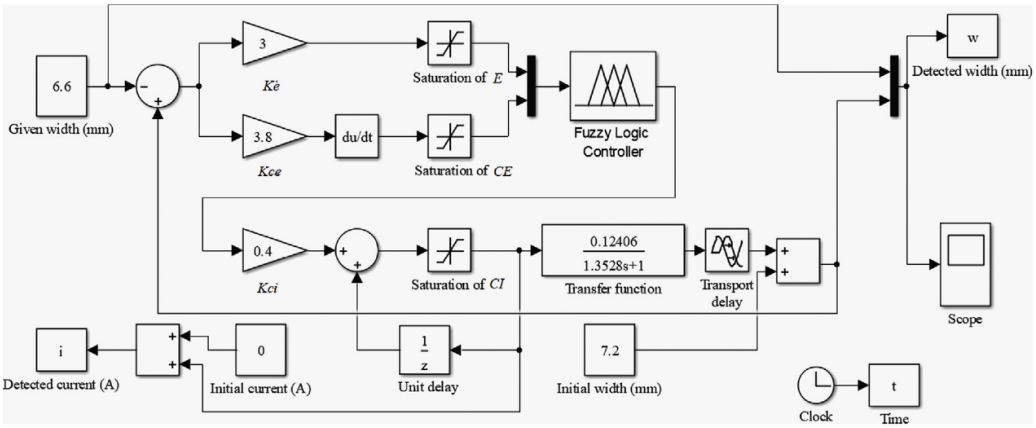

Figure 12 Simulated block diagram of fuzzy controller based on the first-order transfer function (Xiong, J. & Zou, SY., 2019)

The simulation results show that the optimal control performance of fuzzy controller can be obtained by setting the improved controller parameters.

To combine the fuzzy logic and Neural Networks could control the system with time delay. Chen, Wu and Wang (1997) designed a neural network compensator to replace the classical Smith predictor to attenuate the detrimental effects of time delays in an uncertain system. Figure 13 and Figure

14 shows the PMN's network structure and the control system with Smith predictor.

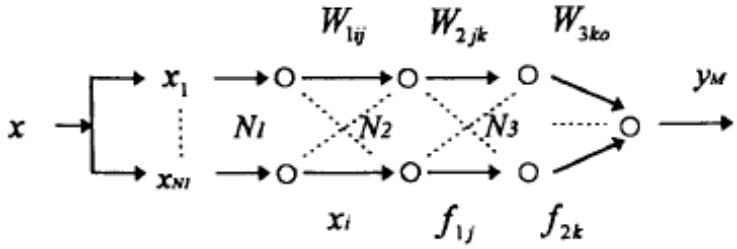

Figure 13 Neural network model of PMN (Chen, SB., Wu, L. & Wang, QL., 1997)

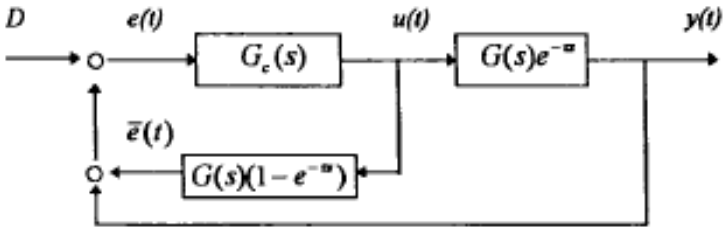

Figure 14 Control system with Smith predictor (Chen, SB., Wu, L. & Wang, QL., 1997)

A dynamic SISO model for controlling pulse TIG welding is established. (Chen, SB., Wu, L. & Wang, QL., 1997) The output and input of the weld pool head pass width and the weld travel speed. The neural network model of this process is established by using input and output to batch test data and off-line learning algorithm. The scheme has been applied to the dynamic control of the weld pool in the arc welding process, and experimental results show that the control scheme is feasible.

2.4.4. Control and algorithms

The effectiveness of the process control system depends strongly on the preciseness of the system behavior analytical model in the conventional

control methods. Nevertheless, the AM process is complex and nonlinear, what's worse, it is hard to develop an accurate mathematical model due to the fact that process variables couple each other. Nowadays, complex system with highly nonlinear and complex task requirements, followed by uncertain mathematical models, are controlled by intellectual control algorithms specifically developed for this use. Intellectual control methods were also applied in AM control area.

A fuzzy logic based PID controller designed by Y. Hua et al. (2005) alters laser power during the laser deposition process in order to track reference height. Though fuzzy logic-based control requires knowledge and experience in the process, it does not need an accurate mathematical model. PID parameter transformed adaptively can deal with the time-varying system of a fuzzy logic system.

Basing on the fuzzy logic, Meysar Zeinali et al (2010) creative a dynamic model for the laser cladding process. Process dynamics of scanning speed and layer height was modeled. In order to deal with uncertainties, some model arguments were estimated online in this fuzzy model. This characteristic of online learning provides adaption for real-time control applications.

Volker Renken et al (2017) suggested a concept of control approach in laser additive manufacturing. In order to make process stability at a fix point, an adapted self-learning strategy was suggested in this control approach, this can be achieved by updating the data of the multidimensional model which is used

to restrain the environmental influences or machine shifts during the process. The molten pool size including the height and width was correlated to the intensity of RGB signals as the temperature using data from the RGB sensor. In order to achieve polynomial and radial basis function (RBF) model in real time, the integrated data comes into the calculation, updating the parameters of the model.

A study on a hybrid control system that improved the dimensional preciseness of geometrically complex parts was run by Song et al. in 2011. In the study a triangulation device that controls the pool height using three high-speed charge-coupled device cameras was designed.

The maximum increase in the height of metal deposition is limited by a height controller. The height of the cladding is controlled and altered using three lenses, with a spacing of 45 degrees with the laser beam in the x-y plane and a spacing of 120 degrees for the three lenses. The detection threshold of the pixel luminance is set, while an image processing unit is made by calculating the centroid of the cladding height from the cladding image. Reference height is the thickness of the layer which matches the height increment. Three cladding heights are been calculated and then compared with the reference height. If the cladding height exceeds the limit, the sending of a trigger signal to the laser will reduce the laser power in order to avoid exceeding the cladding for 10 milliseconds at the current location.

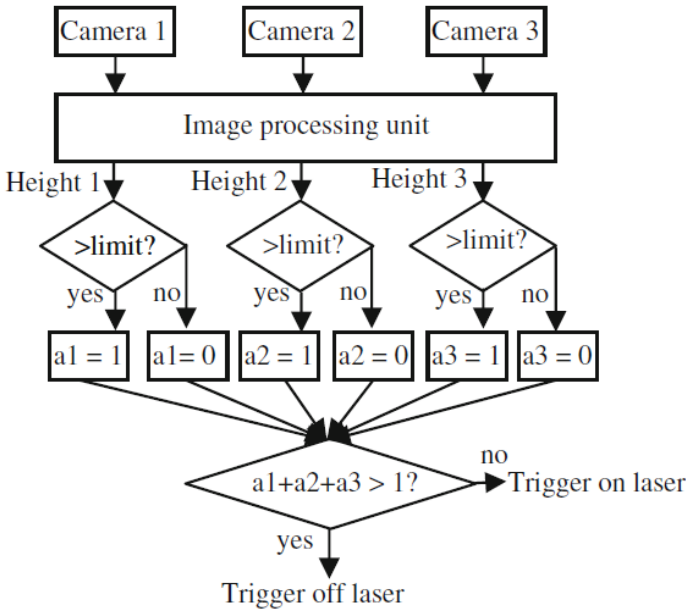

Figure 15 Height Controller Logic for Three High-Speed Cameras (Song, L., et al., 2011)

A two-color pyrometer consists of two inputs and one output control system which controls the height increase and pool temperature of every deposit is the supervisory control of the pool temperature control system. A regular controller with input restraints in its generalized predictive control algorithm is called a height controller.

GPC, comparing with traditional PID controllers, can provide more powerful control behaviors (Rostgaard, M. et al., 1996) enabling it to adapt to the multi-input and multi-output systems much easier. As shown in the following equation, N step prediction $\hat{x}(k+N)$ and $\hat{y}(k+N)$ can be expanded as Equation 2:

$$\begin{cases} \hat{x}(k+N) = A^N x(k) + A^{N-1} B_U(k) + \cdots + B_U(k+N-1) \\ \hat{y}(k+N) = CA^N x(k) + CA^{N-1} B_U(k) + \cdots + CB_U(k+N-1) \end{cases} \text{(Equation 2)}$$

As the height of the pool gets to a point higher than a specified thickness, the main height controller avoids overbuilding by reducing the power of the laser and blocking the effects of the temperature controller. However, when the height of the pool gets below the layer thickness, the process of height controller is absent and the temperature controller only dynamically adjusts the power of the laser to control the welding pool temperature instead. Through heat input control ensuring stable layer growth, the hybrid controller will be capable of avoiding over-construction and low-rise construction.

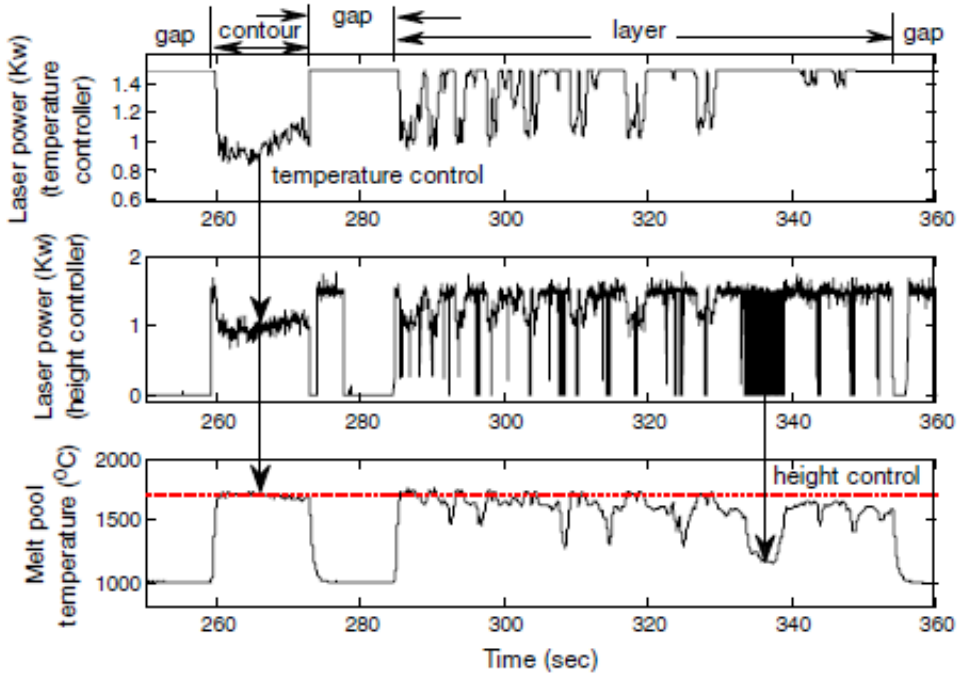

Figure 16 Control Action and Pool Temperature (Song, L., et al., 2011)

Adaptive control has long-term application in welding. In 1996, an adaptive generalized predictive decoupling control scheme is constructed by Zhang, Kovacevic and Li. As shown in Figure 17 (Zhang, Y. et al., 1996), the system consists of four basic parts: decoupling element device, estimator and predictive control algorithm.

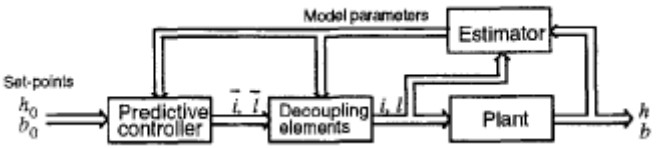

Figure 17 Predictive Decoupling Control Principle (Zhang, Y. et al., 1996)

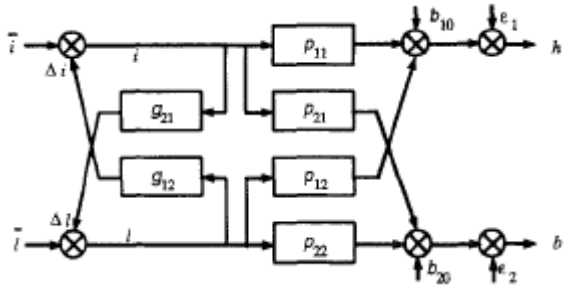

Figure 18 V-canonical decoupling (Zhang, Y. et al., 1996)

Figure 17 is the simple V-canonical decoupling with a P-canonical plant. Where,

$\mathrm{P} = \begin{bmatrix} p_{11} & p_{12} \\ p_{21} & p_{22} \end{bmatrix}$, $\mathrm{G} = \begin{bmatrix} 0 & g_{12} \\ g_{21} & 0 \end{bmatrix}$, $\mathrm{U} = [i, l]^t$, $\overline{\mathrm{U}} = \left[\bar{\imath}, \bar{l}\right]^t$, $\mathrm{Y} = [h - b_{10}, b - b_{20}]^t$, $\mathrm{E} = [\varepsilon_1, \varepsilon_2]^t$, g_{12} and g_{21} are the transfer.

And Equation 3 can be obtained,

$$= PU + E = P(I_{iden} - G)^{-1}\overline{U} + E$$
$$\frac{1}{1 - g_{12}g_{21}} \begin{bmatrix} p_{11} + p_{12}g_{12} & p_{12} + p_{11}g_{12} \\ p_{21} + p_{22}g_{21} & p_{22} + p_{21}g_{12} \end{bmatrix}$$

(Equation 3)

A simple elimination method is employed so that a complete decoupling is accomplished. The complete decoupling condition for g_{12} and g_{21} are shown as Equation 4:

$$\begin{cases} p_{12} + p_{11}g_{12} = 0 \\ p_{21} + p_{22}g_{21} = 0 \end{cases} \quad \text{(Equation 4)}$$

Experiments have shown that there is a delay in the welding process which is due to distance between laser bar and the welding pool is shown through experiments. However, an adaptive decoupling algorithm is designed in order to successfully control the process. The experiments also show that an ideal pool geometry can be reached despite the interference and variations that occurs in the welding conditions. Therefore, developed system provides technology that can be developed for welding quality control.

Xiong and Zhang use the adaptive control on deposited height in GWAM-based layer, later in 2014. In the study, in order to improve the stability of the welding process and at the same time keep the nozzle to the top surface distance (NTSD) constant, an adaptive control system was designed and the controlled process was simplified into a linear system. The vision system is as shown in Figure 19.

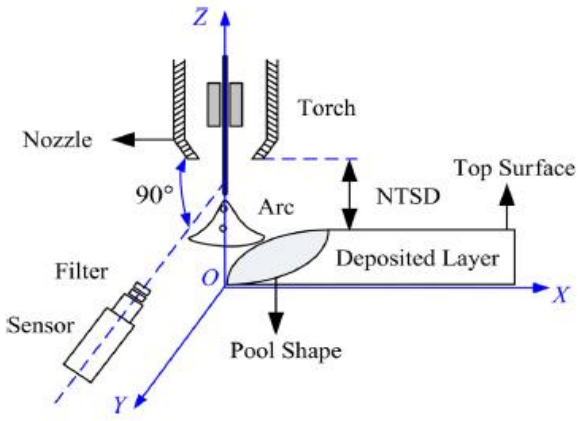

Figure 19 Schematic of the vision sensor system (Xiong, J & Zhang, G, 2014)

An adaptive controller adjusts the controller parameters and complete the online identification process arguments, in this paper. (Xiong, J & Zhang, G, 2014) Among these parameters, the performance index is solved by a generalized minimum variance algorithm, while the adaptive controller is determined as Equation 5:

$$u(k) = \frac{-G(z^{-1})y(k)}{A+B(z^{-1})F(z^{-1})} \quad \text{(Equation 5)}$$

In which $A = \lambda^2/b_0$, λ is the weighting coefficient of able, and $F(z^{-1})$ $G(z^{-1})$ are expressed as Equation 6:

$$\begin{cases} F(z^{-1}) = 1 + f_1 z^{-1} + \cdots + f_{d-1} z^{-(d-1)} \\ G(z^{-1}) = g_0 + g_1 z^{-1} + \cdots + g_{n-1} z^{-(n-1)} \end{cases} (n = n_a - 1)$$

(Equation 6)

With the process structural arguments constant, the algorithms can be written as Equation 7:

$$u(k) = \frac{-g_0 y(k) - g_1 y(k-1) - g_2 y(k-2) - b_1 u(k-1) - b_2 u(k-2) - b_3 u(k-3)}{A+b_0}$$

(Equation 7)

where g_0, g_1, g_2, b_0, b_1, b_2, b_3 are calculated by forgetting factor recursive least squares estimator online. Figure 20 shows the principle of the NTSD adaptive controller.

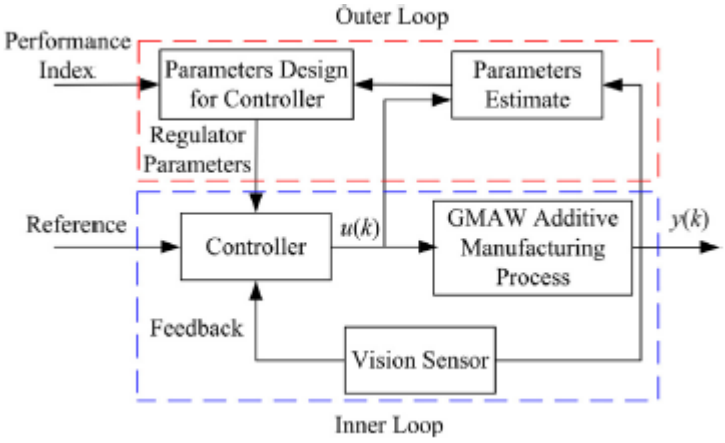

Figure 20 NTSD adaptive controller principle (Xiong, J & Zhang, G, 2014)

This experiment shows the preciseness of the control system can be limited to as low as 0.5mm by the developed adaptive control algorithm. Additionally, the distance between the top surface and the nozzle can be detected effectively by the passive vision sensor system. Nevertheless, a new control strategy needs to be developed because during the welding process a high degree of deviation between the arcing point and the arc stop point is found.

2.5 SUMMARY

By understanding the knowledge of WAAM, this study will use aluminum alloy as welding material, and TIG and MIG welding methods are used.

Additive manufacturing is an effective method for near-clean shape manufacturing. As WAAM is a complex process that integrates many aspects, the molding cannot have stable results. Through the reading of the literature, nowadays WAAM technology is not well regulated and controlled. The visual feedback system of welding process has been used to measure the quality of penetration these years. In order to develop a real-time welding connection

system, speed, current, voltage, and feed speed are controlled based on measured height, mass, and depth. However, the literature on using such techniques to control WAAM in real time is scarce, and although there are a large quantity of research that related to the control method, applying these control methods to WAAM obtained less attention. This research aims to apply these control methods by experiments and simulation model to determine whether they are effectiveness and practical.

The current problems that comes out in the process of additive welding is that as the system stacks to a higher height, the errors caused due to the fact that the height and width of each layer cannot be made uniform built up to a large degree. Additionally, the size of the molten pool may be larger than the range of the soldering during the stacking process making that part of the soldering liquid lower than the expected height, so as this small different adds up the solder layer will become shorter than the ideal height. An error in the additive welding as mentioned above will cause the stacked walls to slant.

Since K-NN requires some data that is already classified, it is not applicable in this study. The treatment of the data in this paper requires the elimination of points that are far away from reality and the selection of the most advantageous to prepare for the later choice of control parameters, hence the genetic or particle swarm optimization algorithm.

Because some of the algorithms used in other devices and technologies have achieved better control, so during the course of the study, similar algorithms

are learned in the next experiment, by using them in WAAM technology such as fuzzy logic, PID control, etc.

Also, by considering the influence of welding speed regulation on the mechanical inertia of the process response, a dynamic model can be established to simulate. In order to improve the accuracy of the control algorithm, a data recognition algorithm will be used to filter and classify the image data. The internal parameters and corresponding system functions of the system can be obtained from the simulation model, which can help to reduce experimental errors and reduce the cost.

CHAPTER 3 EXPERIMENT CONFIGURATION

This chapter introduces the experiment configuration for the dissertation. For applying the computer vision system to the welding process, a complete experiment should include both hardware and software for monitoring welding process and collecting data. The experiment platform is used to generate the raw data during the welding process and then these data will be applied to calculate the proper parameters for the simulation and the algorithms introduced later. Then the experiment will be compared with the simulation data to prove that if the system is valid or not, and this will be a new attempt to build up a connection between control algorithms and welding algorithm for the welding process, which may be useful for applying the WAAM in practical.

3.1 PARAMETER SELECTION

As stated in subsection 1.3.1, the aim of this research focus on developing the process control method for WAAM to provide the stability geometry for each layer and improve the accuracy. In order to achieve a good surface quality, the width of each layer should under control. Hence the weld pool width should be considered as an essential evaluation result. The weld pool width is affected mainly by the heat during the welding process and the wire feed speed. The experiment set the heat as a const and the wire feed speed as a variable, in that the real production, the MIG and TIG requires the base metal not being melt. This requirement causes the welding temperature to be relatively stable. Hence the wire feed speed affects the result significantly.

3.2 HARDWARE CONFIGURATION

Firstly, the hardware should be determined to achieve the basic functions, such as welding, collect data, transport signal between controller and the manipulator. The hardware is consisting of several part for the experiment, a welding torch, a welding power, a wire feeding system, shielding gas, a cooling device and a CCD camera.

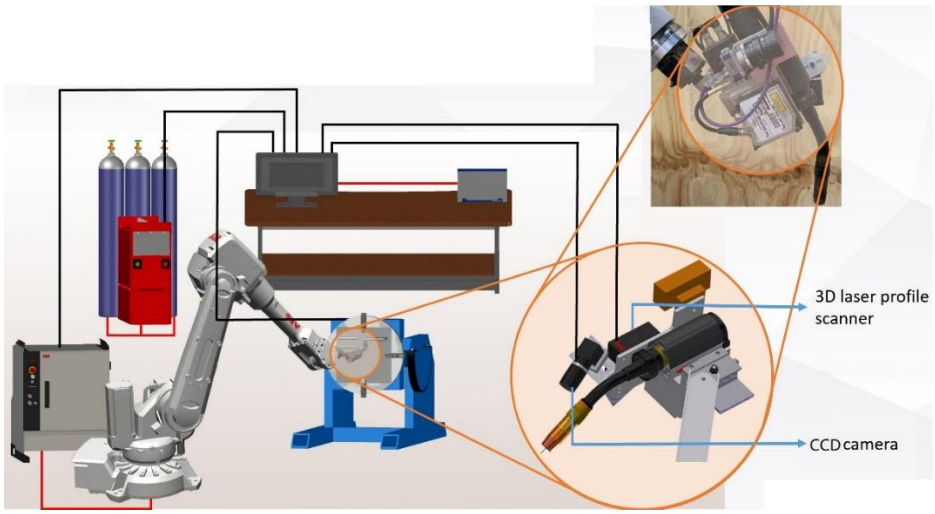

Figure 21 Laboratory equipment

In order to exhibit the hardware configuration visually, figure 21 is created to show the hardware. A CCD camera is fixed at the top of the torch, at the angle of 60 degree relative to the weld orientation on the plan perpendicular to the weld surface. This is the fitted orientation for collecting the typical picture during welding process according to a simple experiment applied. Then the camera is connected to the PC. Another PC port is connected to the ABB central control system to control the parameters, such as the position of the manipulator and the torch moving speed. Furthermore, this could be convenient for operators to control the manipulator if the manipulator is required to stop working urgently, and, operators could observe the weld molding process whenever necessary.

Others such as a power supplier, the shielding gas and wire feed control system are also applied.

The wire, whose material is aluminum alloy 4043, is used as the electrode for additive welding under the action of protective gas. The CCD camera and 3D laser profiles scanner are positioned next to the torch as sensing and surveying equipment, which allows the device to move with the torch during the additive process. The image taken by the camera will be at the specific angle. The scanner will scan the weld in horizontal state after the additive is finished. Detail of selection and configuration for each component are stated in following subsections.

3.2.1. MIG torch

The welding electrode is generally made of the welding material such as aluminum, iron and copper. The typical GWAM welding torch has many critical components, including the electrode tubes and liner, the contact tip, the control switch, the power cable, the gas nozzle and gas hose.

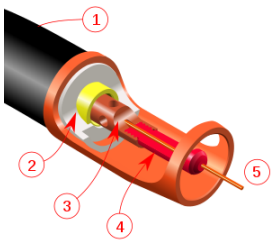

Number	Name
1	Torch handle
2	Molded phenolic dielectric (white) & threaded metal nut inset (yellow)
3	Shielding gas diffuser
4	Contact tip
5	Nozzle output face

Figure 22 The structure of MIG welding torch (Car cooling system, 2020)

Pressing a trigger activates or control switch the wire feed, power and protective airflow, causing the arc to be struck. As the MIG torch uses the welding material as the electrode, this results in a uniform and stable shielding gas to the weld area, while the leads and pads help avoid warping and keep an uninterrupted wire feed.

3.2.2. TIG torch

The electrode, gas nozzle, collet, collet body, and end cup are combined as TIG welding torch. The tungsten wire is used as a welding electrode in welding torch. Because of the high melting point of tungsten, the electrode heats up but does not melt during the TIG welding process. The arc is released within a certain distance between the electrode and the base metal, and the heat generated the melts the external welding material.

Since the welding material of TIG is external, if the welding material is in the contact with the electrode during the welding process, it is easy for the material to stick on the electrode, which may damage the electrode and cause arcing, and also affect the camera's observation of the molten pool.

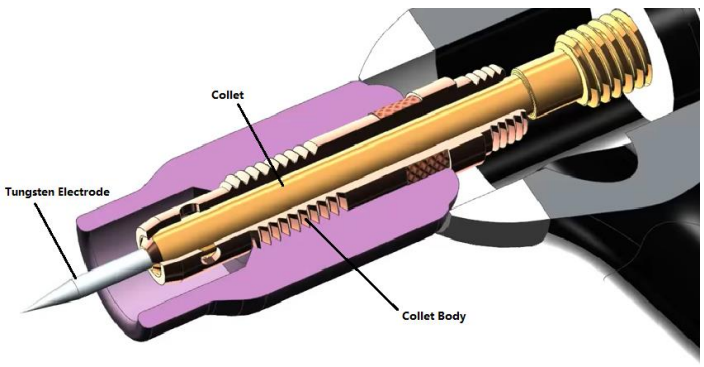

Figure 23 The structure of TIG welding torch

3.2.3. CCD camera selection and configuration

The multi-function CCD with a USB 2.0 port to which the Sony CCD sensor can be connected is used in this laboratory. Since TIG welding requires an external welding material, the camera is not suitable for capturing the melt pool data as directly as the MIG system, and a lens is used for reflection, as shown in Figure 24.

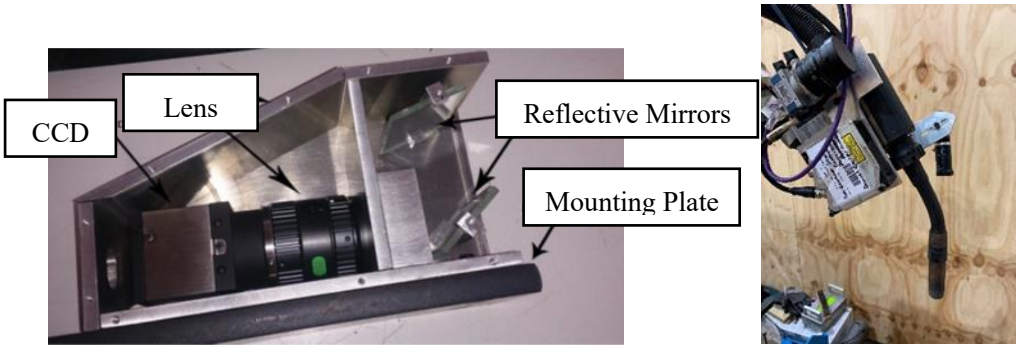

Figure 24 Camera Equipment (top-TIG & bottom-MIG)

The camera takes the UI-2220SE specification, which has a resolution of 786 x 576 pixels. The camera is commonly used in the automotive and industrial fields; therefore, the appearance of the molten pool can be visually observed.

An IR (infrared) cutoff filters with a bandwidth of 15 nm was also used in the surveillance process. There is a requirement for an upper limit of spectral sensitivity because the noise ray in the welding process is UV light (Chen, S. B., 2007). In case the initial version is not applicable for TIG welding, the filter will be followed from the Blu-ray filter.

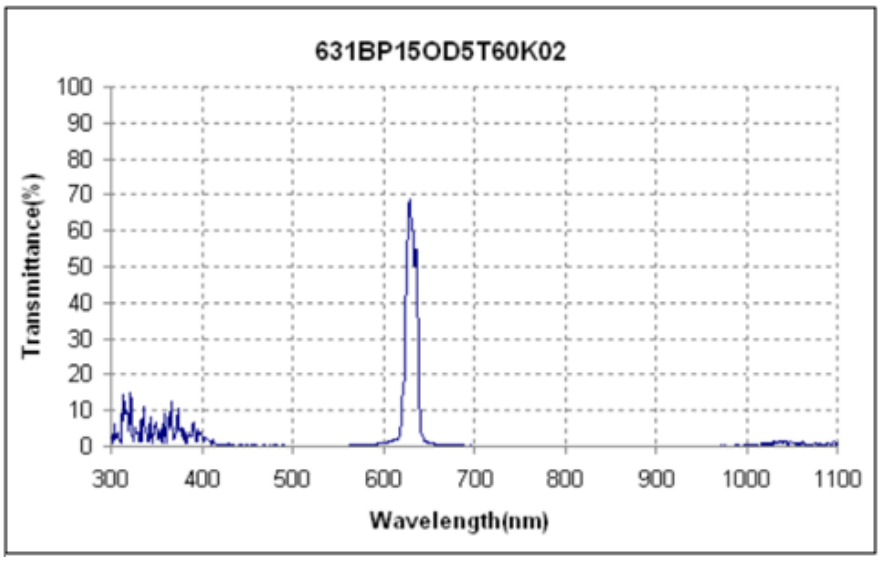

Figure 25 Transmittance Index %

3.2.4. GTAW interface

The GTAW interface is a central element for connecting hardware. It can be connected not only to all the hardware equipment; at the same time, it can be connected to the computer through the USB interface.

The GTAW interface is linked to the computer, which makes it possible to both transmit programs and communicate with control software, which achieve the joint control of software and hardware. In this study, the control signal, after getting the feedback of the melt pool width, is transmitted to the wire feeding system by GTAW interface to control the wire feeding speed.

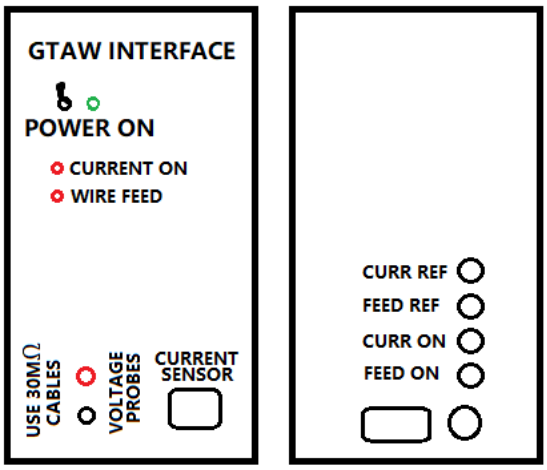

Figure 26 interface of the Device

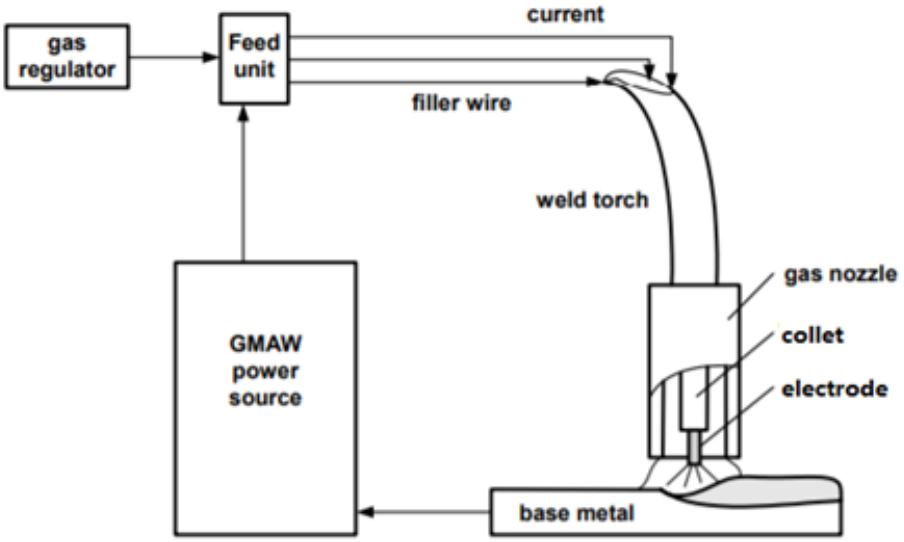

Figure 27 Schematic diagram of GMAW

3.2.5. Wire feed controller and wire feeding speed selection

The wire feeding machine is a kind of computer and the program control under the control of continuous and stable according to set parameters to feed the automatic wire feeding equipment.

The driving part of the wire feeder typically consists of an adjustment pretension pressure bar, a drive wheel and a driven wheel. The adjustable preload lever is used to hold the wire in place and the swivel handle

allows for adjustment of pressure. The motor provides motive force for the wire feed drives by driving the rotation of the drive wheel. The smooth feeding of the wire depends on the increased friction between the wire and the wire feed wheel, which is achieved by pressing the wire into the wire feed channel on the wire feed wheel by the driven wheel of the welder. The semi-automatic GMAW wire feeding speed is generally between 2 ~10 meters/minute.

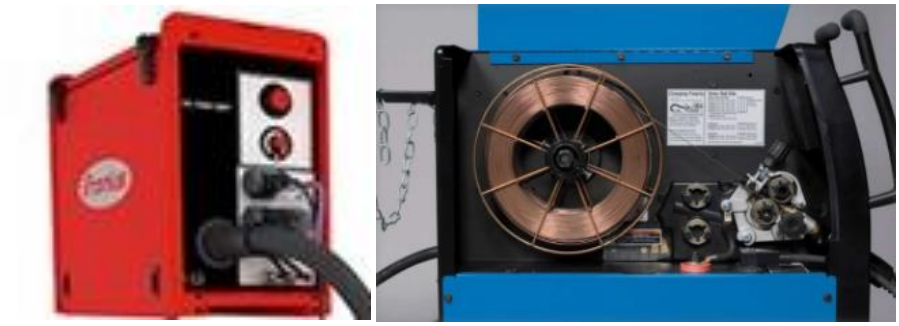

Figure 28 Structure of Wire Feed Controller (Car cooling system, 2020)

3.2.6. Primary power

In the welding process, the direct current (DC) welding is applied. First of all, there is no "zero junction" in the output current of the current welding machine, which reduces the welding process to an unlikely arc break and stabilizes the arc. Furthermore, the peak secondary voltage of the transducer is constant. Since the no-load voltage of a DC welder is higher than the alternate current (AC) welding machine, the welding process is more likely to initiate an arc.

Stepped current instead of the DC current is helpful to extract the peak and base values of the welding pool condition in the DC inverter arc

welder. Therefore, in the following study, the step current will be applied.

For both TIG and MIG welding, the main power supply is a constant voltage source. It can be seen that any variation in arc length directly associated with the voltage will lead to differences in the input thermal and current. Constant power supplies and wire feeding machines sometimes need to be used in combination.

Figure 29 Voltage Power Supply & 4000/5000 CMT Power (Globalrobots.com, 2020)

3.2.7. Shielding gas

Shielding gas is used to prevent the melt pool from being exposed to oxygen, nitrogen and hydrogen gas. The shielding gas is continually sprayed from the nozzle of the torch during the welding process to form a gas shield around the arc to keep out the air and prevent detrimental impacts on the tungsten electrode, the melt pool and the surrounding thermal influenced areas to obtain a high-quality weld layer.

In this study, the shielding gas is argon gas. The shielding gas valve was opened before welding. During the welding process, the shielding gas is normally held at 5-10 litres.

3.2.8. Cooling system

The radiator is driven only by the thermosiphon effect in the coolant pump. The liquid pump first uses a downward vertical flow, and during the heating process, the coolant becomes less dense, so the coolant pump rises; when the radiator cools the liquid, the coolant becomes denser, so the coolant pump falls.

Working as a radiator, the heater core remove heat from the cabin. This provides for the efficiency and stability of the welding process.

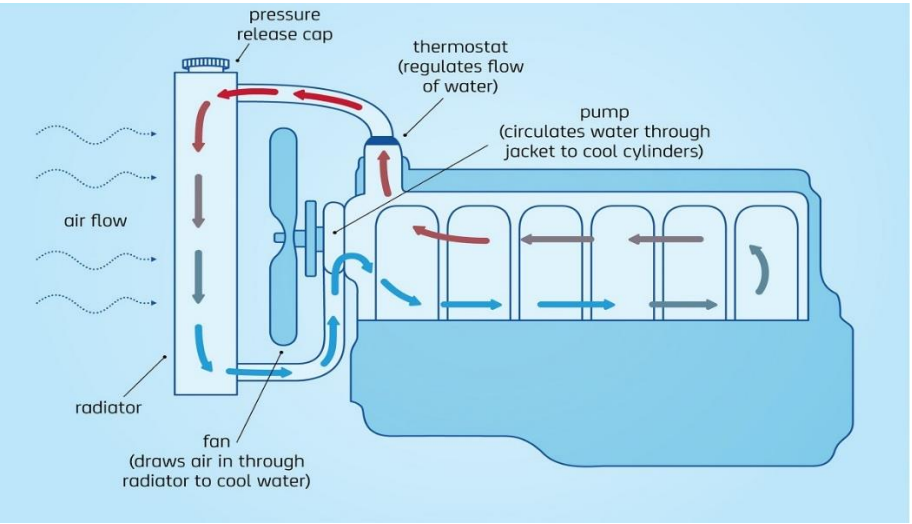

Figure 30 Water flow & Gas pressure interlock (Car cooling system, 2020)

3.2.9. 3D laser profiles scanner

ScanCONTROL 3D laser profile (as shown in Figure 31) is used in this

study to record, measure and evaluate the external profile of the weld bead under test, which is the high-end industrial automated contour scanner. ScanCONTROL intelligent profilers are suitable for applications that require calculating common parameters while measuring profile information, such as step height, clearance width and relative position.

In this study, a 3D scanner is used to scan the weld at the end of addition to determine if the width of the layer is the same as that obtained by the vision system; and to obtain the height of layer to determine the feasibility of the control algorithm and whether geometric stability has been achieved.

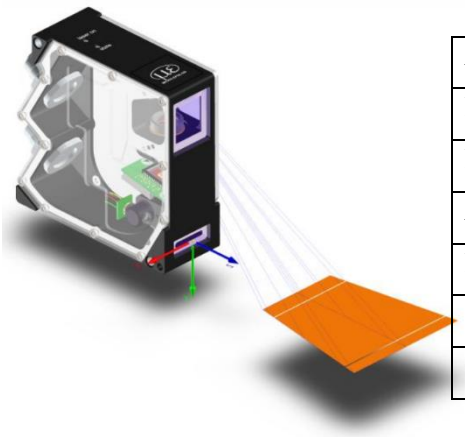

Ambient Light	10000 lx
Property range - Z axis	$\leq 240mm$
Property range - X axis	$\leq 100mm$
Absolute error - Z-axis	$\leq \pm 0.16\%$
Resolution - X-axis	1280 measuring point/ contour
Scanning frequency	$\leq 2000Hz$
Operating temperature	0℃ ~ 45℃

Figure 31 Parameter of ScanCONTROL 3D laser profile scanner

3.3 SOFTWARE CONFIGURATION

Secondly, after the physics has been configured, and the data has been collected, the data obtained from the image system should be processed. Following software are used to determine the key parameters, and these parameters will be used to assist to develop the simulation model. The image processing will

determine how quickly we respond to changes in the system and thus the overall welding quality.

3.3.1. ABB RobotStudio

ABB RobotStudio is the simulation and off-line software that allows programming and simulation of robots at computer interface. Simulation reduces the actual risk and cost of performing the process. At the same time, the CAD format files can be imported into the software, and for equipment not available in the software database, the model can be combined and simulated in ABB RobotStudio after it is built in CAD. Meanwhile, the software has its unique logic language. Thus, a welding simulation platform is built for the experiment in the software, as shown in Figure 32.

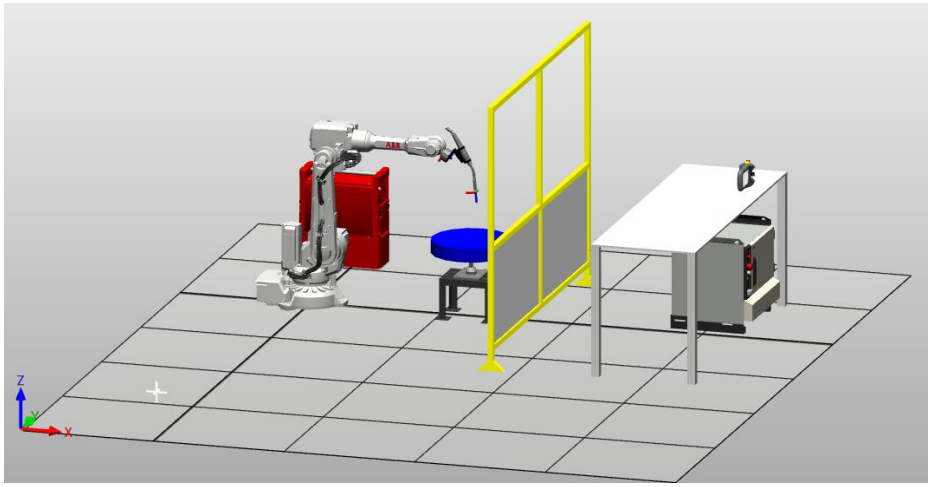

Figure 32 Simulation diagram of welding experiment

The welding path can be planned using the software. After welding the first weld layer, the second layer can be welded precisely to the start of the transverse plane and the change of the longitudinal welding height can

also be adjusted precisely. This prevents the electrode from being too far away from the mother plate to form an arc, or too far away to stick to the weld.

The ABB RobotStudio connects the welder to the image acquisition system during operation. It enables the operation of the robot arm and the welder. Also, the geometry of the melt pool can be captured via LabVIEW due to the operation of the arm.

3.3.2. LabVIEW

Figure 33 LabVIEW Program Interface

Laboratory Virtual Instrument Engineering Workbench (LabVIEW) is a graphical programming language that uses symbols in place of lines of text to build applications. LabVIEW is a general-purpose programming system that, as C and BASIC languages, has a large database of functions that can be used for virtually programming processes. The database consists of data display, data acquisition, data storage, data analysis, serial

port control and GPIB. The traditional program modifications that LabVIEW has make it debug programs easily, such as single-stepping, displaying the results of data and its subroutines in animation, and setting breakpoints.

The most significant difference between LabVIEW and other computer language is that it uses a graphical editing language to code programs that are generated in the form of block diagrams, whereas other computer languages use a textual language to create code. The resulting program is in the form of a block diagram. While traditional text-based programming languages identify the order in which programs are executed based on the order of instructions and statements, LabVIEW uses data flow programming. The data flow between nodes in the block diagram determines the order of execution of execution of the VI (LabVIEW program module - virtual instrument) and functions.

Several traditional instruments are provided as controller by the front panel of LabVIEW, which makes it simpler for programmers to create interfaces. Using wires and icons, the items on the front panel can be programmed and controlled. Figure 34 shows the graphical source code programmed for the experiment. Since the graphical source code of LabVIEW resembles a flowchart, it is also known as block diagram code.

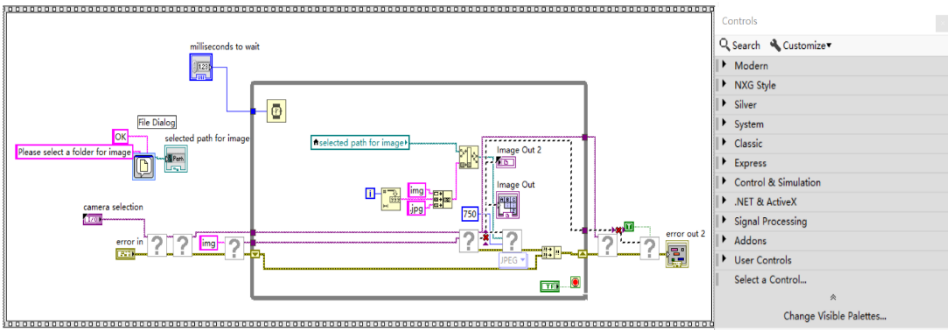

Figure 34 Block - Programming Interface

After programming, the control interface can be set up in LABVIEW, as shown in the Figure 35. With controls (the red part), the required buttons and Windows can be built. For this study, the wire feeding speed will be adjusted through the green part, and the welding pool status will be observed through the visual window in real time. At the same time, the video will be stored for later image recognition and width measurement. Each button in the control interface will be associated with the programming interface, which will unify the system.

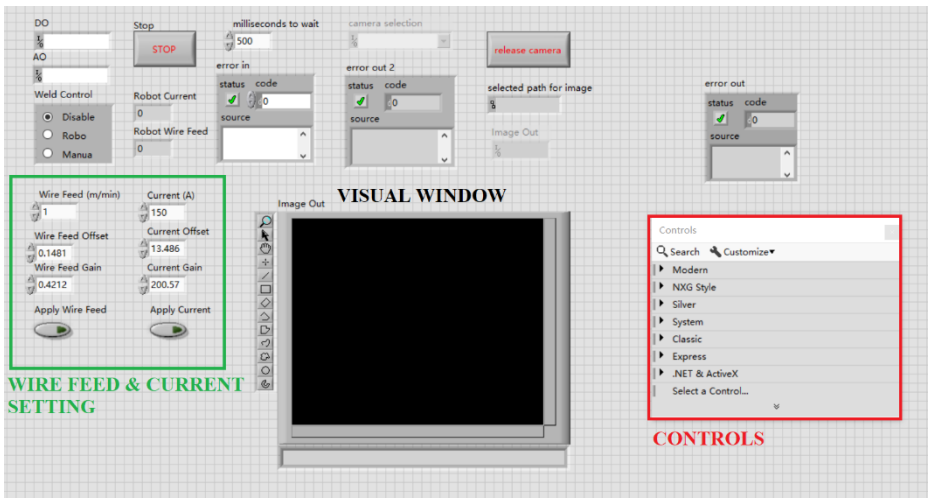

Figure 35 Control Interface

3.3.3. MATLAB

MATLAB is used in this study to do the camera calibration, the image processing get the width of the melt welding pool and the simulate the algorithms used in the experiments.

MATLAB data visualization function can be vector and matrix with graphics, and can mark and print graphics. This provides a good assistant for the image processing of this study. At the same time, MATLAB has hundreds of packages for internal functions, thus making function calls easier and faster.

The camera's aberrations can be dealt with directly using the 'Camera Calibrator' module that comes with MATLAB. By importing the image data, the module learns to correct the aberrations and obtains the corresponding mathematical conversion formula.

In terms of image data processing, since this study needs to extract the melting pool widths, some operators from the packages that identify the edges are used, as shown in Figure 36.

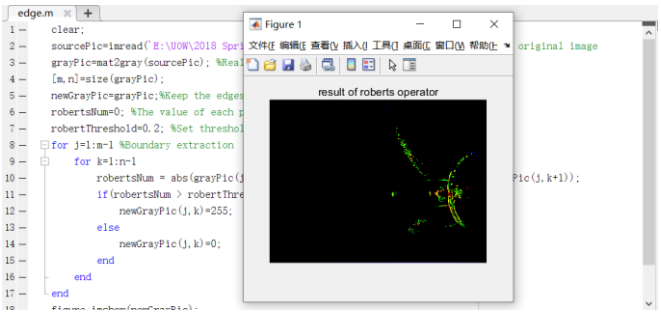

Figure 36 Image processing in MATLAB

Simulink, a visual simulation tool, also a block diagram design environment based on MATLAB. An integrated environment which includes comprehensive analysis, simulation and dynamic system modelling is provided by Simulink.

The logic is relatively complex to implement a feedback control that eliminates latency for WAAM control. The control logic can be made clearer by not requiring extensive programming in this environment.

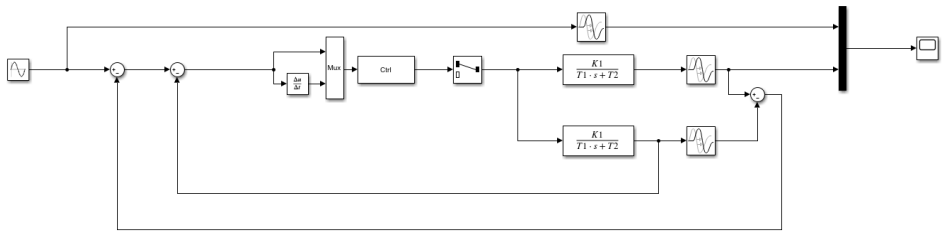

Figure 37 Model be built in Simulink

The control algorithm in this study is simulated with Simulink for use in the experiments. The SIMULATION part can greatly reduce the errors in the experimental process, reduce the waste of funds, and get the appropriate experimental parameters more efficiently.

CHAPTER 4 DATA COLLECTION

In this chapter, different methods on data collecting and data processing will be list, and will explain the benefit with these methods. Also, with the camera itself has distortion, the camera calibration will be applied.

4.1 CAMERA CALIBRATION- ZHANG ZHENGYOU METHOD

The three-dimensional geometric position of a point on the plane $X_C OY_C$ of a spatial object and its relationship to the corresponding point in the image is established by the camera calibration. (Jin, F. & Wang, X., 2015) The camera calibration could establish a relationship between the capture plane $X_c OY_c$ and the world plane $X_W OY_W$, and hence the corresponding point and a spatial point on an object could be reflected. The geometric model of the camera image is established, and its parameters are the parameters of camera. Distortion in the camera lens can result in inaccuracies in dimensions of the digitized image and the actual image size. Figure 38 shows the relationship between the position of object and image points in the camera model.

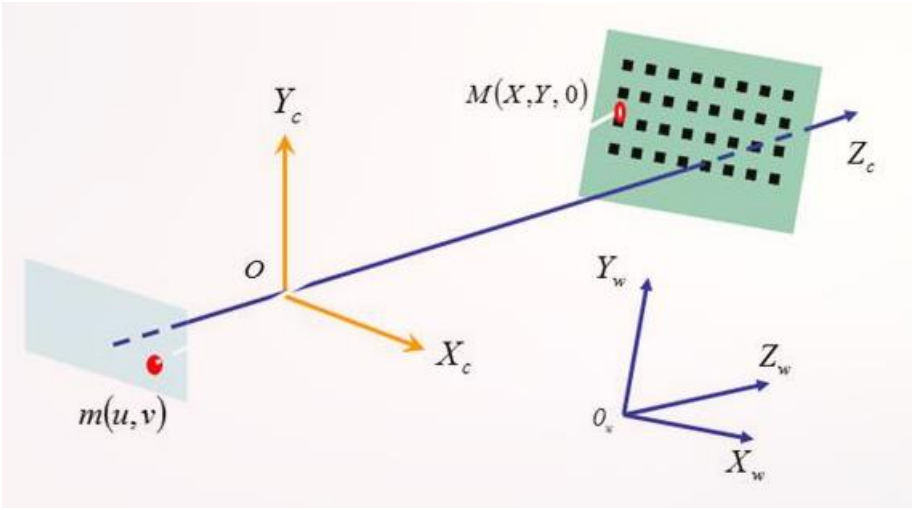

Figure 38 The schematic diagram of the relationship between the imaging coordinate system, world coordinate system and camera coordinate system

The principle of the camera calibrated algorithm is as follows.

The template plane is assumed to be on the plane of the world coordinate system with $z = 0$. O_{uv} is the pixel coordinate, O_{xy} is the image coordinate and $O_w X_w Y_w Z_w$ is the world coordinate system, $O_c X_c Y_c Z_c$ is the camera coordinate system.

The Equation 8 expresses the transformation relationship between the image coordinate system and corresponding pixel coordinate system:

$$s\begin{bmatrix} u \\ v \\ 1 \end{bmatrix} = K[r_1 \quad r_2 \quad r_3 \quad r_4]\begin{bmatrix} X \\ Y \\ 0 \\ 1 \end{bmatrix} = K[r_1 \quad r_2 \quad t]\begin{bmatrix} X \\ Y \\ 1 \end{bmatrix}$$

(Equation 8)

where *K* is the camera's intrinsic parameter matrix; s is an arbitrary scaling coefficient; $[X \quad Y \quad 1]^T$ is the homogeneous coordinate of points on the template plane; $[u \quad v \quad 1]^T$ is the homogeneous coordinates of points projected onto the image plane from the template plane; and $[r_1 \quad r_2 \quad r_3 \quad r_4]$ is the rotation matrix of the camera coordinate system with respect to the world coordinate system; and *t* is the translation vector.

$[X \quad Y \quad 1]^T$ The distortion of the camera lenses can be usually classified into radial and tangential distortion. Therefore, the ideal pinhole model is not fully applicable to it. Since the influence of the tangential distortion is typically small, it is not considered in this study. For the calibrating the nonlinear model of a camera that only considers radial distortion, two methods, the Tasi two-step

method and Zhang Zhengyou plane constraint template calibration method, are commonly used. In this study, the camera is calibrated based on Zhang Zhengyou plane method, and the distortion characteristics are calculated using MATLAB.

Obtain a 10×10 black-and-white checkerboard pattern on A4 paper with a size of 20×20mm for each chessboard grid. And the planar coordinate system of the chessboard is specified as the calibration template, as shown in Figure 39. A CCD camera was used to capture images in the calibration board from different angles to provide data for the image calibration.

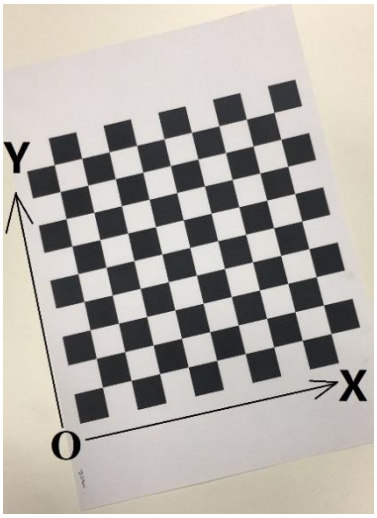

Figure 39 Calibration Plane

Processing of the collected images with 'Camera Calibrator' module in MATLAB allows the rotation matrix to be calculated.

Where $[r_1 \quad r_2 \quad r_3] = \begin{bmatrix} f_1 & 0 & 0 \\ 0 & f_2 & 0 \\ 0 & 0 & 1 \end{bmatrix}$, and $f_1 = 0.0120,\ f_2 = 0.3214.$

Intrinsic matrix could be solved as $K = 1.0e^3 \times \begin{bmatrix} 1.7894 & 0 & 0 \\ 0.0007 & 1.7888 & 0 \\ 0.5457 & 0.9540 & 0.0010 \end{bmatrix}$.

The verification leads to a slight error in the camera distortion values, which is due to the fact that only radial distortion is being considered. While the influence of tangential distortion is not significant, it cannot be neglected.

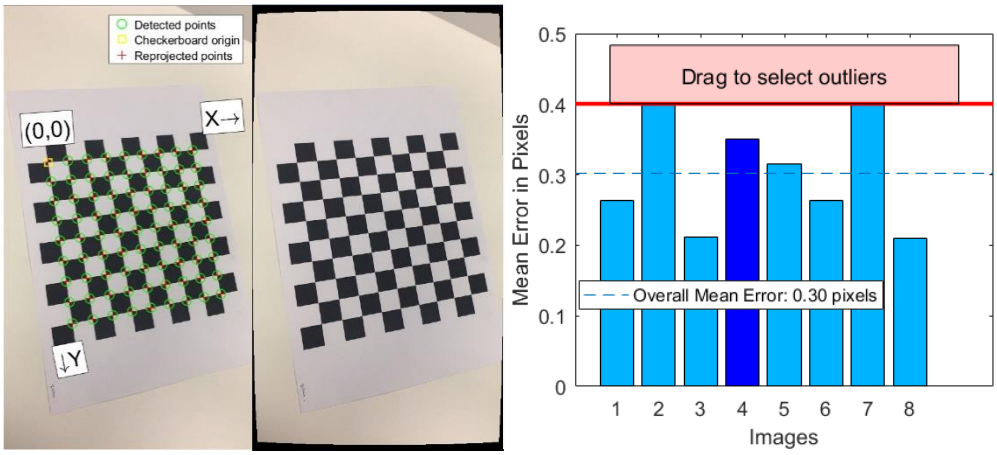

Figure 40 Undistorted Image VS. Corrected Image, Reprojection Errors

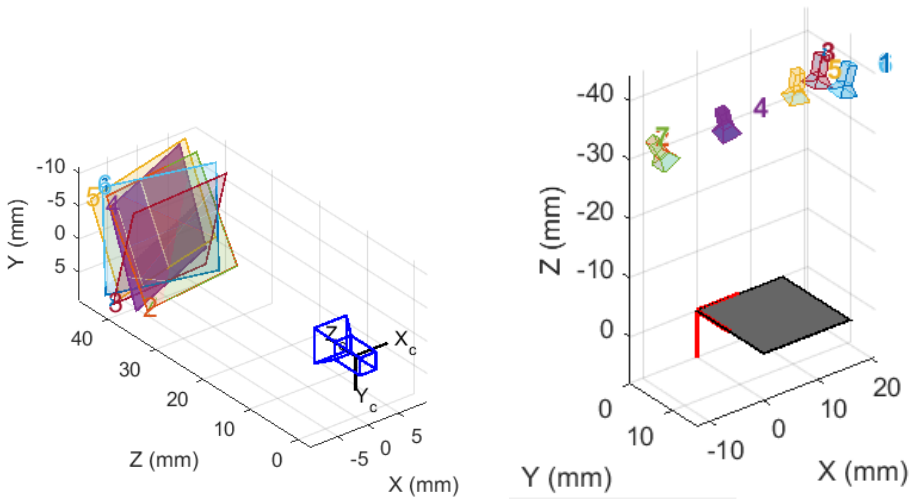

Figure 41 Centric View of Pattern (left) & camera (right)

4.2 OBTAIN EXPERIMENTAL DATA

In the process of collecting data, perform the following series of operations on the controller:

1. Connect welding machine, the CCD camera and computer equipment;
2. Set the coordinates for the ABB robot arm and move the arm to the initial welding position;
3. Set the parameters of TIG/MIG welding in the LabView control panel;
4. Run the LabView program. The computer stores the welding image and the welding machine records the welding parameters;
5. Start the welder. LabView will activate the TIG/MIG welding machine;
6. Start the ABB robot arm. The torch and camera shift along with the welding path;
7. Start the wire feed. LabView will activate the wire feed process;
8. Stop feeding the wire. LabView will halt the wire feed process;
9. Stop welding. LabView will halt the welding current;
10. Stop the robotic arm and back to the initial position.

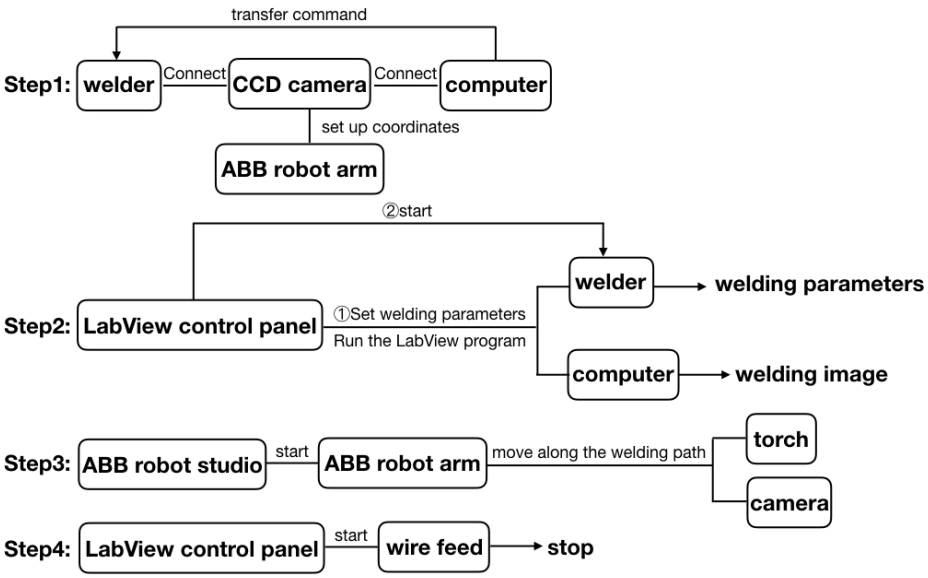

Figure 42 System interconnection

4.2.1. TIG Welding

Through the above welding process, using DC pulse current for experiments, good welding results were obtained, as shown in Figure 43. Set the base value of 30A, the peak value of 150A, which is more than 5 times the base value, wire feed speed is set to 0.4 m/min and feed speed set to 2mm / s. From the figure shows that the welding began without wire feed, so the molding of the welding material does not add process. Black appears around the weld, indicating that during the welding process the shielding gas is unstable.

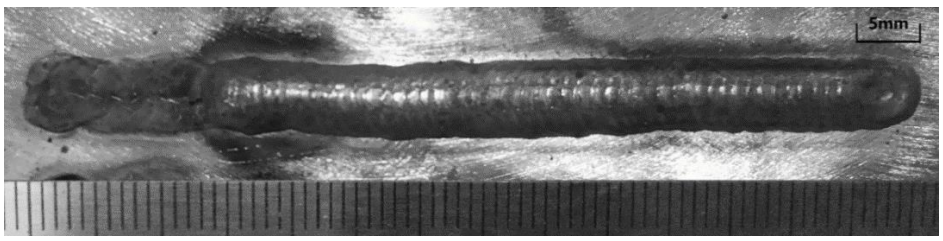

Figure 43 Formation of Weld

The captured images can also view this phenomenon. As shown in Figure 44, at the beginning of the wire feed, the welding arc is exceptionally large because the protective gas does not work, making it impossible for the filter to filter out the excess arc, resulting in the camera to capture contours of the pool unclearly. Therefore, the intermediate and post data are captured and extracted from the image.

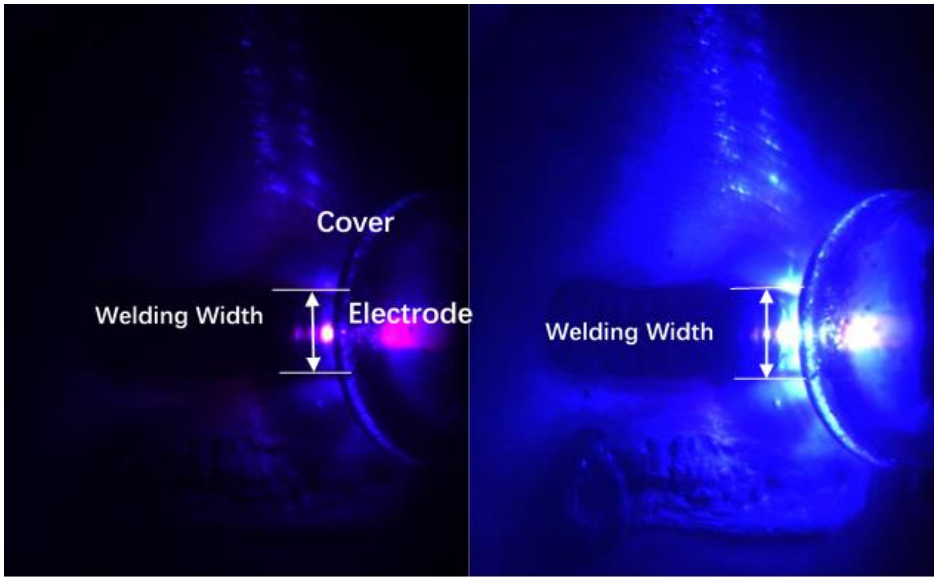

Figure 44 Welding Image of the Front Section of the Weld (Left-Base Value Right-Peak Value)

By intercepting the middle and back melt pool images, we get different base and peak images. The images are acquired in current time'. The ‘avi’ format was intercepted by LabVIEW program and then by MATLAB program (vide Appendix A) to get the base and peak of the pulse of the image was processed. The program extracts it to the melt pool location and the weld melt pool profile is obtained using MATLAB software, vide Appendix for the code.

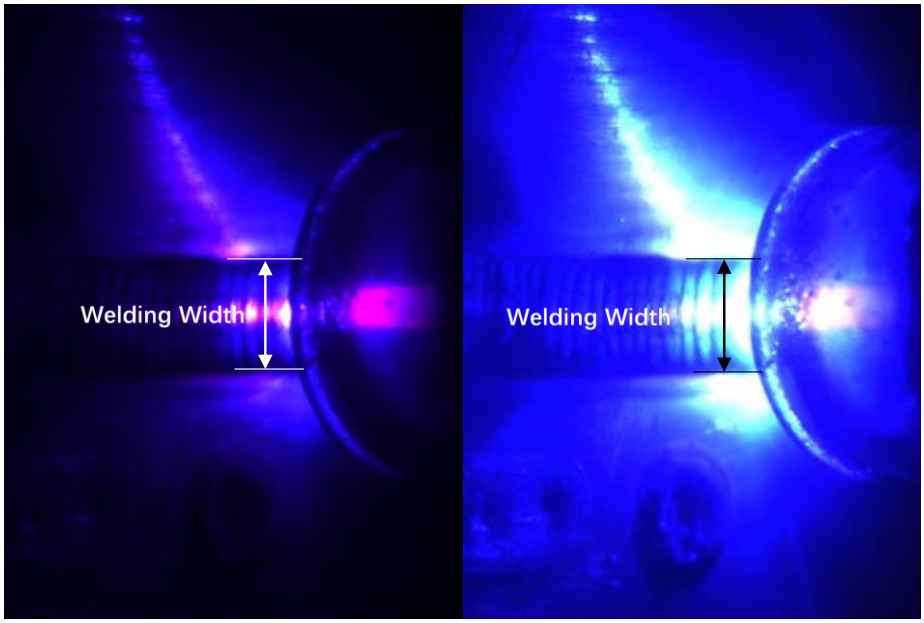

Figure 45 Left-Pool at Base Value-24.96s Right- Pool at Peak Value-25.28s

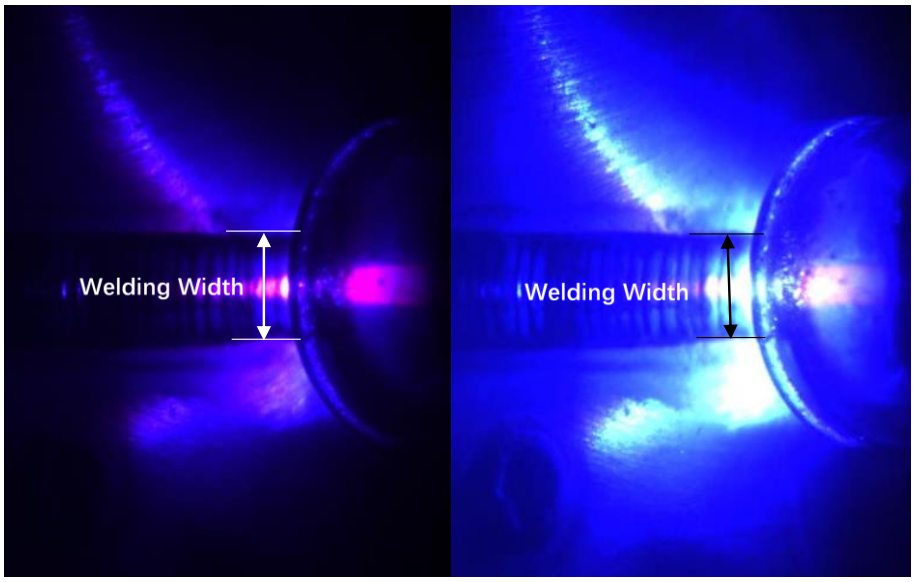

Figure 46 Left-Pool at Base Value-324.96s Right- Pool at Peak Value-35.28s

4.2.2.MIG welding

During the welding process, the MIG system is more stable than the TIG system. The two welding methods control the weld layer in

different ways: TIG welding changes the weld width by controlling the current, and MIG changes the weld width by controlling the wire feeding speed. The experimental results show that the wire feeding speed is controlled between 1 m/min ~ 10 m/min in MIG welding, and the weld layer did not appear to be collapsed or over-welded.

Because of the stable welding process, the same type of camera and filter used for TIG welding are used for MIG welding. The images obtained by MIG welding are clearer and the filtering effect is better.

Figure 47 Welding Image of the MIG (Left to Right: 2s, 34s & 57s)

4.3 DATA PROCESSING

4.3.1. Edge detection operator

The vision system collects video information and performs image extraction by MATLAB for one extraction every 0.05s. In this paper, three methods are used for edge extraction. The first one is differential edge detection, the second one is Robert operator detection, and the third one is a combination of Robert operator and swelling corrosion detection.

Differential edge is the most primitive and basic method. Its first-order difference on the x-axis is divided into $X_D = f(i+1,j) - f(i,j)$ and the first-order differences on the y-axis are divided into $Y_D = f(i,j+1) - f(i,j)$. This operator is directional and thus preserves indiscriminately any edge in the image, but in this study, it is necessary to extract the horizontal edge of the weld layer.

The Roberts operator detects edges using an approximate gradient magnitude of the difference between two adjacent pixels in the diagonal direction, which is more accurate than the differential edge algorithm and more sensitive to both horizontal and vertical edges. Its first-order difference on the x-axis is divided into $X_R = f(i,j) - f(i-1,j-1)$ and the first-order differences on the y-axis are divided into $Y_R = f(i-1,j) - f(i,j-1)$, and difference of Roberts operator is $|X_R - Y_R| = \sqrt{{X_R}^2 - {Y_R}^2}$. In a weld layer identification scenario, where the weld layer is horizontal and the arc and electrode discharge edges are often inclined, the Roberts operator is more suitable than the differential edge algorithm. However, the Roberts operator is sensitive to noise, so it requires additional erosion and expansion processes to reduce the noise of the image to extract a sharper weld edge, which provides a guarantee for the extraction width.

4.3.2. Processing result comparison

The weld pool area of the obtained image data is first cropped. The image A in the following figures were processed using the Roberts edge detection operator for the cropped image. And the image B was processed with a combination of the expansion and corrosion operator on top of the result obtain in image A.

Grayscale processing, black and white (binary) processing and edge contour detection to obtain the three processing results, shown in Figure 48-51 C, D and E. All the data were collected during the welding process and analyzed for, 24.96s (Figure 48), 25.28s (Figure 49), 34.96s (Figure 50) and 35.28s (Figure 51), four different moments.

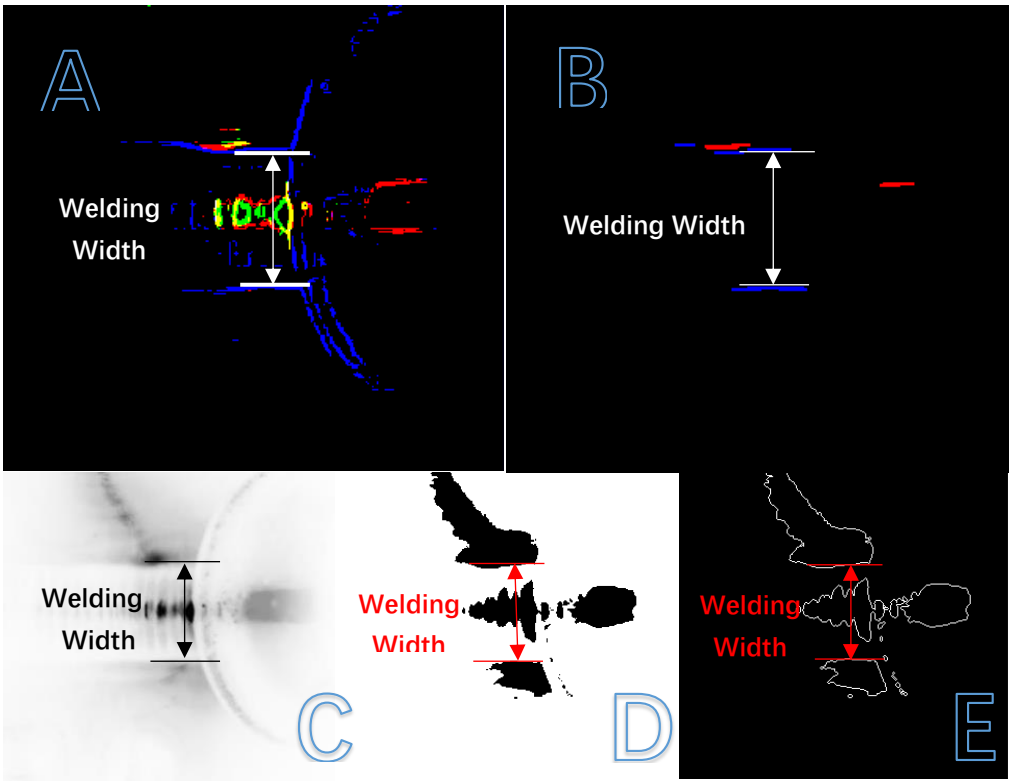

Figure 48 MATLAB processed images of the base Value -24.96s

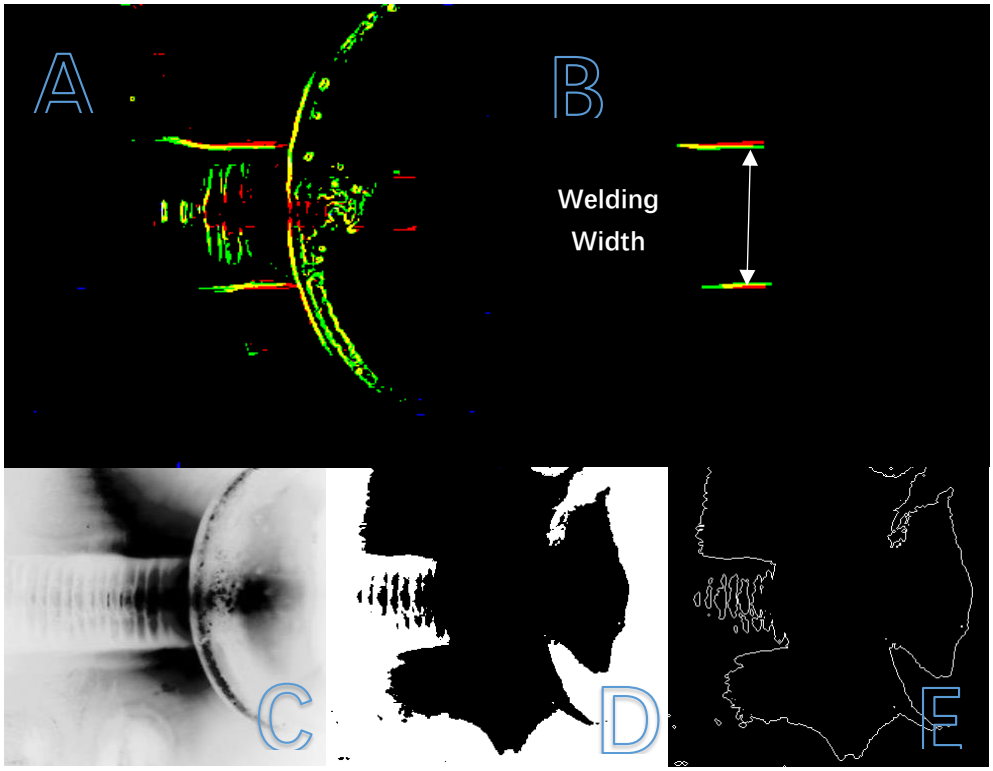

Figure 49 MATLAB processed images of the peak value-25.28s

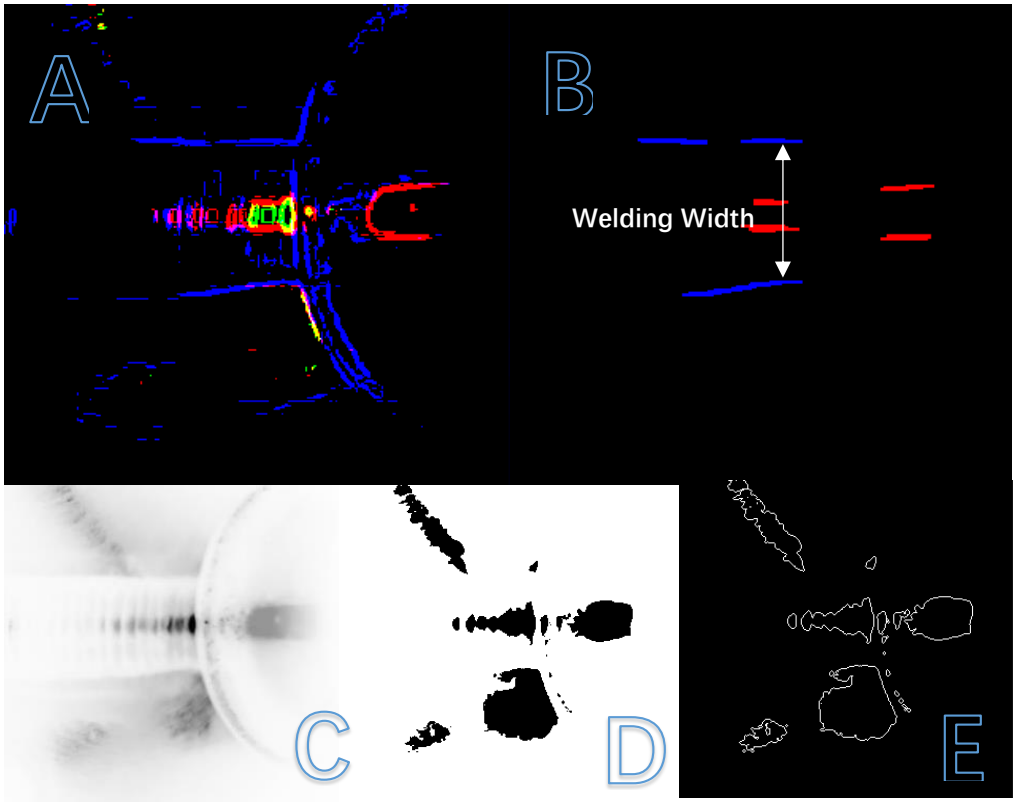

Figure 50 MATLAB processed images of the base value-34.96s

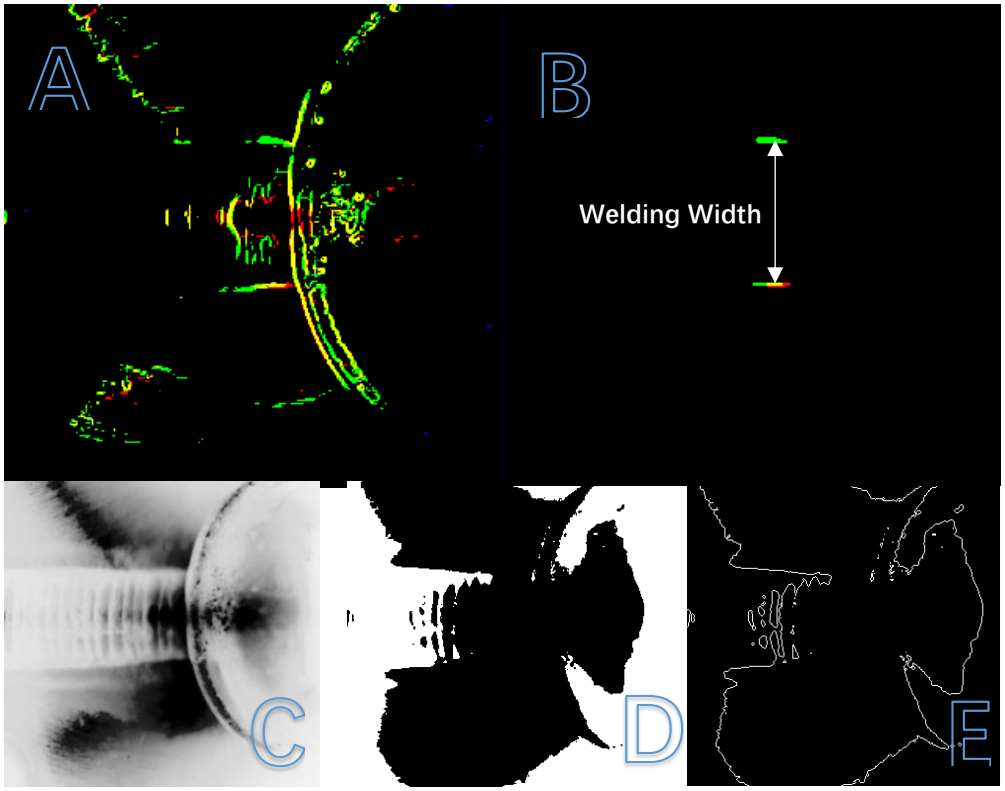

Figure 51 MATLAB processed images of the peak value-35.28s

The images are processed and analyzed for different times, different peaks and base values, in the case of the same welding parameters. All the results of the processing basically measure the width of the molten pool. In specially, the weld pool width can be extracted more accurately after processing by the Roberts edge detection operator and then by the combined operation of expansion and corrosion, as shown in Figure 48-51 B.

Due to the different arc sizes during welding, the images sensitivity of the video captured through the filter varies, so that the image after the combined process displays different colours. In the subsequent image processing, the image will be grey-scaled in order to make the measurement of the molten pool width easier.

By tuning the parameters, the Roberts edge detection operator was found to get the appropriate width of the welding pool. The pixel value was calculated for the pixel locations. However, as seen in figure 50-B, with the same parameters, the Roberts edge detection operator does not filter out all ambiguous pixels. When this happens, since the longitudinal maximum and minimum position difference is the principle of the width extraction algorithm, the arcing of the intermediate electrode (red lines) does not affect the melt pool width extraction and the exact width of the melt pool can still be determined, as shown in Figure 52.

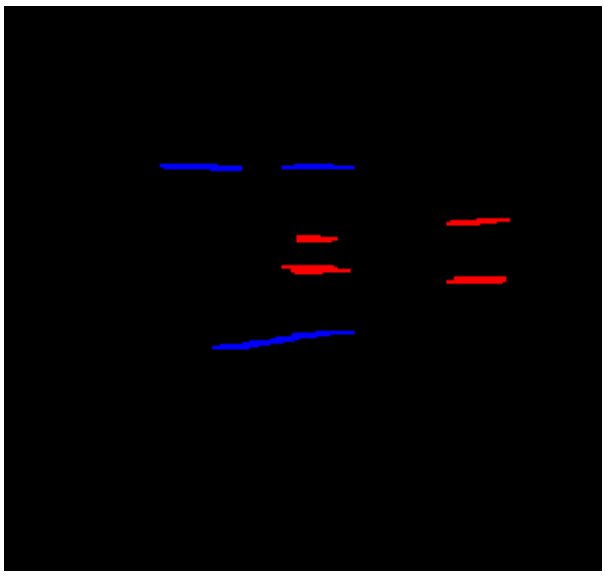

Figure 52 Error Width with the Same Parameter

There is a better filtering of the welding pool image resulting from MIG welding than from TIG welding, therefore there is no need to extract the boundaries with the Roberts edge detection operator.

Due to the camera placement, in order to obtain the width of the molten pool, the image after extraction to the melt pool region needs to be reversed 60 degrees in counter-clockwise. As shown in Figure 53.

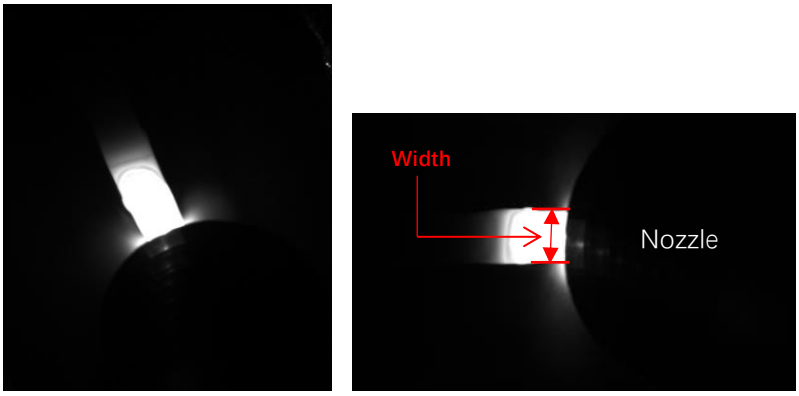

Figure 53 Welding Image of the MIG with 60°

Since the MIG welding hardware is relatively stable, the different wire feeding speeds correspond to relatively constant weld widths. Therefore, the wire feeding speed can be set to the desired weld width.

While the wire feeding speed of the CMT could be programmed to be 1-10 m/min, only 5-8 m/min was used in the present study to determine the width of the weld pool. Meanwhile, the weld feeding speed was programmed at 500mm/min and the current value is 30A. By analysing a number of data, the average pool width was obtained and an approximation of the linear relationship between the wire feeding speed and the width of the welding pool was obtained. The weld layer for which parameters were provided for the data acquisition are shown in the Appendix.

NO.	Wire feeding speed (m/min)	Width of melt pool (mm)	Width of pixel
1	5.0	5.38	73
2	5.5	5.72	77
3	6.0	6.19	85
4	6.5	6.67	89
5	7.0	7.18	98
6	7.5	7.60	102
7	8.0	7.81	105

Table 3 Feed welding speed, width of the pool & width of pixel

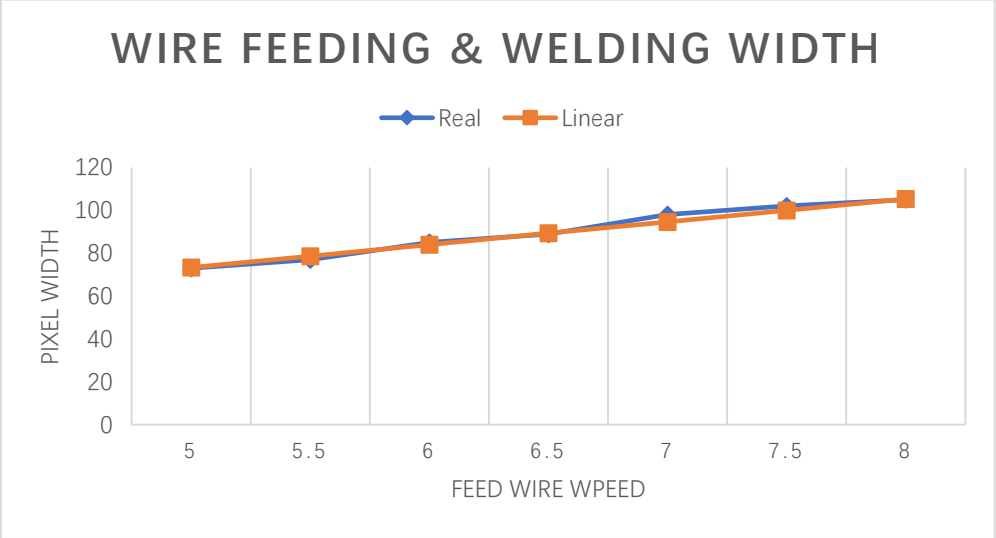

Figure 54 Linear relationship between the wire feeding speed and the welding width

The weld formation can be seen as a narrower width before the end of the additive process. Because of the thermal accumulation, the longer the weld is allowed to proceed, the higher its temperature will be, which may lead to excessive melting of the solder and material causing build-up. Consequently, the welding operation should continue to feed the torch for 2 second after the wire is stopped to ensure that the weld width remains stable.

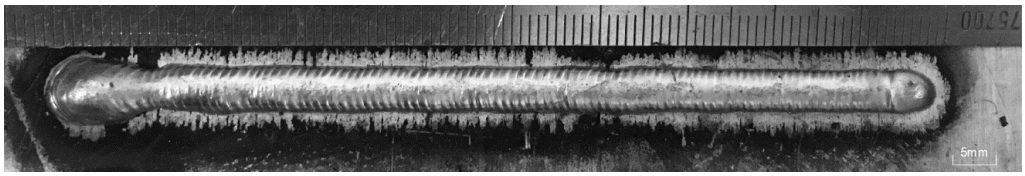

Figure 55 Feed wire speed-5.0 m/min

CHAPTER 5 PARAMETER IDENTIFICATION FOR SIMULATION MODEL

Before setting up the simulation model, the reasonable parameter should be determined whatever algorithms are used. Here, the wire feeding speed is chosen to be analyzed due to its significant effect for welding process. However, excessive spending, such as budget and materials will be cost if the feasible parameter is achieved by repeated experiments. Here, a new identification algorithm is applied to solve out the practicable parameter for the simulation model.

5.1. RANDOM SIGNAL ACQUISTION

As stated in the first two chapters, the existed control algorithm does not present a stable molten pool with related parameter. This could be affected by several aspects. For example, the external environment and internal control system error. Here, the external environment is controlled to be the same for the experiment. Hence, the internal control system error could be justifiably suspected.

To prove that a system error does exist, a random signal algorithm experiment is determined for the equipment same as in the previous chapter. Here, the wire feeding speed is set as a random variable, and the range is defined between 3m/min and 12m/min. This is changed each second and the values, wire feeding speed and pool width, are recorded in each half second.

Figure 56 shows the result of the association among three parameters. The blue line illustrates the relationship between the time and the wire feeding speed, and the red line represents the relationship between the time and the pool width. Hence through the figure, the connection between wire feeding speed and the

pool width could be determined. As normal, the pool width should simultaneously change with the wire feeding speed. If not, a system error could be determined.

From figure 56, we can observe that the width of the molten pool is not synchronized with the change of wire feeding speed as we expected, and a time difference here is about 1s (as 2 samples will be taken per second), which known as systematic time delay.

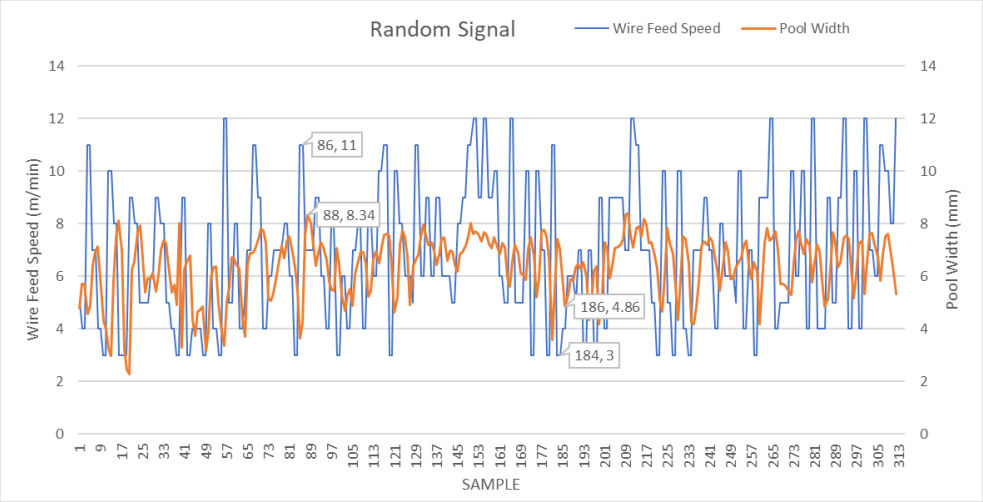

Figure 56 Random Wire Feeding Speed & Width of Molten Pool from Experiment

In order to more intuitively understand the impact of delay on the experimental results, the width of the molten pool corresponding to different wire feeding speeds with the elimination of the delay (1s) was analyzed in a discretely way, and figure 57&58 was obtained.

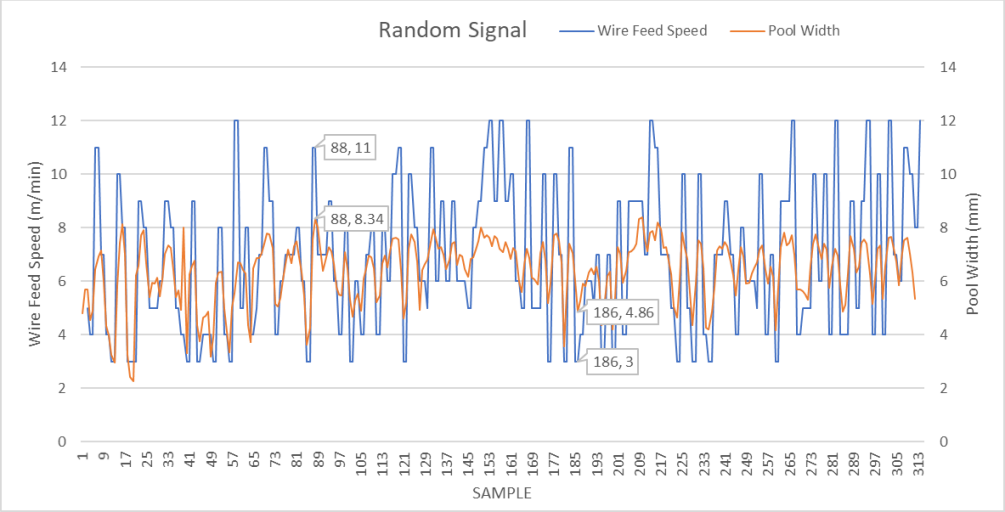

Figure 57 Random Wire Feeding Speed & Width of Molten Pool without time delay

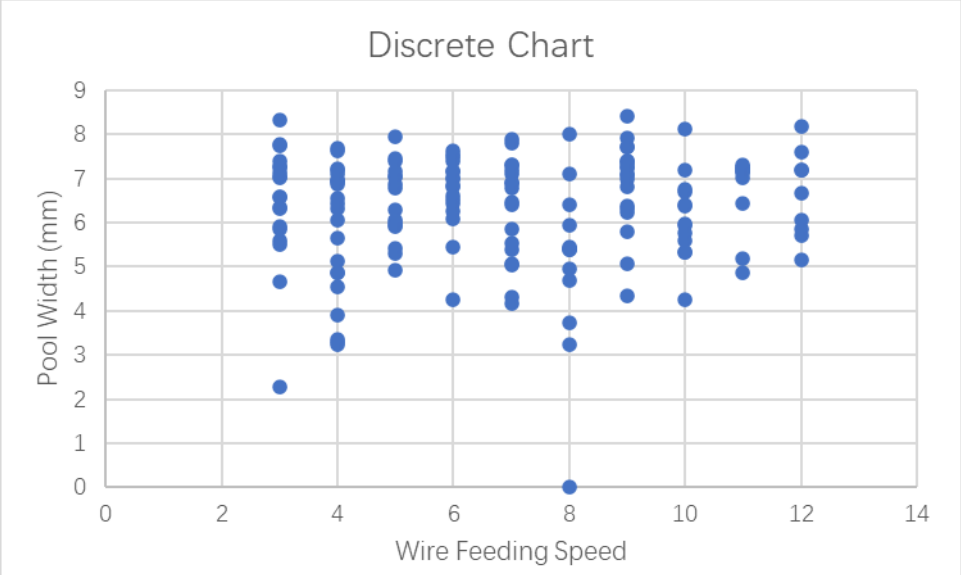

Figure 58 Discrete Chart for Pool Width in different Wire Feeding Speed without time delay

As can be seen from figure 58, a relatively stable molten pool width is not obtained when the wire feeding speed is the same, but demonstrates a relatively discrete state. This shows that, due to the delay, the wire feeding speed at the last moment has a great influence on the width of the current moment. Therefore, in the following work, an algorithm should be used to predict the width of the molten pool, to realize real-time control. It is also necessary to identify and

process the data to eliminate any data that is larger than the true situation in order to prepare for obtaining accurate control parameters.

5.2. GENETIC ALGORITHM (GA)

One of the optional algorithms is genetic algorithm (GA). This algorithm is created by Professor John. H. Holland (1975) based on Naturalistic evolutionism by C. R. Darwin and Mendel's theory of genetic variability by Mendel.

5.2.1. Basic principle

Genetic algorithm is a bionic algorithm based on the principle of biological evolution, simulating the evolution of life and searching for the optimal solution. Starting with the initial population, the selection, crossover, and mutation operations are repeated to make the population evolve and get closer to the optimal result.

The selection operation makes it easier to select individuals with larger fitness values in the next step, and the outcome of the selection depends on the initial population. The crossover operation pairs individuals in the group in pairs, and exchanges some genes of the paired individuals with a certain probability, that is, the crossover probability (P_c), thereby generating new individuals, which fully demonstrates the idea of information exchange between individuals. The mutation operation provides the possibility of generating new individuals, in which certain gene values of individuals change with a certain probability, that is, mutation probability (P_m), thereby generating new individuals.

5.2.2. Realization process

The operation steps of the standard genetic algorithm are as follows:

1.Coding: the conversion from parameters or solutions in the search space to chromosomes in the genetic space, that is, mapping from phenotype to genotype;

2.Population initialization: randomly generate N individuals, all N individuals form the initial population, and set the maximum evolutionary generation number T;

3.Fitness function: According to different problems, the definition of fitness function is also different, but the fitness function value indicates the advantages or disadvantages of individuals or solutions;

4.Selection: Select the group;

5.Crossover: Cross-operating group;

6.Mutation: Perform mutation operation on the group;

7.Termination condition judgment, if the termination condition is satisfied, then terminate, if not satisfied, transpose *Step 3*.

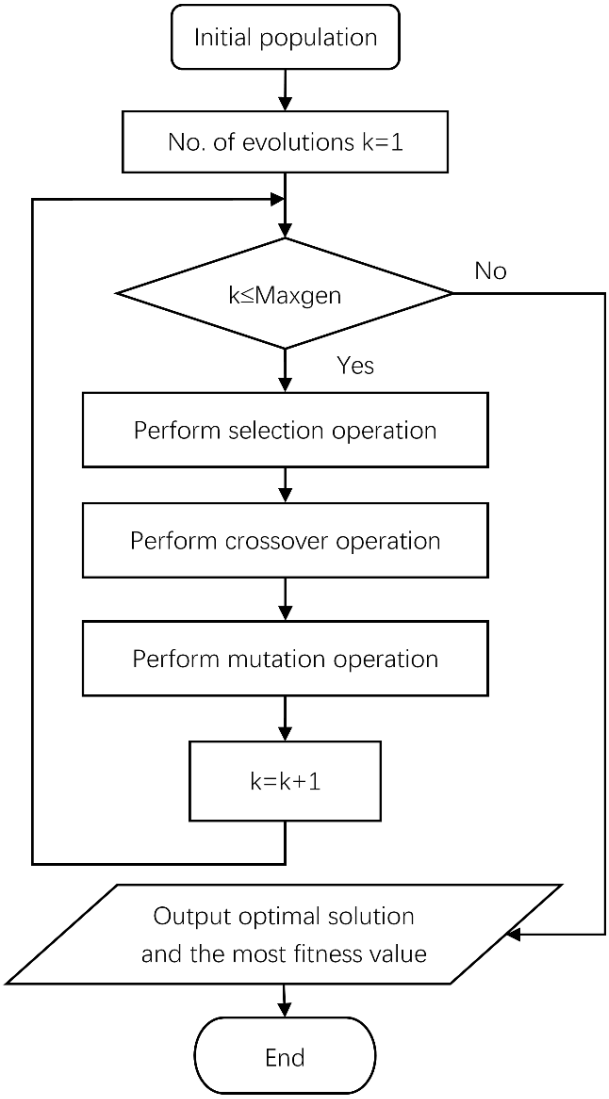

Figure 59 Flow chart of standard genetic algorithm

5.2.3. Application

The genetic algorithm has cross-variation operation. During the period of searching data, the motion of the entire population is relatively uniform and does not easily fall into the local optimum, but to the global one. Therefore, in this paper it is possible to filter out the appropriate melting pool widths well.

5.3. PARTICLE SWARM OPTIMIZATION (PSO)

5.3.1. Standard particle swarm optimization

PSO is initially set up as a set of random particles, which is a random solution, and then gets the optimal solution repeatedly. The particle renews itself in each iteration by following two extreme values, the first extreme value is the best solution discovered by the particle itself, which is known as the individual extreme value, and the other extreme value is the optimal value discovered by the whole population solution currently, which is the overall extreme value. Additionally, instead of using the entire population, only a part of the neighbors of the particles can be used. Then the extreme values in all neighbors are local extreme values.

Suppose that in a D-dimensional target search space, M is the group size. It is not suitable for the group size to be too large or too small, too large will affect the convergence speed and increase the running time, too small is not suitable.

Position (Criteria for evaluating the position of particles):

$$X_i = (x_{i1}, x_{i2} \cdots x_{iD}), i = 1,2, \cdots m$$

Flying speed (Determine the size and direction of particle movement):

$$v_i = (v_{i1}, v_{i2} \cdots v_{iD}), i = 1,2, \cdots m$$

The best searched local optimal position of the individual:

$$p_i = (p_{i1}, p_{i2} \cdots p_{iD}), i = 1,2, \cdots m$$

The best global optimal position searched by the whole particle group:

$$p_g = (p_{g1}, p_{g2} \cdots p_{gD})$$

In the iterative process, the formula for particles to update the speed and position of particles is as Equation 9:

$$\begin{cases} v_{id}^{k+1} = w \times v_{id}^{k} + c_1 \times r_1 \times \left(p_{id} - z_{id}^{k}\right) + c_2 \times r_2 \times \left(p_{gd} - z_{id}^{k}\right) \\ z_{id}^{k+1} = z_{id}^{k} + v_{id}^{k+1} \end{cases}$$

(Equation 9)

Which $i = 1,2,\cdots m$, $d = 1,2,\cdots D$, k is the current number of iterations, v_{id}^{k} represents the velocity of the d-th dimension of the i-th particle during the k-th evolution, z_{id}^{k} represents the scalar position d dimension of the ith particle during the kth evolution, p_{id} represents the d-th position scalar of the i-th particle at the current optimal position, p_{gd} represents the d-dimensional position scalar of the group at the current optimal position, w is the inertial weight of velocity, describing the effect of particle inertia on velocity, r_1, r_2 is two random positive real numbers, which are independent of each other and satisfy the uniform distribution of the interval [0,1], which plays a role in maintaining the diversity of the group; c_1, c_2 is the acceleration factor, also known as the learning factor.

In the algorithm, it plays a role in enabling each individual to self-summarize and learn from the outstanding individuals in the group. At the same time, the individual is encouraged to approach its own historical optimal position and the historical optimal position within the group. The generally recommended value range is [0,4].

According to formulas, a single particle i moves from position z_i^k to position z_i^{k+1} as follow:

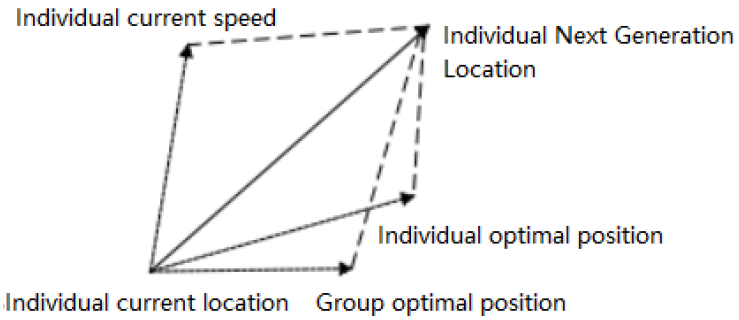

Figure 60 Schematic diagram of single particle position movement

The particle swarm mainly follows the following five principles, defined as follows:(Ji, Z. et al., 2010)

1) Quality principle: Particle groups should be able to respond to the quality factors of the surrounding environment;
2) Proximity principle: Particle groups should be able to perform simple spatial and temporal calculations;
3) The principle of adaptability: Particle swarms should be able to appropriately adjust their behavior at an appropriate time under the condition of acceptable computational cost;
4) Qualitative principle: the particle group should not change its behavior every time the environment changes slightly;
5) Diversity response principle: Particle swarms should not move in a too narrow range;

5.3.2. Realization process

According to the basic principles of the standard particle swarm algorithm, the following is the algorithm implementation process:

1. Determine the parameters in the particle swarm optimization algorithm, group size M, inertia factor w, learning factors c_1 and c_2, and maximum speed V_{max}. The initial population records the position of the initial particle group as the historical optimal position, and the fitness value of the initial particle is recorded as the historical optimal fitness value.
2. Calculate the fitness value of each particle in the population according to the position of the particles.
3. Update the individual historical optimal position and group historical optimal position of the particle. First, compare the individual's current fitness function value with the individual's historical maximum value. If the fitness function value is better than the individual's historical optimal position, then replace the historical optimal position with the current position. Then compare the current global optimal value with the historical global optimal value g_{best}, if it is better than the historical global optimal value, then replace the historical global optimal position with the current global optimal position.
4. Update the speed and displacement according to equation 9.
5. Determine whether the termination condition is satisfied. If it is satisfied, stop it. If it is not satisfied, go to *Step2* and continue the loop until the termination condition is satisfied.

The particle swarm algorithm flow chart is as follows:

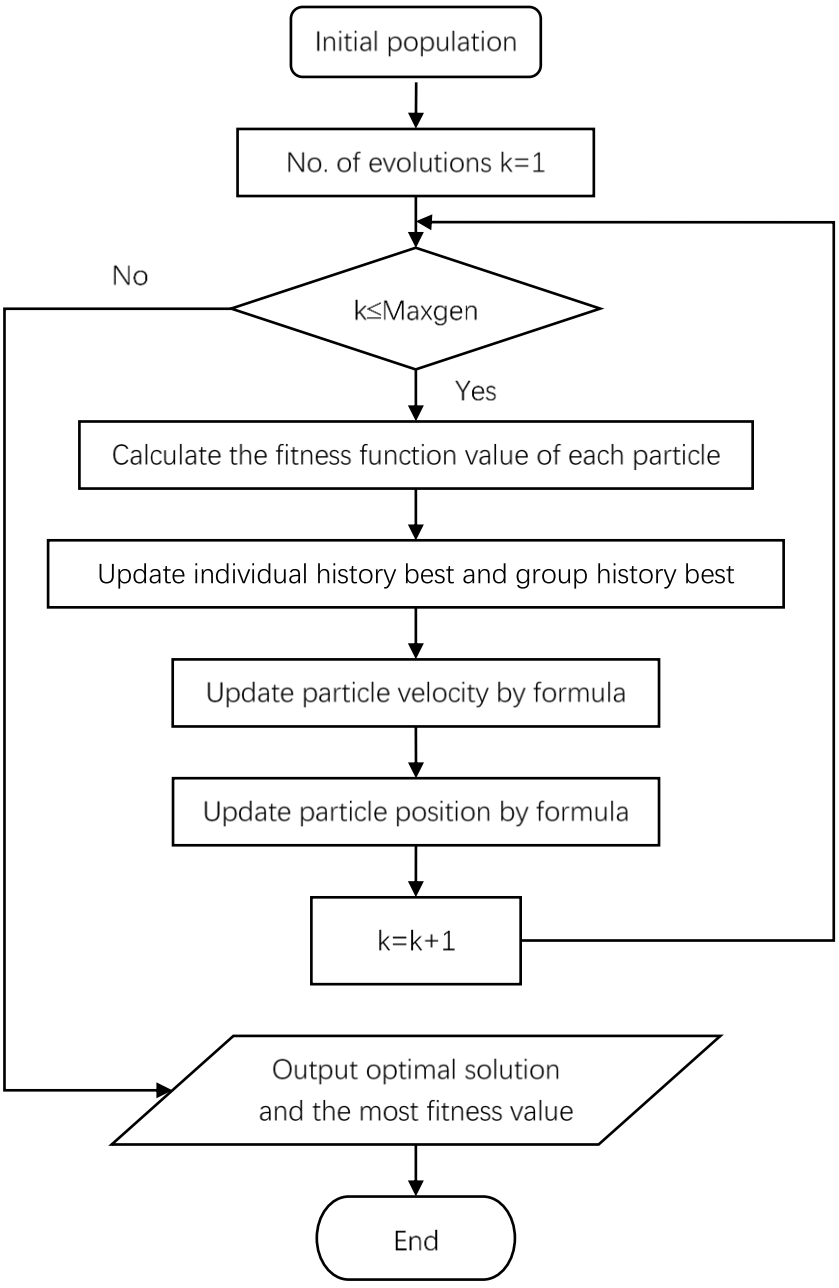

Figure 61 Flow chart of standard particle swarm optimization

5.3.3. Application

The PSO algorithm is overlaid for use before the genetic algorithm because it is a stochastic search algorithm and is therefore scalable, self-organizing, and adaptive, three properties that allow melting pool width data to

cooperate with each other without a given classification criterion, indirectly sharing information and preserving its own memory work.

The robustness of the algorithm makes the data processing process independent of the continuous and deducible mathematical properties of the optimization problem itself, as well as the structural features of the objective function and constraints, so that when using the particle swarm algorithm, there is no need to modify the rest of the algorithm, only the corresponding functions.

At the same time the inherent parallelism of the algorithm allows it to achieve larger gains with less computational effort.

5.4. COMPARISON BETWEEN GA AND PSO

Section 5.2 and Section 5.3 introduced two available algorithms that could be used to distinguish the valid data from the raw data. Each algorithm has some significant advantages and disadvantages.

The advantage for GA is generalized and strong global search ability. The GA code the feasible solution of a practical problem to a series structure of data in gene type, and the process of coding makes it possible to directly operate the structure but not only the parameters during calculation. This could decrease the effect of the parameter to the final solution, and increase the generality. Moreover, the GA implements the search and operation actions in group but not in individual, which means that the item to be operated is not the single valid

solution but the group of the valid solutions. Thus, the strong global search ability could be achieved with using this kind of algorithm.

Meanwhile, there are also some disadvantages shown by GA. Firstly, Due to the generality, no standard could be applied to summarize the coding method of this algorithm. Hence the results relatively could not be clear under the uncertainty. Secondly, GA only judges the superior and inferior of the individuals by their fitness with the function. For example, if there is an individual that is better than others, the possibility to choose its feature to next generation will increase obviously, and the gene will be spread in the population. The method means the next generation will be trend to this sample. This will cause the result to lose the diversity to be premature convergence.

For PSO algorithm, the self-organization and adaptability optimize fitness by memorize the superior of the sample in the uncertain population. The two features could keep the diversity of the population compared to the GA algorithm. Furthermore, the stability of the PSO algorithm is also better than GA, because this algorithm does not depend on some mathematical quality such as the continuity and differentiability. However, it should be mentioned that the PSO algorithm is not easy to be convergence, especially when this algorithm is applied to solve the high dimensionality optimization problem.

5.5. PARTICLE SWARM GENETIC HYBRID ALGORITHM (PSO-GA)

Due to the strength and weakness stated before, a new algorithm maybe created to integrate the strengths of both the algorithms shown before to keep the

diversity and is easy to be convergence. The particle swarm genetic hybrid algorithm (PSO-GA) is a horizontal combination of the both genetic algorithm and particle swarm optimization these two algorithms. Through this algorithm, the PSO offers the diversity of the population and GA increase the convergence of the result. Yao et al. (2007) combined the advantages of the two algorithms, and used a mixed probability to divide the particle swarm into two subgroups, one part was PSO evolution, and the other was GA evolution. A novel PSO-GA hybrid algorithm (PGHA) was proposed. The selection of the combination algorithm is expected to yield accurate data.

5.5.1. Principle

In this study, the particle swarm genetic algorithm (PSO-GA) after initializing the population.

The size N of the population is used, the particle swarm optimization algorithm first evolves the population by a certain algebra T, and then depending on the fitness value of the function.

The fitness function in the population (M_k) individuals whose value is better than the average value of the group suitable function is directly extracted and enter the next generation, leaving ($N - M_k$) individuals. Based on the remaining ($N - M_k$) individuals, GA evolution is performed to generate ($N - M_k$) individuals, and combine the remaining ($N - M_k$) individuals with the GA evolved ($N - M_k$) individuals to select the first half ($N - M_k$) individuals.

Finally, M_k individuals that were directly suggested by PSO evolution and $(N - M_k)$ individuals obtained by GA evolution are combined to create a new particle swarm group N, and the next evolutionary operation is continued. The schematic diagram of particle swarm genetic hybrid algorithm is as follows:

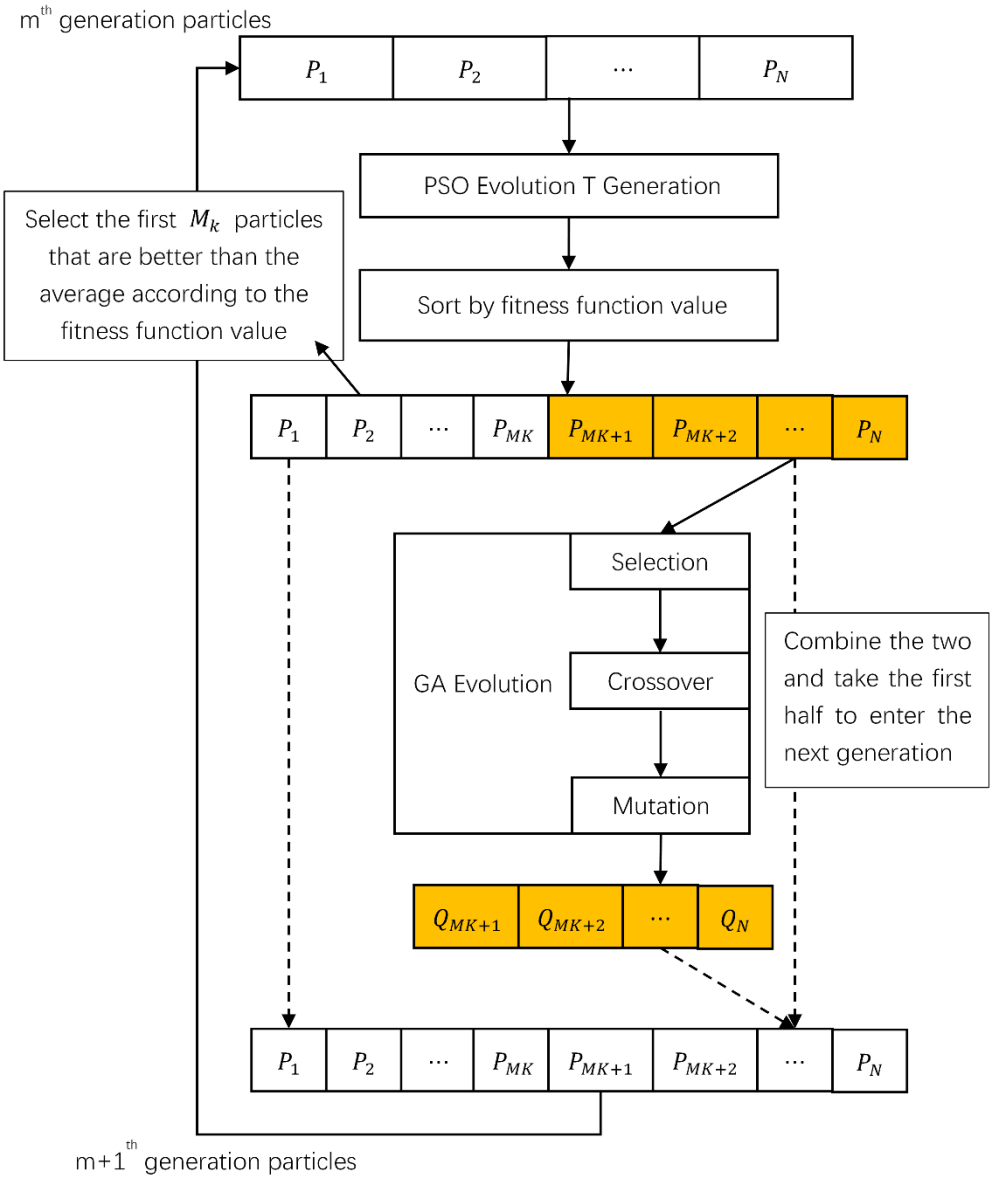

Figure 62 Schematic diagram of PSO-GA

5.5.2. Realization process

Specific steps of particle swarm genetic hybrid algorithm:

1. Initialize the population parameters, population size N, total evolution of hybrid algorithm $Maxgen$, two learning factors in particle swarm algorithm c_1, c_2 , maximum speed V_{max}, and algebra of particle swarm evolution T; probability of parameter cross in genetic algorithm P_c and mutation probability P_m;
2. Initialize the population in the space and give N particles randomly;
3. Calculate the suitable function value based on the suitable function set in advance;
4. Setting the count of algebraic sum $k = 1$;
5. Judge whether $k \leq Maxgen$ or not. If $k \leq Maxgen$, continue to the next step, otherwise turn to Step15;
6. Setting the PSO evolutionary algebra count $t = 1$;
7. Judge whether $t \leq T$ or not. If $t \leq T$, continue to the next step, otherwise jump to Step10;
8. Speed and position of the particle swarm are updated based on equation 9;
9. $t = t + 1$;
10. Sort the N individuals based on the suitable function value, and calculate the average $faverage$ of each particle fitness function value, and directly propose M_k suitable value of individuals whose is higher than the average value;
11. Use GA to evolve the remaining $N - M_k$ individuals;

12. Combine 2 sets of $N - M_k$ individuals, and select the higher one based on the suitable function value.
13. The M_k individuals directly proposed by PSO evolution and stem from GA evolution ($N - M_k$) individuals form a new particle swarm group;
14. $k = k + 1$, back to Step5;
15. Output the optimal solution, namely the particle position, and the optimal fitness function value.

The flow chart of particle swarm genetic hybrid algorithm is as follows:

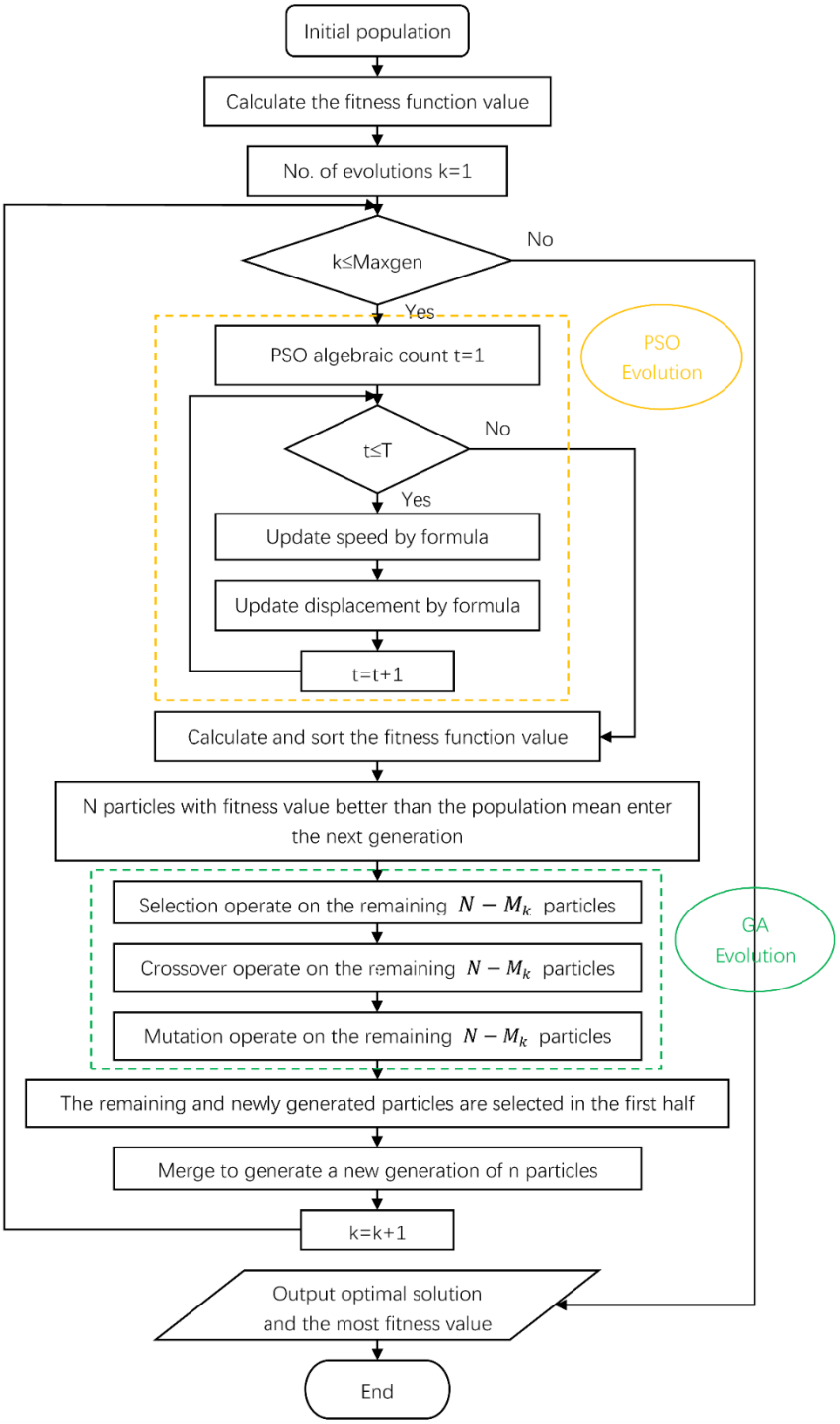

Figure 63 Flow chart of particle swarm genetic hybrid algorithm

5.6. APPLY PSO-GA IN PARAMETER DEFINATION

The results show the difference between the current identification data and the output of the model after the introduction of parameters, which also known as the difference of the identification parameters.

Figure 64 shows the simulation process to get the raw data for creating Figure 65 to Figure 67. The MTLAB function is setting to $y = 0.2\sin(0.5t) + 0.5\sin(0.2t) + 0.3\cos(0.4t)$, and the transfer function is defined as the first-order system $G(s) = \frac{K_1}{T_1 s + T_2}$, which $K_1 = 1$, $T_1 = 0.05$ and $T_2 = 1$.

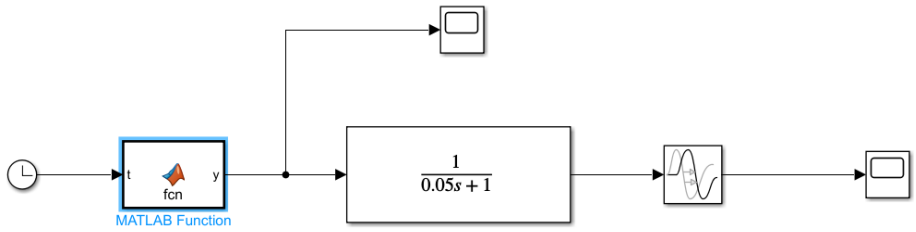

Figure 64 Simulation to get data

The random input data obtained is periodically put into the PSOGA algorithm, and the output is compared and the error is taken as the standard for selection operation.

In population is setting as 20, the first start learning factor value c_{s1} is 2.5, the end of the first learning factor value c_{e1} is 0.5, the second learning factor starting value c_{s2} is 0.5, the end of the second learning factor value c_{e2} is 2.5, the starting of inertia weight w_s is 0.9, at the end of the inertia weight w_e is 0.4, the biggest negative probability p_{max} is 0.4, the smallest mutation probability p_{min} is 0.001, by changing the number of iterations M of 20, 50

and 100 respectively, the following PSOGA results were obtained in figure 65-67.

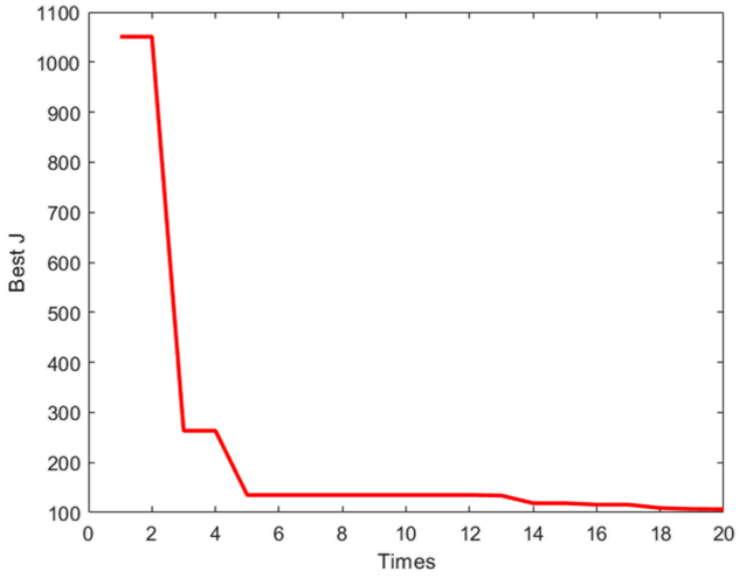

Figure 65 The PSOGA results with $M = 20$

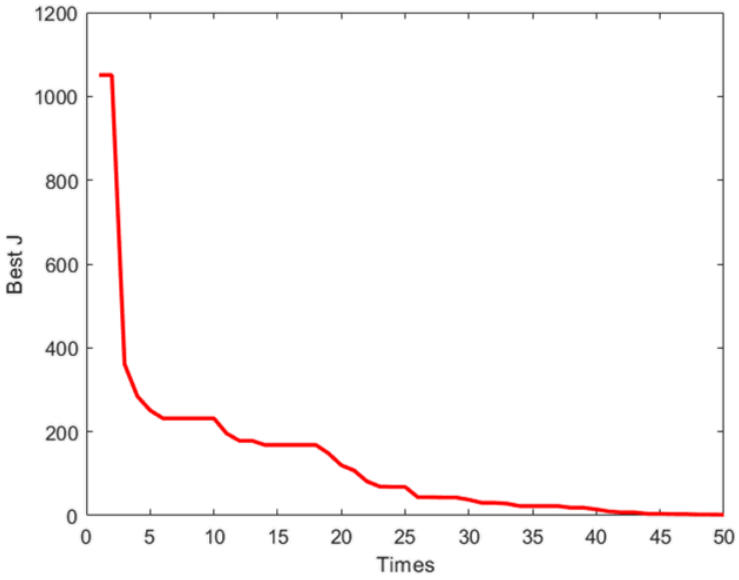

Figure 66 The PSOGA results with $M = 50$

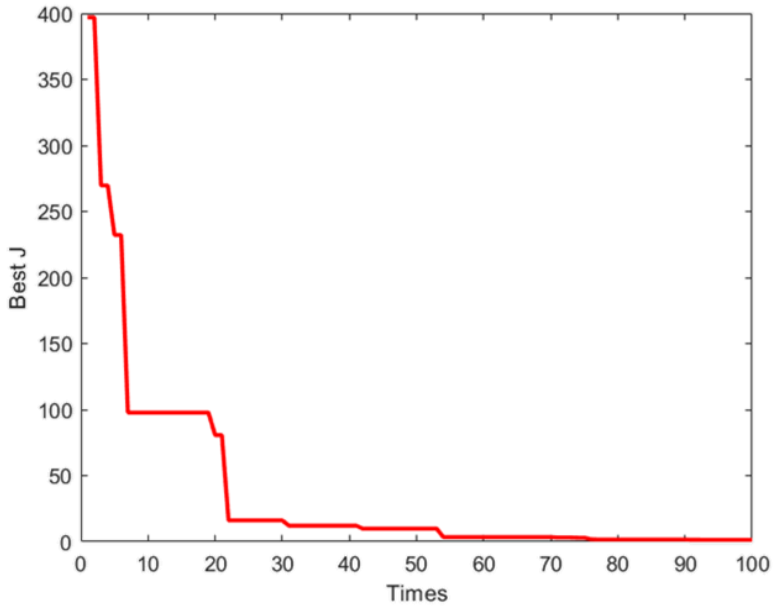

Figure 67 The PSOGA results with $M = 100$

The vertical axis, Best J, shows the convergence of the data, and the horizontal axis shows the convergence time. It can be seen from the figures that the convergence speed can be faster and more stable by increasing the number of iterations. In this study, particle swarm optimization algorithm is used to identify the data, which makes it easier for us to get the data used by the control algorithm.

From the data results, as shown in figure 68, it can be seen that the filtered melt pool width is the same as the actual linear change pattern when the wire feed speed is 3-9 m/min but when the wire feed speed exceeds 10 m/min, the melt pool width from the random signal does not match the actual situation. This may be due to the large variation of the wire feed, which prevents the welder from reaching the required power in a short time.

Therefore, the wire feed speed of 10 m/min will not be taken into account later in the simulation.

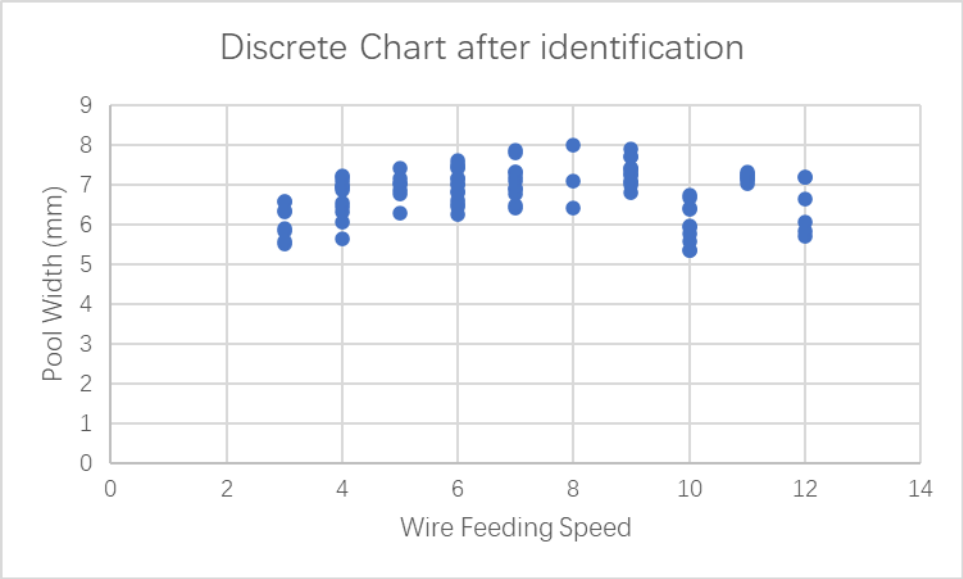

Figure 68 Discrete Chart for Pool Width in different Wire Feeding Speed without time delay after data identification

Particle swarm genetic hybrid algorithm (PSO-GA) is a new identification algorithm used in WAAM. From the figure, it can be seen that the PSO algorithm initially classifies the data and then applies the genetic algorithm for optimal screening to obtain data that is consistent with the actual changes and is expected to improve the control algorithm in the further study.

CHAPTER 6 SIMULATION RESULT

In this chapter, it will show the control algorithms which use in this study, all the algorithms are simulated in MATLAB. A dynamic model will be developed to simulate the welding control process, to investigate whether the new algorithm can achieve real-time control of the welding process.

Through the study of the extant literature, closed-loop control should be applied to the welding control. Because the feedback system is a vital part of process to achieve real-time control.

This study will use PID and difference equations, which are often used in WAAM control algorithm, but also will use fuzzy PID control algorithm and adaptive control algorithm. Due to the delay of data acquisition and control in actual WAAM operation, the Smith estimation system is adopted. (Lai, C.L. & Hsu, P.L., 2009) For the adaptive algorithm, RBF network is added to the controller for feedback control.

6.1 Difference equation

The difference equation is used to express the relationship between the wire feeding speed and the welding width. The output at a moment is determined by the one at the previous moment, which the function as Equation 10:

$$y(k) = 0.8\sin\big(y(k-1)\big) + 15u(k-1) \qquad \text{(Equation 10)}$$

where the period of data collection is 0.02s; the number of collections is 500 times.

It can be seen from the results that the output results are stable after about 3s. However, due to the inherent delay of the system and the heat transfer during the welding process, if the stability is reached after 3 second, the actual welding stability will fluctuate greatly in the early stage, which will result in the inability to obtain a stable weld.

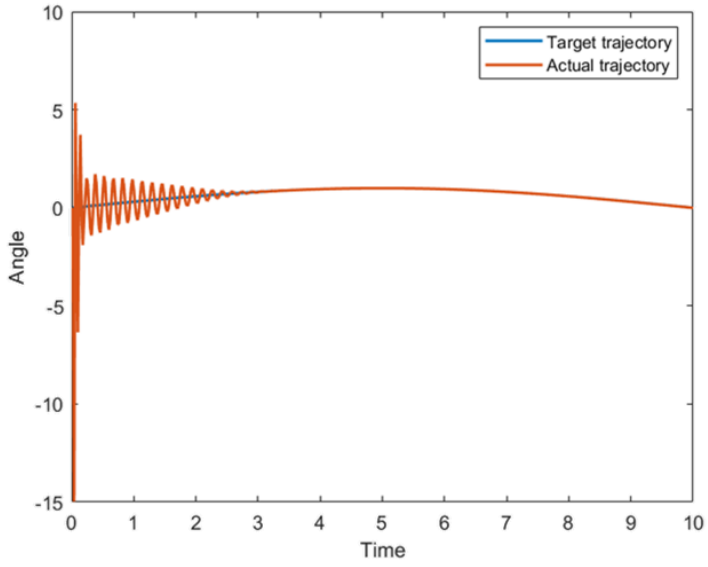

Figure 69 Difference equation control result

6.2 PID control with Fuzzy logic

6.2.1. Fuzzy logic

In this study, the fuzzy logic is used to determine the coefficient of PID control. So, the fuzzy logic inputs take the error of wire feeding speed e and its rate of change ce, the output take the coefficients K_P, K_I and K_D.

The steps of design a fuzzy controller are as follows:

1. Select the input and output variables for fuzzy control, and the values are generally e, ce and u.

2. Determine the fuzzy language value of each variable and the corresponding membership function, that is, perform fuzzification.
3. Establishing fuzzy control rules or control algorithms is the central link in the transition from actual control experience to fuzzy controllers. The fuzzy control rule table can directly query the control quantity u from e and ce.
4. Determine fuzzy reasoning and defuzzification methods. The common fuzzy reasoning methods include maximum and minimum reasoning and maximum opportunity reasoning. The method of defuzzification includes maximum membership method, center number method, weighted average method and so on.

Input and language variables generally take the systematic error e and its rate of change ce. For the actual input quantity, the scale must first be transformed to the required domain.

Among them, if the actual input is x_0^*, the range is $[x_{min}^*, x_{max}^*]$, and the required domain is $[x_{mix}, x_{max}]$, then $x_0 = \frac{x_{max}-x_{mix}}{2} + k\left(x_0^* - \frac{x_{max}^*-x_{min}^*}{2}\right)$.

The quantization factor $[0, e_{max}]$ continuously changes the error into n intervals to make it discretized. And the fuzzy set of the error takes the domain of: $X = \{-n, -n+1, \cdots, 0, \cdots, n-1, n\}, where\ k_e = \frac{n}{e_{max}}$.

The scale factor $[-u_{max}, u_{max}]$ is the basic domain of the change of the control quantity u, and n is the quantized interval number of the basic domain. For the change of the system control quantity, the definition error, the error change rate and the change of the control quantity are generally divided into three levels: large, medium and small. Its value corresponds to a fuzzy set in its domain. The fuzzy set is described by the membership function.

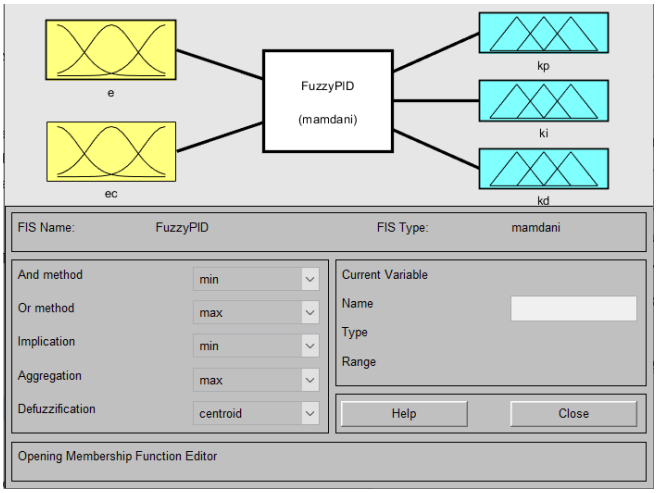

Figure 70 The structure of Fuzzy logic

The membership functions are setting into 7 level: negative big (NB), negative medium (NM), negative small (NS), zero (Z), positive small (PS), positive medium (PM) and positive big (PB). The range for the function is $[-1,1]$.

The membership function of Gaussian normal distribution can reflect the thinking characteristics of people judging things. The Gaussian function has good smoothness and symmetry, the graph has no zeros, and it has a relatively clear physical meaning, which can describe and approximate the

membership function well. It is appropriate to use Gaussian membership function to describe the fuzzy concept of human control, so the membership functions in this study are all Gaussian.

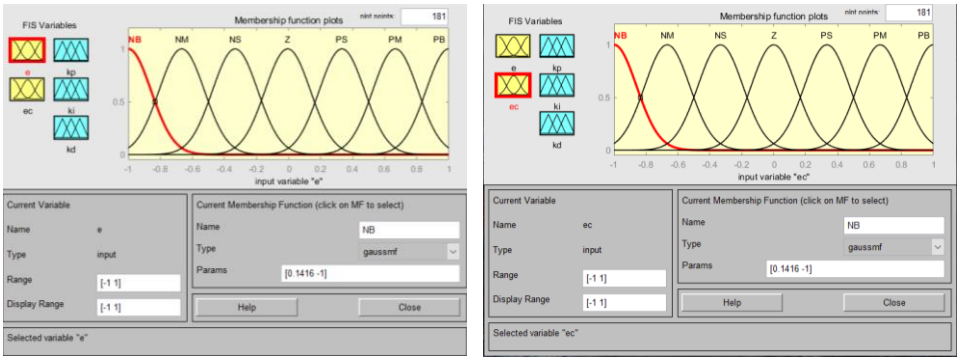

Figure 71 The membership function of input

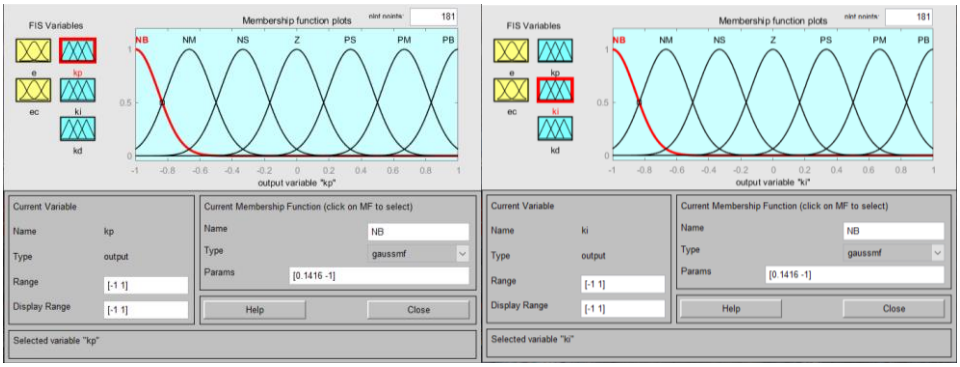

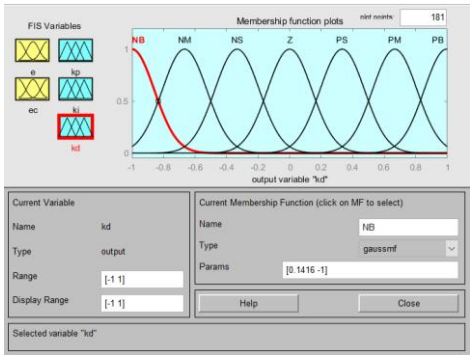

Figure 72 The membership function of output

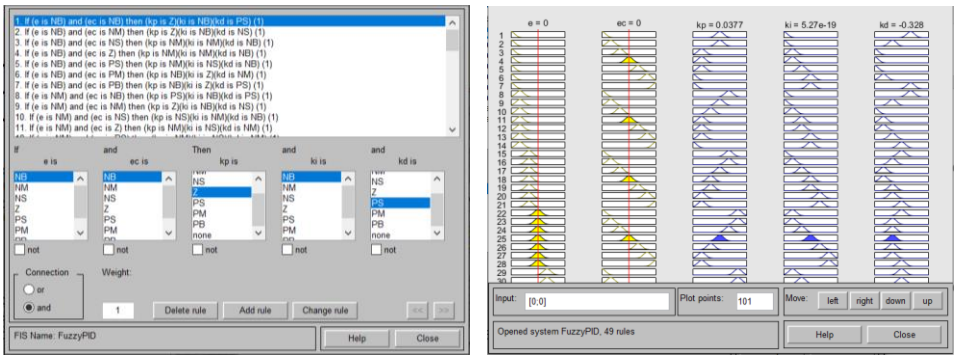

Figure 73 The rules of the fuzzy logic

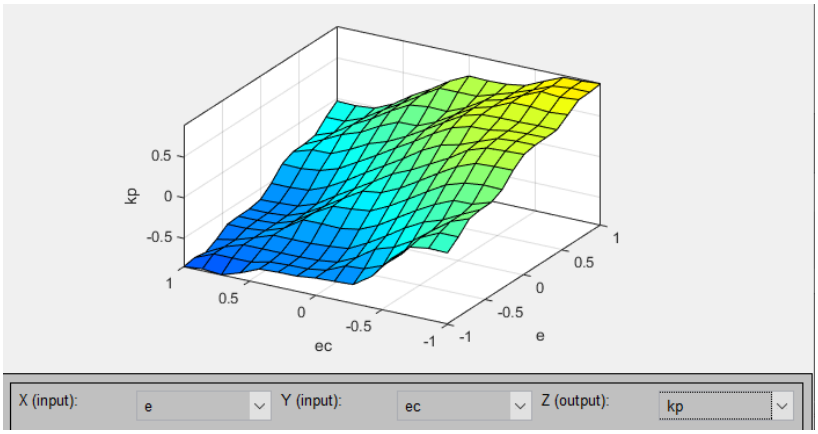

Figure 74 The surface between the input (e and ce) & output K_P

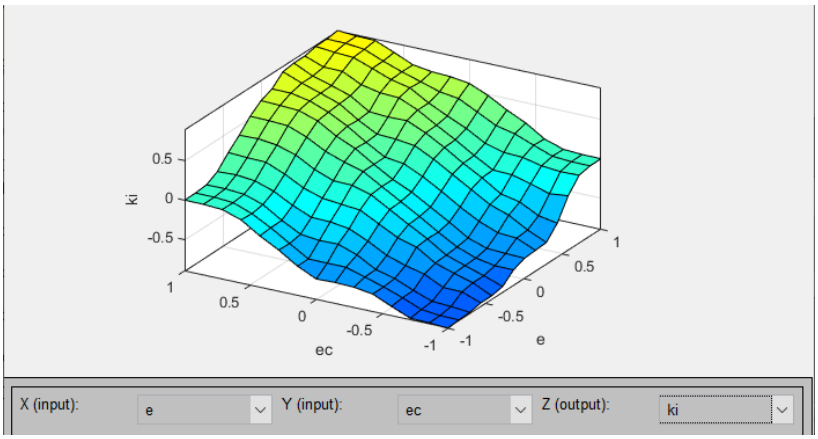

Figure 75 The surface between the input (e and ce) & output K_I

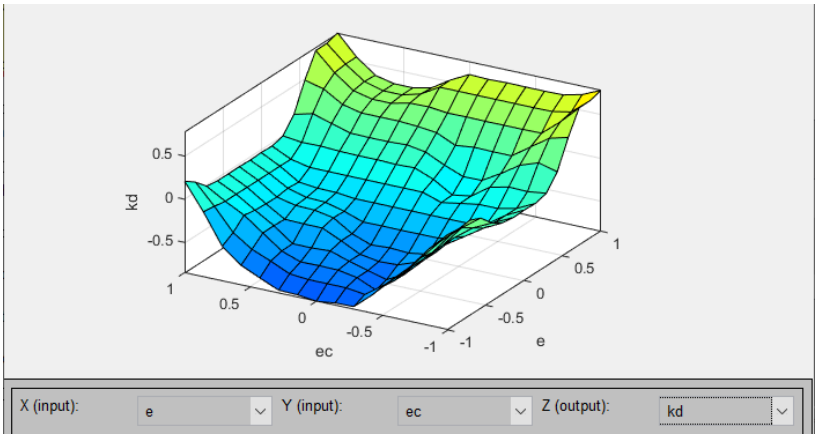

Figure 76 The surface between the input (e and ce) & output K_D

6.2.2. PID control

After correcting by fuzzy logic, the suitable PID coefficients are obtained to act on the PID control, and the simulation model is shown in the figure 77.

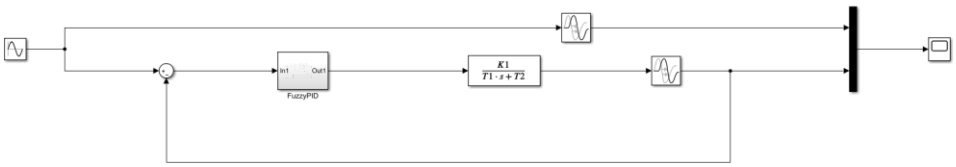

Figure 77 The Simulink model of Fuzzy PID control

The internal structure of 'Fuzzy PID' block is shown in the figure 78. Through the understanding of the literature and the results of previous experiments, the selected PID parameters are: $K_P = 7.5$, $K_I = 2.8$ and $K_D = 0.7$.

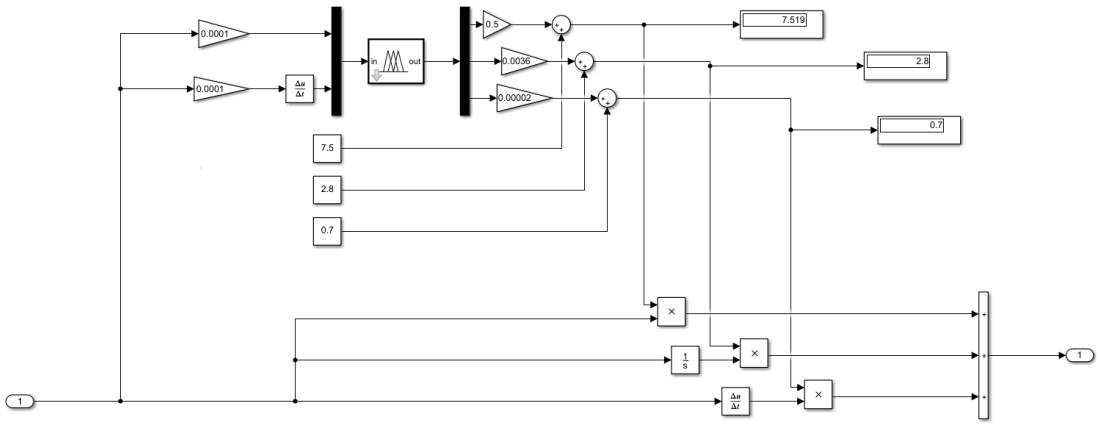

Figure 78 The block for Fuzzy PID

Through the adjustment of 'FuzzyPID' block, its coefficient is changed to: $K_P = 7.519,\ K_I = 2.8$ and $K_D = 0.7$.

Since the selected coefficients are more appropriate and because the derivative and integral have a greater impact on the stability of the control, the proportion of their effects is smaller and the value changes less.

6.2.3. Result

Taking the sine wave as the input signal, after the fuzzy PID adjustment, the adjustment result is shown in the Figure 79. The blue trajectory is the target trajectory, and the red trajectory is the fitting result adjusted by the control function.

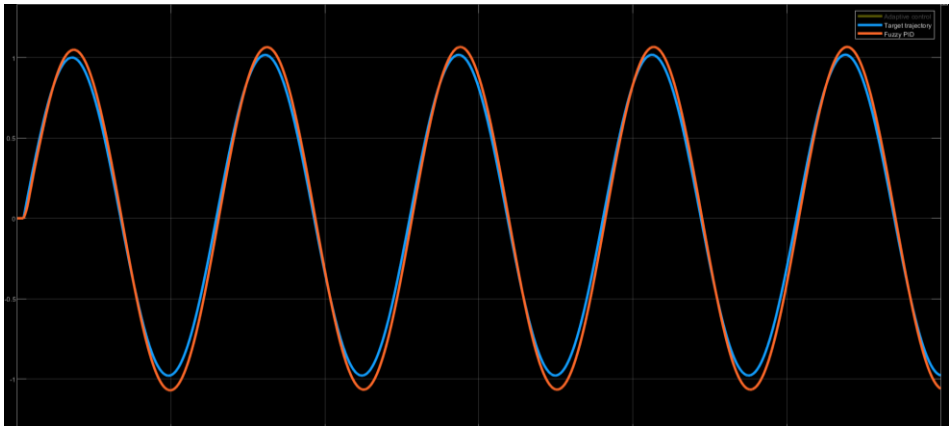

Figure 79 The result for Fuzzy PID control

It can be seen from the fitting results that there is still an error of about 0.05 at the peak and trough (the extreme value), which means that the overshoot is still large. It is found through simulation that no significant improvement is achieved by adjusting the integral coefficient, so adaptive control is added as a control function.

6.3 Adaptive control

6.3.1. Continuous Smith predictive control

Smith predictive control is a pure lag compensation control, which weakens and eliminates the pure lag by introducing a compensator connected in parallel with the controlled object. The general pure lag is the lag caused by the transmission speed limit.

The single-loop control system with pure delay is shown in the Figure 80.

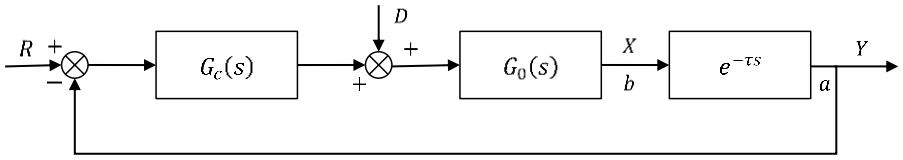

Figure 80 Single loop control system with pure delay

Which its closed-loop transfer function is illustrated by Equation 11:

$$\phi(s) = \frac{Y(s)}{R(s)} = \frac{G_c(s)G_0(s)e^{-\tau s}}{1+G_c(s)G_0(s)e^{-\tau s}} \quad \text{(Equation 11)}$$

And the characteristic equation is determined by Equation 12:

$$1 + G_c(s)G_0(s)e^{-\tau s} = 0 \quad \text{(Equation 12)}$$

It can be seen from the characteristic equation that there is a pure delay link, which is the decrease of system stability. As shown in the Figure 81, if the return signal can be drawn out of point b, the pure delay link is moved to the external of the control loop. With the delay time of τ, the adjusted quantity Y will get the same change of X.

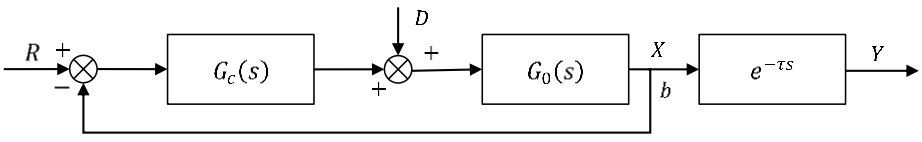

Figure 81 Improved single loop control system with pure delay

Since there is no delay in the feedback signal X, the response of the system will be greatly improved. But in actual systems, point b is usually restricted by physical conditions or does not exist, making it impossible to elicit

feedback signals from point b. In response to this problem, O. J. M. Smith proposed the use of artificial models, known as the Smith predictive control system.

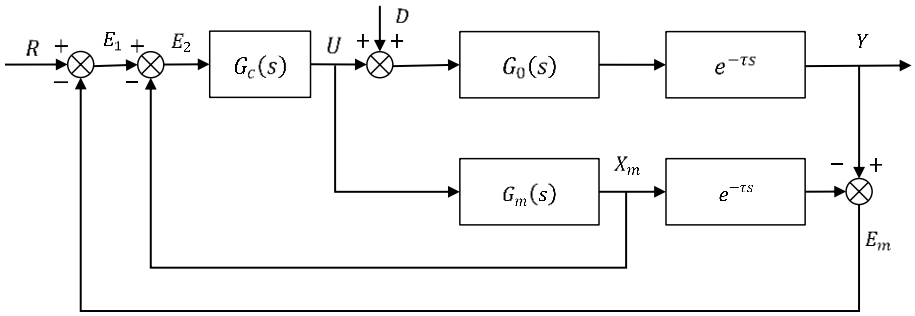

Figure 82 Smith predictive control system

If the model is accurate, that is $G_0(s) = G_m(s)$, $\tau = \tau_s$, and there is no load disturbance $(D = 0)$, then $Y = Y_m$, $E_m = Y - Y_m = 0$, $X = X_m$. Then X_m can be used to replace X as the first feedback loop to move the pure delay link to the external of the control loop. If the load disturbance occurs or model is not accurate, then X is not equal to X_m, $E_m = Y - Y_m \neq 0$, and the control accuracy is not satisfactory. For this reason, E_m is used to implement the second feedback loop. This is the Smith predictor's control strategy.

In actual situations, the predictive model is not connected in parallel to the process, but in reverse parallel to the controller, so it can be transformed to the equivalent diagram of the Smith predictive control system.

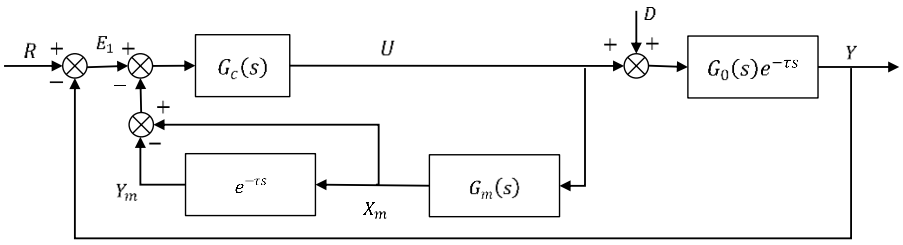

Figure 83 Equivalent diagram of Smith predictor control system

6.3.2. Radical Basis Function (RBF) Neural Network

The RBF neural network is a three-layer neural network, including input, hidden and output layers. The flow diagram is as follows:

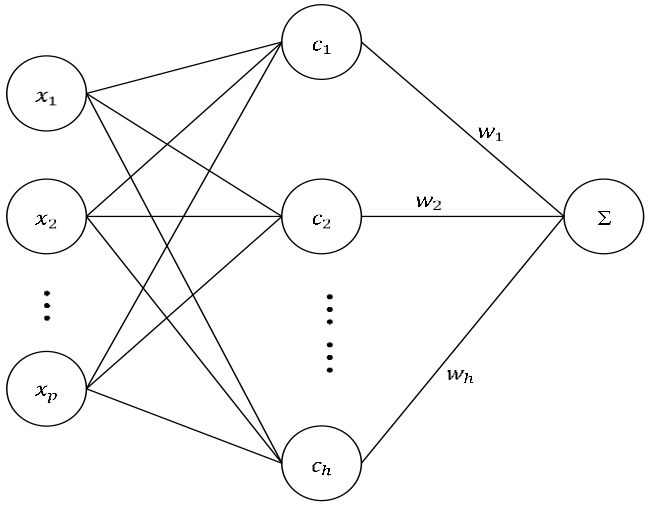

Figure 84 The Schematic diagram of RBF neural network

The mapping of the network from input to output is nonlinear, while the mapping from the hidden space to the output space is linear. In other words, the output of the network is a linear weighted summary of the hidden unit output, in which the weights are the adjustable parameters of the network. The linear equation can be used to solve the weights of the network directly,

which greatly speeds up the process of learning and avoids the problem of local minimum.

The function of the hidden layer is to map the vector from the low dimension p to the high dimension h, so that the low-dimensional linear inseparability can be transformed into the linear separability of the high-dimensional.

The RBF neural network learning algorithm needs to solve three parameters: the center of the basis function, the variance, and the weight from the hidden layer to the output layer. The function derivation process of RBF network is as follows:

Consider 2nd order system determined by Equation 13:

$$\begin{cases} \dot{x_1} = x_2 \\ \dot{x_2} = f(x) + g(x) \cdot u \end{cases} \quad \text{(Equation 13)}$$

Error $e = y_d - y = y_d - x_1$

RBF function is shown by Equation 14:

$$\begin{cases} h_{ij} = g\left(\|x - C_{ij}\|^2 / b_j^2\right) \\ f = w^T h(x) + \varepsilon \end{cases}, where\ x = \begin{bmatrix} e \\ \dot{e} \end{bmatrix} \quad \text{(Equation 14)}$$

Parameter:

x: Network input

i: Number of network inputs

j: The j[th] node of the network hidden layer

h: Gaussian output

w: The weights of the network

ε: Approximation error

Controller:

$$\begin{cases} u = \dfrac{1}{g(x)}\left[-\hat{f}(x) + \ddot{y}_d + K^T E\right] \\ \hat{f}(x) = \hat{w}^T h(x) \end{cases}$$

The adaptive rate:

$$\dot{\hat{w}} = -\gamma E^T P b h(x)$$

Stability analysis:

$$\ddot{e} = -K^T E + \left[\hat{f}(x) - f(x)\right]$$

$$\dot{E} = \Lambda E + B\left[\hat{f}(x) - f(x)\right]$$

The optimal weights:

$$w^* = argmin\left[sup\left|\hat{f}(x) - f(x)\right|\right]$$

Approximation error:

$$w = \hat{f}(x|w^*) - f(x)$$

$$\dot{E} = \Lambda E + B\left[\hat{f}(x) - f(x|w^*) + w\right]$$

$$= \Lambda E + \boxed{B[(\hat{w} - w^*)^T h(x) + w]} \rightarrow (M)$$

Define Lyapunov function as Equation 15:

$$V = \underbrace{\frac{1}{2}E^T P E}_{V_1} + \underbrace{\frac{1}{2\gamma}(\hat{w}-w^*)^T(\hat{w}-w^*)}_{V_2} \qquad \text{(Equation 15)}$$

for P satisfies $\Lambda^T P + P\Lambda = -Q$

The function for V_1 and V_2:

$$\dot{V}_1 = \frac{1}{2}\dot{E}^T P E + \frac{1}{2}E^T P \dot{E}$$

$$= -\frac{1}{2}E^T QE + E^T PM$$

$$= -\frac{1}{2}E^T QE + (\hat{w} - w^*)^T E^T PBh(x) + E^T PBw$$

$$\dot{V}_2 = \frac{1}{\gamma}(\hat{w} - w^*)^T \dot{\hat{w}}$$

The 1st derivative of the Lyapunov function is shown in Equation 16:

$$\dot{V} = \dot{V}_1 + \dot{V}_2 = -\frac{1}{2}E^T QE + E^T PBw \leq 0 \qquad \text{(Equation 16)}$$

The figure 85 shows the combination of RBF neural network and adaptive algorithm in the control system.

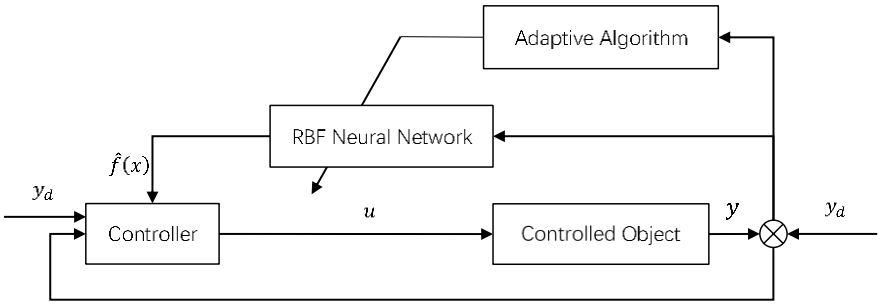

Figure 85 Control logic of adaptive algorithm

6.3.3. Adaptive control

In this study, the adaptive control algorithm '$Ctrl$' roughly divided into three part. The MATLAB code is shown in appendix and the Simulink model is shown in Figure 86.

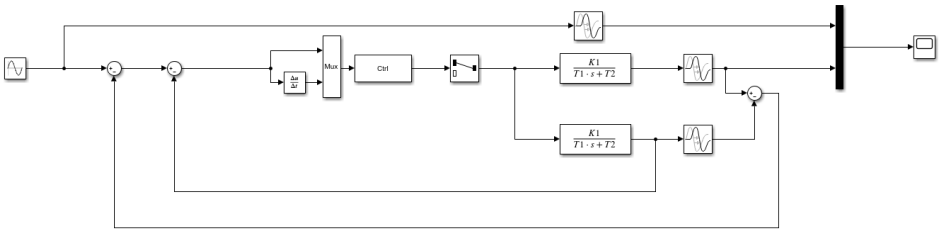

Figure 86 The Simulink model of adaptive control

The first part is to use neural network to approximate the objective function. Defined neural network intervals $sizes.NumContStates = 5$, control inputs $sizes.NumInputs = 2$, control outputs $sizes.NumOutputs = 2$. The input is the error e and the change of the error ∂e (the first derivative of the error). The output is the output of the controller, which is the wire feeding speed and the approximate value (estimated value). The approximation value is obtained by the RBF network.

The second part is the differential equation, which is obtained from the adaptive rate. The gamma coefficient is set to 12, dyd is the first-order derivative of the target trajectory, and $ddyd$ is the second-order derivative of the target's non-trajectory. The base value of the proportional differential function is defined as $K_P = 190$, $K_I = 0.01$, and the approximation term obtained through the RBF network h_j is added for compensation during the control process. The differential equation is shown by Equation 17:

$$S = -\gamma * E' * P * B * h \qquad \text{(Equation 17)}$$

The third part is the output of the function. fxp is an unknown item. The unknown item is obtained by multiplying the neuron and the full-value matrix: $fxp = W' * h$, and the full-value matrix is obtained by

approximating itself. The unknown term (disturbance term) function compensates for adaptive control.

The transfer function is setting as first-order function could be calculated as :

$$\frac{K_1}{T_1 \cdot S + T_2}$$

where $K_1 = 5$, $T_1 = 10$, $T_2 = 1$ and the time delay $T_{o1} = 0.2$.

6.3.4. Result

After adaptive control, the following results are obtained, in which the blue trajectory is the target trajectory, and the yellow trajectory is the trajectory after adaptive control fitting.

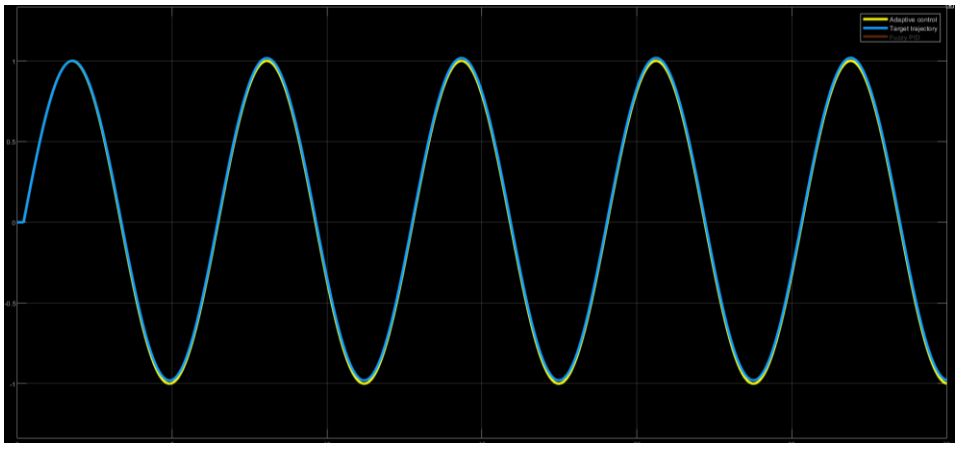

Figure 87 The result for adaptive control

It can be seen from the fitting results that the error value is less than 0.01, and the overshoot is reduced to the expected error range.

Therefore, it can be seen from the simulation control (Figure 88) that the adaptive control algorithm can effectively eliminate the system delay while approaching the target value.

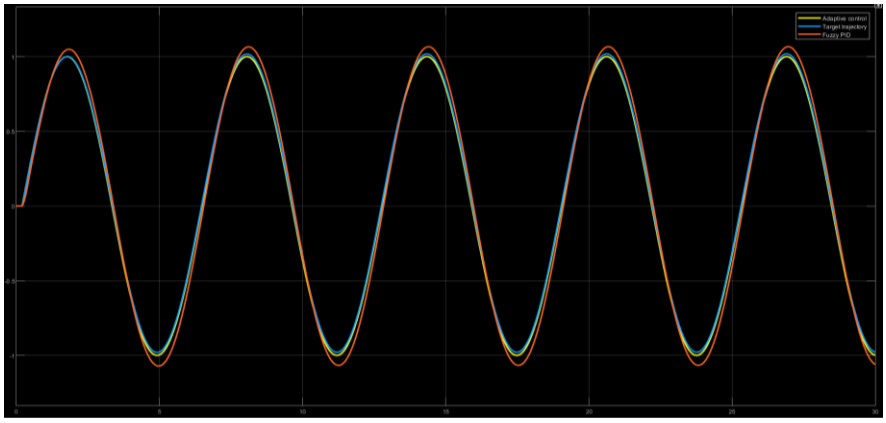

Figure 88 Compare the result between the Fuzzy PID control and adaptive control

CHAPTER 7 RESULT & DISCUSSION

In this chapter, the welding layers will be compared and analyzed to verify the feasibility of the welding control algorithm used.

The initial value of the wire feeding speed in the experiment is given as $5\,m/s$. The result is shown in the figure 89 without control. It can be seen from the figure that the weld has pores, and the width of the weld changes greatly during the additive process. The difference in specific width can be seen from the scan results.

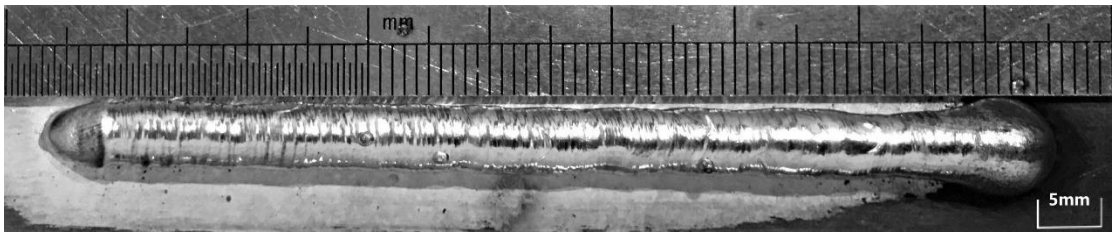

Figure 89 The first level of welding layer without control

At the same initial wire feeding speed, the following experimental results were obtained using fuzzy PID control. As can be seen from the figure 90, due to the pre-judgment and control of the weld width, the wire feeding speed is relatively stable and there is no large width difference. The relative stability of the welding temperature prevents the generation of pores.

Figure 90 The first level of welding layer with fuzzy PID control

Scanning the width and height of the weld can see the stabilizing effect of the control algorithm on the weld. The following table and figures compare the geometric parameters of the weld at different times.

Time (second)	Width-with control	Width-without control	Hight-with control	Hight-without control
1	10	12	4.11	3.475
2	10	9	4.185	4.4
3	10	9	4.2	4.095
4	10	8	4.27	4.625
5	9	9	4.29	4.005
6	9	8	4.32	4.36
7	9	9	4.23	3.94
8	9	6	4.16	3.995
9	8	7	4.06	4.12
10	9	8	4.09	3.875

Table 4 The geometric parameters for different layer-first layer

Through the collection of geometric data at different times, it can be found that after passing the control algorithm, the width of the additive process is relatively stable, but there is a trend of fluctuation in the later period. At the same time, it can be seen that the stable weld width can effectively control the weld height.

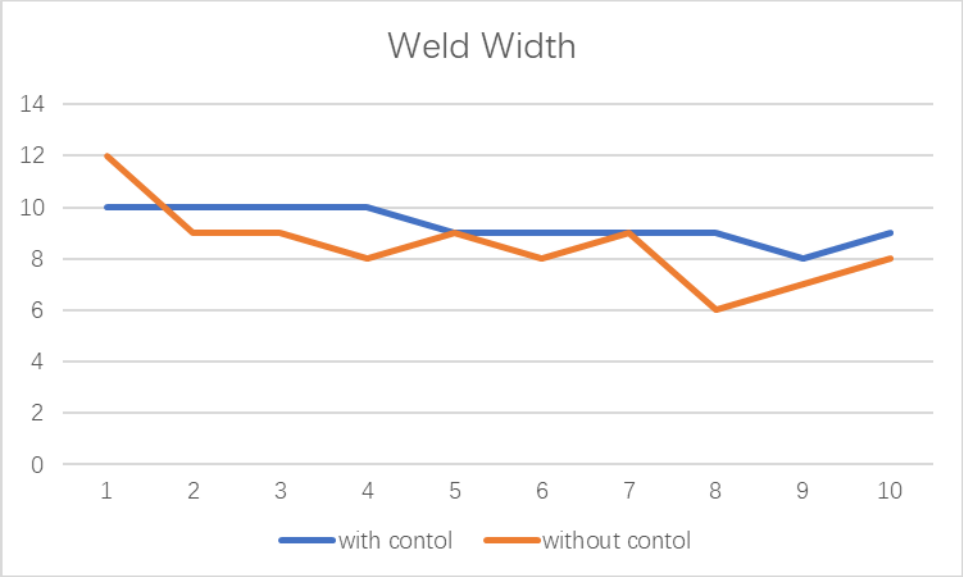

Figure 91 Compare the width with & without control-first layer

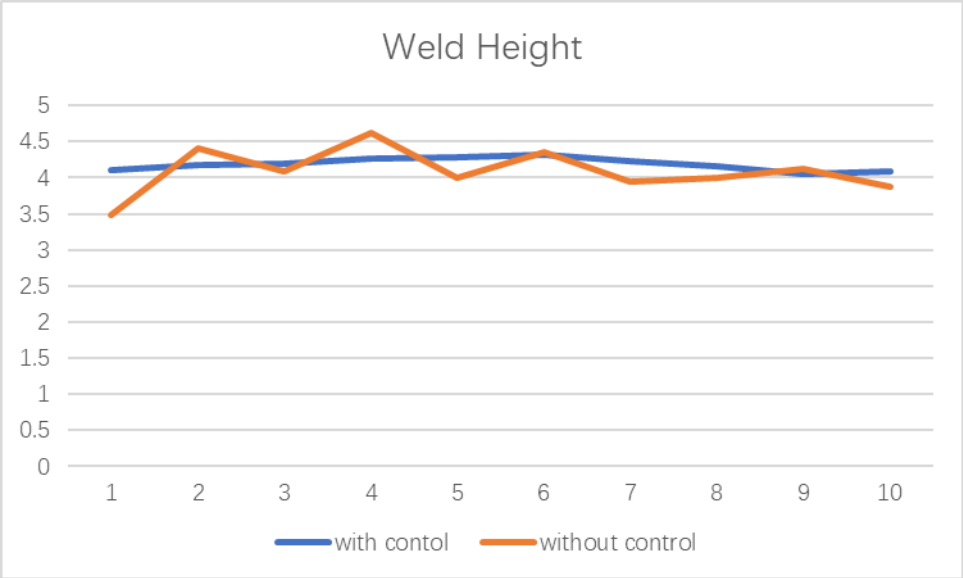

Figure 92 Compare the height with & without control-first layer

The process of additive manufacturing needs to realize the superposition of materials, so each layer of the additive needs to be relatively accurate to prevent the subsequent superposition from being affected. Therefore, during the experiment, the first layer of welds was superimposed, and the following figure was obtained.

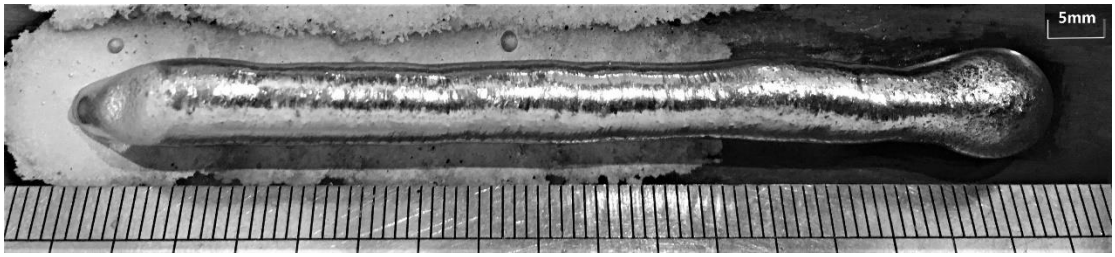

Figure 93 The second level of welding layer without control

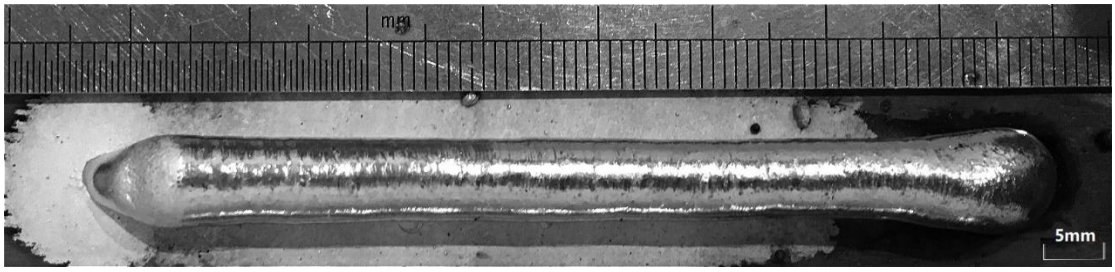

Figure 94 The second level of welding layer with control

Just comparing the uncontrolled single-layer welds and double-layer welds, the shape of the welds of the previous layer has a certain influence on the subsequent additives. It can be seen that due to the collapse of the first layer in some places (the width of the weld is relatively narrow), the same problem still occurs after the second layer is added. At the same time, although the pores disappear, it still has an impact on the internal structure of the weld. If it is used in the manufacture of some parts, such as gears or propellers, it is easy to cause hidden dangers such as broken teeth and propellers.

Similarly, for the geometric parameters of the second layer of welds, the following table compares the control and non-control.

Time (second)	Width-with control	Width-without control	Hight-with control	Hight-without control
1	11	11	7.26	6.365
2	10	11	7.065	6.735
3	10	11	6.915	7.115
4	11	10	6.6	6.395
5	9	7	7.21	6.6
6	11	10	6.2	6.93
7	10	10	6.73	7.015
8	11	11	6.375	6.605
9	9	9	6.51	8.645
10	11	10	6.475	6.495

Table 5 The geometric parameters for different layer-second layer

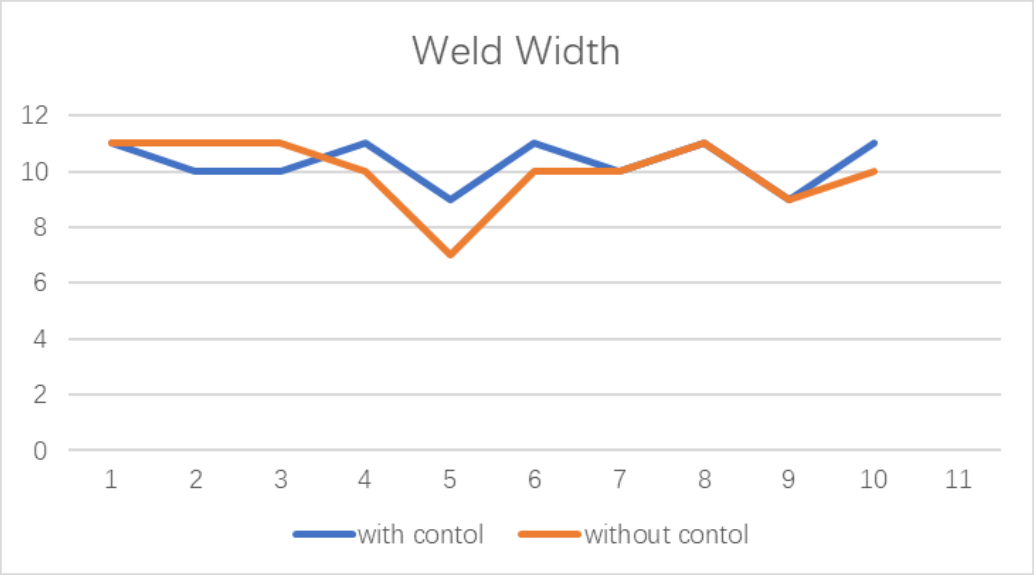

Figure 95 Compare the width with & without control-second layer

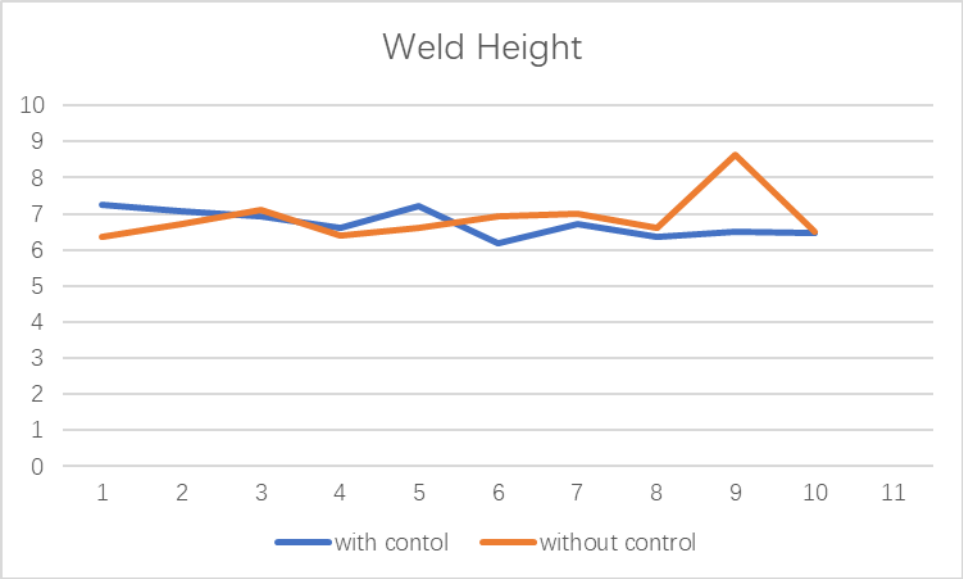

Figure 96 Compare the height with & without control-second layer

By observing the comparison table, it can be seen that even for welds controlled by algorithms, the weld width still fluctuates. But from a height perspective, it is relatively stable. At the same time, by comparing the height of the first layer and the second layer, it can be seen that there is a certain difference in height when the wire feeding speed is the same. This shows that the collapse of welding materials needs to be considered in the process of adding materials. Adding materials to existing welds is different from adding materials to steel plates. When the foundation is relatively narrow, the collapse will be serious.

1st layer	C	4.11	4.185	4.2	4.27	4.29	4.32	4.23	4.16	4.06	4.09
	NC	3.475	4.4	4.095	4.625	4.005	4.36	3.94	3.995	4.12	3.875
2nd layer	C	3.15	2.88	2.715	2.33	2.92	1.88	2.5	2.215	2.45	2.385
	NC	2.89	2.335	3.02	1.77	2.595	2.57	3.075	2.61	4.525	2.62

Table 6 Compare the height of each layer (C-control, NC-non-control)

CHAPTER 8 CONCLUSION

This chapter is a conclusion of this study and prospects for the future. Mentioned the research results and existing problems, and expounded the direction of the next work.

8.1. Conclusion

This study has made certain innovations and applications of WAAM's control algorithm to stabilize the additive process through geometric parameters. Since WAAM's own control process is relatively stable, how to eliminate interference such as delay and improve its accuracy is a big challenge for this study.

In order to have a better analysis of the experimental data, this study uses the method of combining genetic algorithm (GA) and particle swarm optimization (PSO) algorithm, namely particle swarm genetic hybrid algorithm (PSO-GA), to carry out the preliminary data identification of the simulation process. Data identification makes the data used in the simulation more accurate, and can later obtain some parameter values of the control algorithm more efficiently.

The simulation control algorithm uses the common difference equation and fuzzy PID in the control algorithm. At the same time, an adaptive control algorithm containing continuous Smith predictor and RBF neural network is used, which can effectively compensate the system. It can be seen from the simulation results that the adaptive control algorithm is better than the previous two algorithms, and the fitting result is the closest to the target trajectory.

The process of carrying out the experiment mainly used the fuzzy PID control algorithm. It can be seen from the results of the additive that the fuzzy PID control algorithm can better control the first layer of welds, but after superimposing the second layer of welds, there is a slight local collapse. This problem needs to be improved in the future work.

8.2. Future work

In future research, the fuzzy PID control needs to be improved to achieve the stability of the additive process. At the same time, due to the good simulation results of adaptive control, it is expected that the adaptive control algorithm containing continuous Smith predictor and RBF neural network will be applied to actual experiments.

After improving the control accuracy of WAAM, WAAM technology can be applied to some aspects that require precision manufacturing, which will become a new breakthrough in this field.

Reference

1. Acquaviva, P., Chen, C.A., Chun, J.H. and Ando, T., 1997. Thermal modeling of deposit solidification in uniform droplet spray forming, Trans. ASME119, pp.332–340.
2. Bi, G., Gasser, A., Wissenbach, K., Drenker, A. and Poprawe, R., 2006. Characterization of the process control for the direct laser metallic powder deposition. *Surface and Coatings Technology*, *201*(6), pp.2676-2683.
3. Car cooling system: why engine coolant is so important (2020). Available at: https://www.mynrma.com.au/cars-and-driving/car-servicing/resources/engine-cooling-system-care (Accessed: 20 November 2020).
4. Chaib, S., Netto, M.S. and Mammar, S., 2004, June. H/sub/spl infin//, adaptive, PID and fuzzy control: a comparison of controllers for vehicle lane keeping. In *IEEE Intelligent Vehicles Symposium, 2004* (pp. 139-144). IEEE.
5. Chen, S.B., 2007. Visual information acquirement and real-time control methodologies for weld pool dynamics during pulsed GTAW. In *Materials science forum* (Vol. 539, pp. 3996-4001). Trans Tech Publications Ltd.
6. Chen, S.B., Wu, L. and Wang, Q.L., 1997. Self-learning fuzzy neural networks for control of uncertain systems with time delays. *IEEE Transactions on Systems, Man, and Cybernetics, Part B (Cybernetics)*, *27*(1), pp.142-148.
7. De Microinformatique, L. and Godjevac, J., 2007. Comparison between PID and fuzzy control.
8. Devesse, W., De Baere, D., Hinderdael, M. and Guillaume, P., 2016. Hardware-in-the-loop control of additive manufacturing processes using temperature feedback. *Journal of Laser Applications*, *28*(2), p.022302.

9. Ding, D., Pan, Z., Cuiuri, D. and Li, H., 2015. Wire-feed additive manufacturing of metal components: technologies, developments and future interests. *The International Journal of Advanced Manufacturing Technology*, *81*(1-4), pp.465-481.
10. Ding, J., Colegrove, P., Mehnen, J., Ganguly, S., Almeida, P.S., Wang, F. and Williams, S., 2011. Thermo-mechanical analysis of Wire and Arc Additive Layer Manufacturing process on large multi-layer parts. *Computational Materials Science*, *50*(12), pp.3315-3322.
11. Feng, Z. ed., 2005. *Processes and mechanisms of welding residual stress and distortion*. Elsevier.
12. Globalrobots.com. 2020. Robots. [online] Available at: http://www.globalrobots.com/default.aspx [Accessed 20 November 2020].
13. Goldberg D.E.Genetic Algorithms in Search, Optimization and Machine Learning[A].New York, USA: Addison-Wesley Publishing Company,Inc,1989
14. Hagqvist, P., Heralić, A., Christiansson, A.K. and Lennartson, B., 2015. Resistance based iterative learning control of additive manufacturing with wire. *Mechatronics*, *31*, pp.116-123.
15. Heralić, A., Christiansson, A.K. and Lennartson, B., 2012. Height control of laser metal-wire deposition based on iterative learning control and 3D scanning. *Optics and lasers in engineering*, *50*(9), pp.1230-1241.
16. Heralić, A., Christiansson, A.K., Ottosson, M. and Lennartson, B., 2010. Increased stability in laser metal wire deposition through feedback from optical measurements. *Optics and Lasers in Engineering*, *48*(4), pp.478-485.

17. Hofman, J.T., Pathiraj, B., Van Dijk, J., De Lange, D.F. and Meijer, J., 2012. A camera based feedback control strategy for the laser cladding process. *Journal of Materials Processing Technology*, *212*(11), pp.2455-2462.
18. Holland J. H. Adaption in Natural Artificial Systems[M]. MIT Press, 1975:1-17
19. Hu, D. and Kovacevic, R., 2003. Sensing, modeling and control for laser-based additive manufacturing. *International Journal of Machine Tools and Manufacture*, *43*(1), pp.51-60.
20. Hua, Y. and Choi, J., 2005. Adaptive direct metal/material deposition process using a fuzzy logic-based controller. *Journal of Laser Applications*, *17*(4), pp.200-210.
21. Ji, Z., Zhou, J.R., Liao, H.L. and Wu, Q.H., 2010. A novel intelligent single particle optimizer. *Chinese journal of computers*, *33*(3), pp.556-561.
22. Jin, F. and Wang, X., 2015, September. An autonomous camera calibration system based on the Theory of Minimum Convex Hull. In *2015 Fifth International Conference on Instrumentation and Measurement, Computer, Communication and Control (IMCCC)* (pp. 857-860). IEEE.
23. Karunakaran, K.P., Suryakumar, S., Pushpa, V. and Akula, S., 2010. Low cost integration of additive and subtractive processes for hybrid layered manufacturing. *Robotics and Computer-Integrated Manufacturing*, *26*(5), pp.490-499.
24. Kennedy, J. and Eberhart, R., 1995, November. Particle swarm optimization. In *Proceedings of ICNN'95-International Conference on Neural Networks* (Vol. 4, pp. 1942-1948). IEEE.
25. Lai, C.L. and Hsu, P.L., 2009. Design the remote control system with the time-delay estimator and the adaptive smith predictor. *IEEE Transactions on Industrial Informatics*, *6*(1), pp.73-80.

26. Mandal, L. and Jana, N.D., 2019, December. A Comparative Study of Naive Bayes and k-NN Algorithm for Multi-class Drug Molecule Classification. In *2019 IEEE 16th India Council International Conference (INDICON)* (pp. 1-4). IEEE.

27. Metawa, N., Hassan, M.K. and Elhoseny, M., 2017. Genetic algorithm based model for optimizing bank lending decisions. *Expert Systems with Applications*, *80*, pp.75-82.

28. Morrow, W.R., Qi, H., Kim, I., Mazumder, J. and Skerlos, S.J., 2007. Environmental aspects of laser-based and conventional tool and die manufacturing. *Journal of Cleaner Production*, *15*(10), pp.932-943.

29. Mughal, M.P., Fawad, H. and Mufti, R.A., 2006. Three-dimensional finite-element modelling of deformation in weld-based rapid prototyping. *Proceedings of the Institution of Mechanical Engineers, Part C: Journal of Mechanical Engineering Science*, *220*(6), pp.875-885.

30. Ngo, T.D., Kashani, A., Imbalzano, G., Nguyen, K.T. and Hui, D., 2018. Additive manufacturing (3D printing): A review of materials, methods, applications and challenges. *Composites Part B: Engineering*, *143*, pp.172-196.

31. Renken, V., Albinger, S., Goch, G., Neef, A. and Emmelmann, C., 2017. Development of an adaptive, self-learning control concept for an additive manufacturing process. *CIRP Journal of Manufacturing Science and Technology*, *19*, pp.57-61.

32. Reynolds, C.W., 1987, August. Flocks, herds and schools: A distributed behavioral model. In *Proceedings of the 14th annual conference on Computer graphics and interactive techniques* (pp. 25-34).

33. Rostgaard, M., Lauritsen, M.B. and Poulsen, N.K., 1996. A state-space approach to the emulator-based GPC design. *Systems & control letters*, *28*(5), pp.291-301.

34. Santos, E.C., Shiomi, M., Osakada, K. and Laoui, T., 2006. Rapid manufacturing of metal components by laser forming. *International Journal of Machine Tools and Manufacture*, *46*(12-13), pp.1459-1468.

35. Shi, X.H., Liang, Y.C., Lee, H.P., Lu, C. and Wang, L.M., 2005. An improved GA and a novel PSO-GA-based hybrid algorithm. *Information Processing Letters*, *93*(5), pp.255-261.

36. Song, L., Bagavath-Singh, V., Dutta, B. and Mazumder, J., 2012. Control of melt pool temperature and deposition height during direct metal deposition process. *The International Journal of Advanced Manufacturing Technology*, *58*(1-4), pp.247-256.

37. Stoyanov, Stoyan & Bailey, Chris. (2017). *Machine learning for additive manufacturing of electronics.* 2017 40th International Spring Seminar on Electronics Technology (ISSE). pp. 1-6.

38. Wang, F., Williams, S. and Rush, M., 2011. Morphology investigation on direct current pulsed gas tungsten arc welded additive layer manufactured Ti6Al4V alloy. *The international journal of advanced manufacturing technology*, *57*(5), pp.597-603.

39. Wang, F., Zhang, H., Li, K., Lin, Z., Yang, J. and Shen, X.L., 2018. A hybrid particle swarm optimization algorithm using adaptive learning strategy. *Information Sciences*, *436*, pp.162-177.

40. Weiss, L.E., Prinz, F.B., Adams, D.A. and Siewiorek, D.P., 1992. Thermal spray shape deposition. *Journal of Thermal Spray Technology*, *1*(3), pp.231-237.

41. Wong, A., Stancescu, A. and Chen, M., 2019. 3D Printing in Surgery and Medicine. *The Meducator*, *1*(36), pp.8-9. Banks, J., 2013. Adding value in additive

manufacturing: researchers in the United Kingdom and Europe look to 3D printing for customization. *IEEE pulse*, *4*(6), pp.22-26.

42. Xiong, J. and Zhang, G., 2014. Adaptive control of deposited height in GMAW-based layer additive manufacturing. *Journal of Materials Processing Technology*, *214*(4), pp.962-968.
43. Xiong, J. and Zou, S., 2019. Active vision sensing and feedback control of back penetration for thin sheet aluminum alloy in pulsed MIG suspension welding. *Journal of Process Control*, *77*, pp.89-96.
44. Yao K, Li F F, Liu X Y. Hybrid algorithm based on PSO and GA[J]. *Computer Engineering and Applications*,2007,43(6):62-64.
45. Zeinali, M. and Khajepour, A., 2010. Height control in laser cladding using adaptive sliding mode technique: theory and experiment. *Journal of manufacturing science and engineering*, *132*(4).
46. Zhang, Y., Chen, Y., Li, P. and Male, A.T., 2003. Weld deposition-based rapid prototyping: a preliminary study. *Journal of Materials Processing Technology*, *135*(2-3), pp.347-357.
47. Zhang, Y.M., Kovacevic, R. and Li, L., 1996. Adaptive control of full penetration gas tungsten arc welding. *IEEE Transactions on Control Systems Technology*, *4*(4), pp.394-403.

Bibliography

1. Xia, C., Pan, Z., Zhang, S., Polden, J., Wang, L., Li, H., Xu, Y. and Chen, S., 2020. Model predictive control of layer width in wire arc additive manufacturing. *Journal of Manufacturing Processes*, *58*, pp.179-186.
2. Xia, C., Pan, Z., Fei, Z., Zhang, S. and Li, H., 2020. Vision based defects detection for Keyhole TIG welding using deep learning with visual explanation. *Journal of Manufacturing Processes*, *56*, pp.845-855.

Appendix A - MATLAB code

Roberts edge detection operator:

```
clear;
sourcePic=imread('E:\UOW\2018
Spring\ENGG940\TIG\0918\screem\971\971.tif'); %Read
original image
grayPic=mat2gray(sourcePic); %Realize the
normalization of the image matrix
[m,n]=size(grayPic);
newGrayPic=grayPic;%Keep the edges of the image
robertsNum=0; %The value of each pixel calculated by
the roberts operator
robertThreshold=0.2; %Set threshold
for j=1:m-1 %Boundary extraction
    for k=1:n-1
        robertsNum = abs(grayPic(j,k)-
grayPic(j+1,k+1)) + abs(grayPic(j+1,k)-
grayPic(j,k+1));
        if(robertsNum > robertThreshold)
            newGrayPic(j,k)=255;
        else
            newGrayPic(j,k)=0;
        end
    end
end
figure,imshow(newGrayPic);
title('result of roberts operator')
imwrite(newGrayPic,strcat('E:\UOW\2018
Spring\ENGG940\TIG\0918\screem\971\',num2str(1),'.tif
'),'tif');
```

Grayscale processing, black and white (binarization) processing & edge contour detection

```
Y=imread(strcat('E:\UOW\2018
Spring\ENGG940\TIG\0918\screem\971\',num2str(971),'.t
if'),'tif');
I1=255-rgb2gray(Y);
K=im2bw(I1,0.8);
contour = bwperim(K);
%show the images
figure;
subplot(1,3,1);
```

```
imshow(I1);
imwrite(I1,strcat('E:\UOW\2018
Spring\ENGG940\TIG\0918\screem\971\',num2str(2),'.tif
'),'tif');
subplot(1,3,2);
imshow(K);
imwrite(K,strcat('E:\UOW\2018
Spring\ENGG940\TIG\0918\screem\971\',num2str(3),'.tif
'),'tif');
subplot(1,3,3);
imshow(contour);
imwrite(contour,strcat('E:\UOW\2018
Spring\ENGG940\TIG\0918\screem\971\',num2str(4),'.tif
'),'tif');
```

Image expansion and corrosion combined operation

```
clear;
SE = strel('rectangle',[2 12]); %Remove the rectangle
%All lines be deleted, but the rectangle also be
reduced
BW1=imread('E:\UOW\2018
Spring\ENGG940\TIG\0918\screem\971\1.tif');
BW2=imerode(BW1,SE);
%Restore the rectangle to its original size and use
the same structural elements to swell the corrupted
image.
BW3=imdilate(BW2,SE);
subplot(1,2,1),imshow(BW1);
subplot(1,2,2),imshow(BW3);
imwrite(BW3,strcat('E:\UOW\2018
Spring\ENGG940\TIG\0918\screem\971\',num2str(5),'.tif
'),'tif');
```

Crop image

```
clear;
Mat=imread('E:\UOW\2018
Spring\ENGG940\TIG\0918\screem\971\5.tif');
imshow(Mat);
mouse=imrect(gca, [500 250 185 200]);
pos=getPosition(mouse);% x1 y1 w h
Mat_1 = imcrop(Mat,pos);
imshow(Mat_1);
```

```
imwrite(Mat_1,strcat('E:\UOW\2018
Spring\ENGG940\TIG\0918\screem\971\crop\',num2str(5),
'.tif'),'tif');
```

Difference equation control:

```
clear all;
close all;

x_1=0.15;
x_2=0.50;
beta=0.05;

m=0.5*[1;1;1;1;1;1];
n=0.5*[1;1;1;1;1;1];

cij=0.50*[1,1,1,1,1,1];
bj=5*[1;1;1;1;1;1];
h=[0;0;0;0;0;0];

 m1=m;m2=m1;
 n1=n;n2=n1;
 u1=0;y1=0;

 ts=0.02;
 for i=1:1:500
 time(i)=i*ts;

yd(i)=1.0*sin(0.1*pi*i*ts
);

 %Simulate Object;
 y(i)=0.8*sin(y1)+15*u1;

 for j=1:1:6
    h(j)=exp(-norm(y(i)-
cij(:,j))^2/(2*bj(j)*bj(j
)));
 end

 G(i)=m'*h;
 N(i)=n'*h;

 ym(i)=G(i)+N(i)*u1;

 e(i)=y(i)-ym(i);

 d_w=0*m;
 for j=1:1:6
    d_w(j)=x_1*e(i)*h(j);
 end
 m=m1+d_w+beta*(m1-m2);

 d_v=0*n;
 for j=1:1:6

d_v(j)=x_2*e(i)*h(j)*u1;
 end
 n=n1+d_v+beta*(n1-n2);

 u(i)=-
G(i)/N(i)+yd(i)/N(i);

 u1=u(i);
 y1=y(i);

 m2=m1;
 m1=m;

 n2=n1;
 n1=n;
end
figure(1);
plot(time,yd,time,y,'line
width',1.5);
xlabel('Time');ylabel('An
gle');
legend('Target
trajectory','Actual
trajectory');
```

Adaptive control:

```
function
sys=acDerivatives(t,x,u)
global m n
gama=12;
E=u';
Fai=[0 1;-190 -0.01];
F=Fai';

Q=diag([50 50]);
P=lyap(F,Q);

xi=E;
h=[0;0;0;0;0];
for j=1:1:5
    h(j)=exp(-norm(xi-
m(:,j))^2/(2*n^2));
end
B=[0;1];
S=-gama*E'*P*B*h;

sys = S;
function
sys=acOutputs(t,x,u)
global m n
yy = [sin(t);cos(t);-
sin(t)];

K=[190 0.01]';
E=u';
W=x';
xi=E;
h=[0;0;0;0;0;0];
for j=1:1:5
    h(j)=exp(-norm(xi-
m(:,j))^2/(2*n^2));
end
f_xp=W'*h;
g_x=1;

u_t=1/g_x*(-
f_xp+yy(3)+K'*E);

sys(1)=u_t;
sys(2)=f_xp;
```

Appendix B – Weld layer

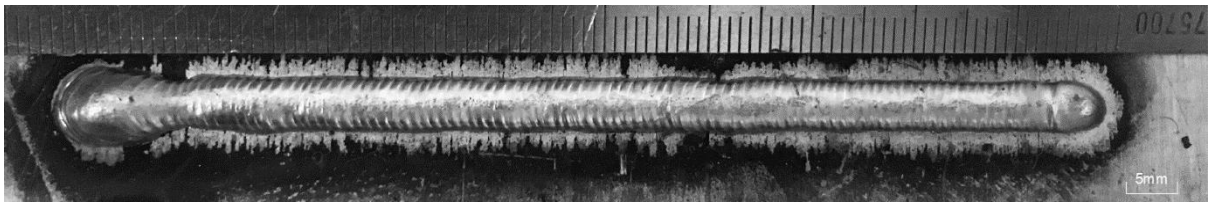

Figure 97 The welding layer with 5.0m/min of feeding wire speed

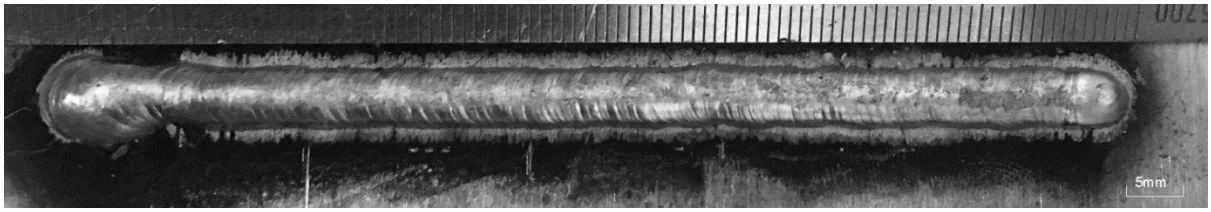

Figure 98 The welding layer with 5.5m/min feeding wire speed

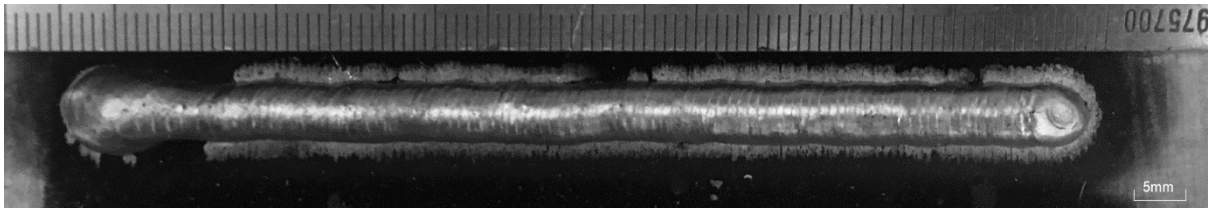

Figure 99 The welding layer with 6.0m/min of feeding wire speed

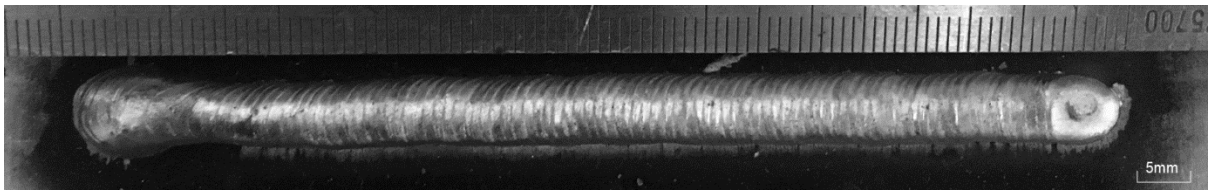

Figure 100 The welding layer with 6.5m/min of feeding wire speed

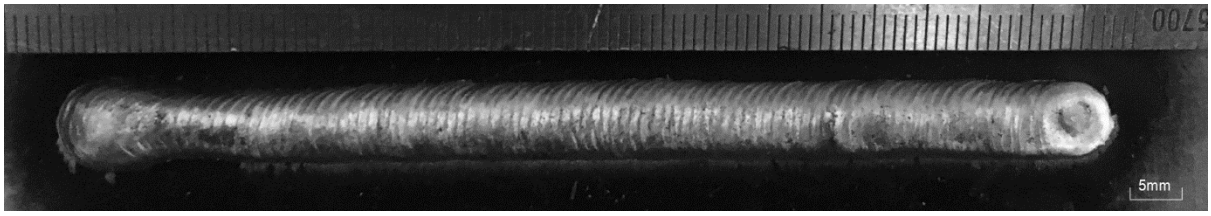

Figure 101 The welding layer with 7.0m/min of feeding wire speed

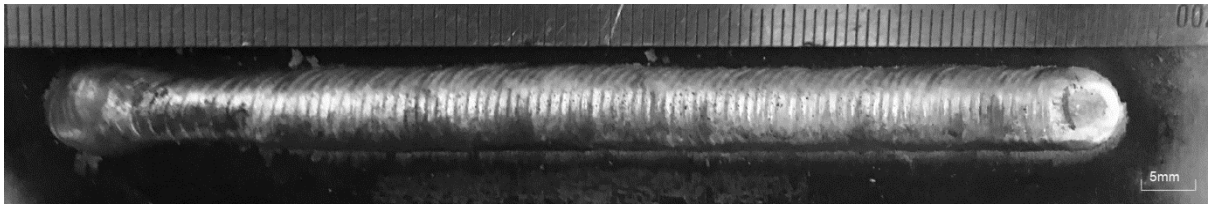

Figure 102 The welding layer with 7.5m/min of feeding wire speed

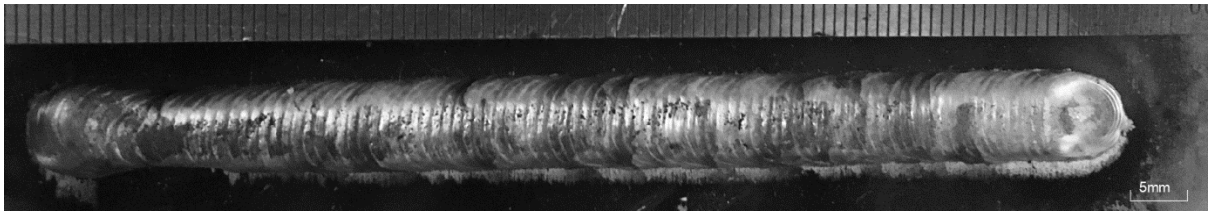

Figure 103 The welding layer with 8.0m/min of feeding wire speed

Appendix C - Scanned data

First layer (Horizontal axis: layer height/mm; Vertical axis: layer width/mm)

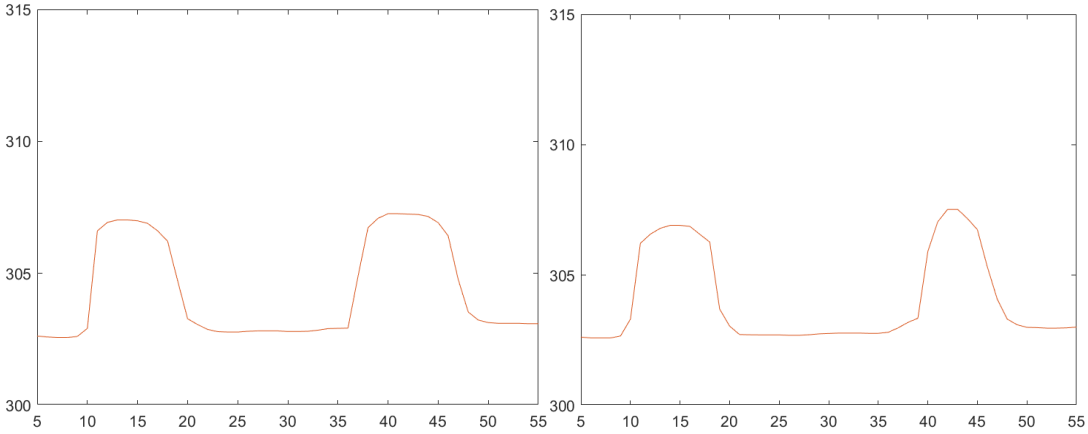

Figure 104 With (left) & without (right) control-1s & 2s

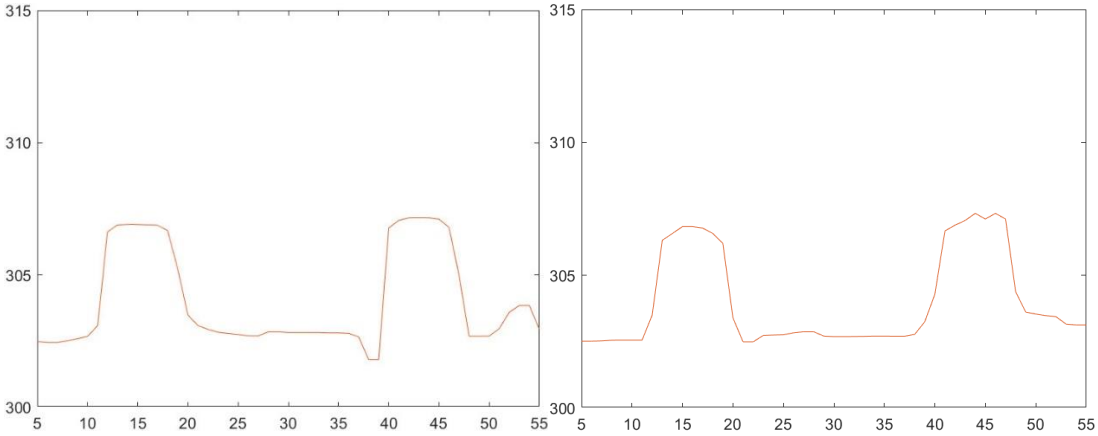

Figure 105 With (left) & without (right) control-3s & 4s

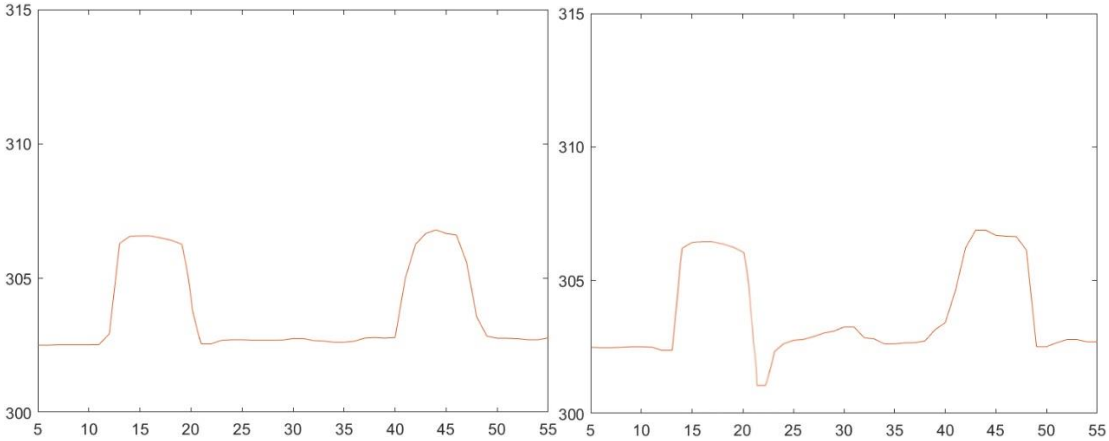

Figure 106 With (left) & without (right) control-5s &6s

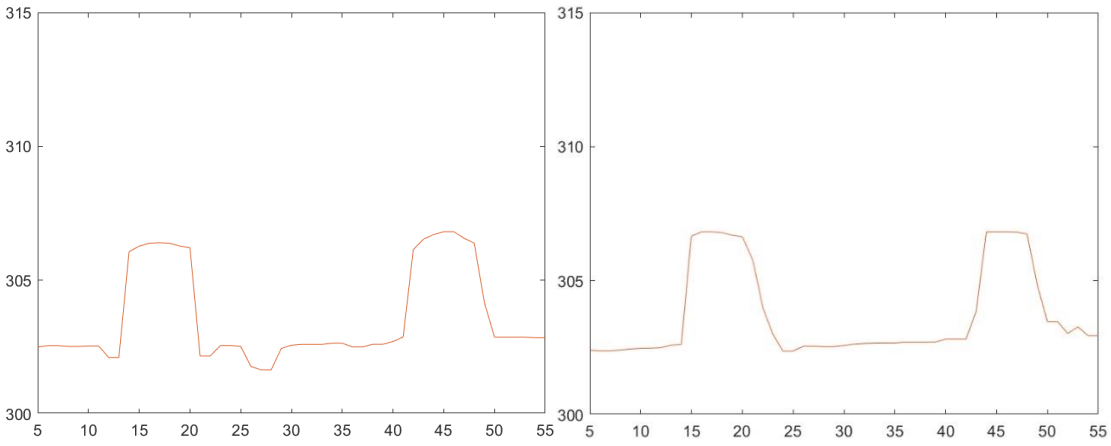

Figure 107 With (left) & without (right) control-7s & 8s

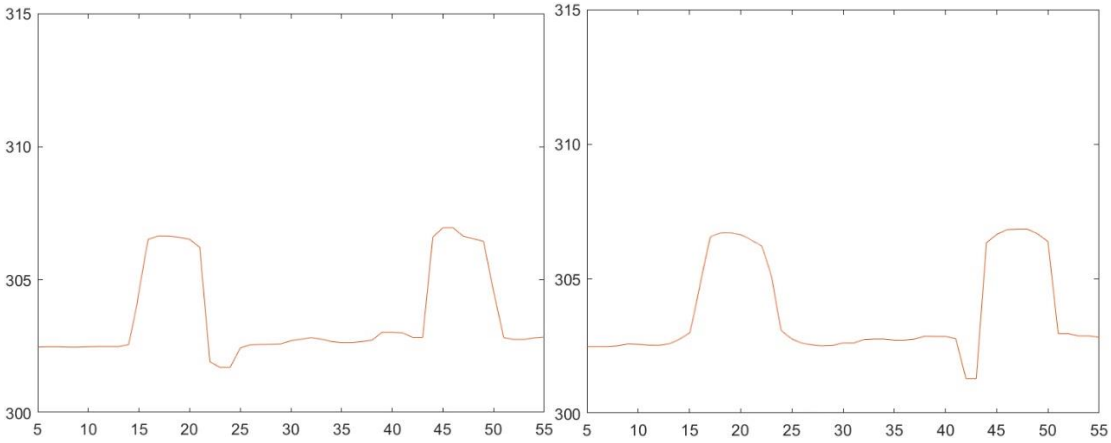

Figure 108 With (left) & without (right) control-9s & 10s

Second layer (Horizontal axis: layer height/mm; Vertical axis: layer width/mm)

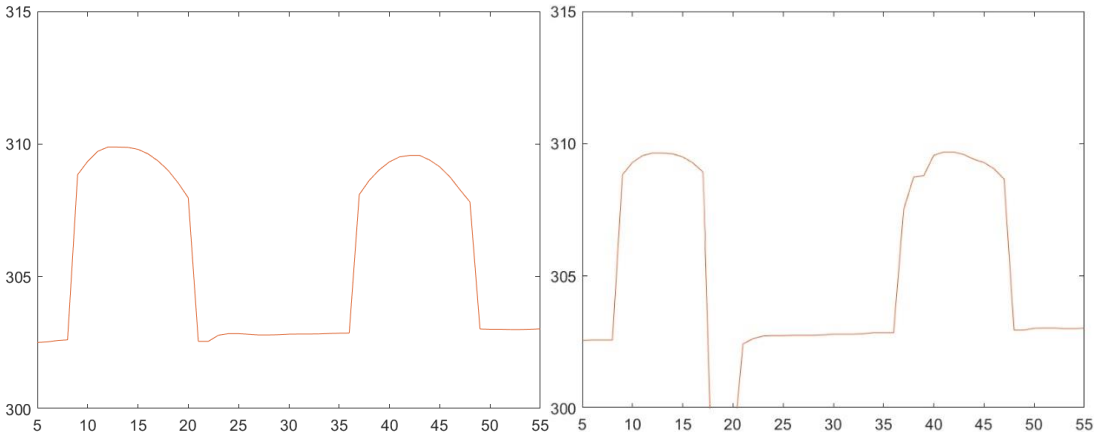

Figure 109 With (left) & without (right) control-1s & 2s

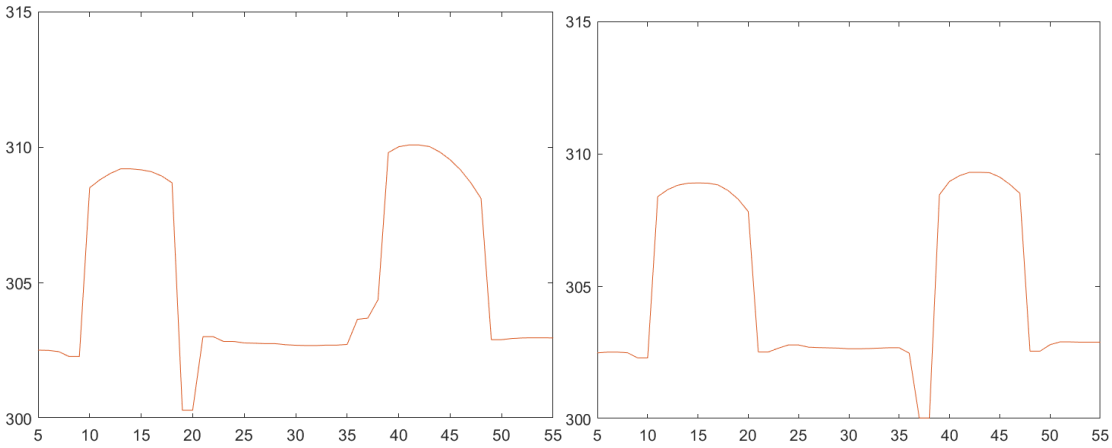

Figure 110 With (left) & without (right) control-3s & 4s

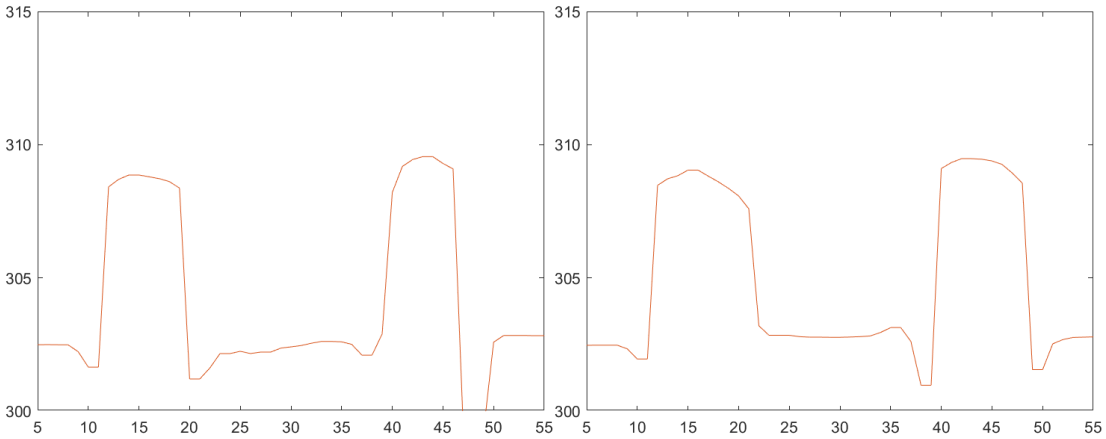

Figure 111 With (left) & without (right) control-5s & 6s

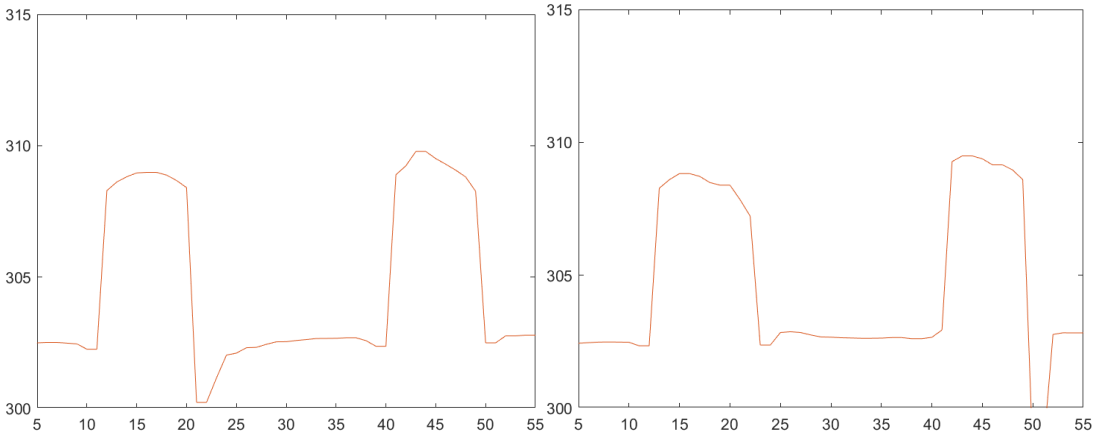

Figure 112 With (left) & without (right) control-7s & 8s

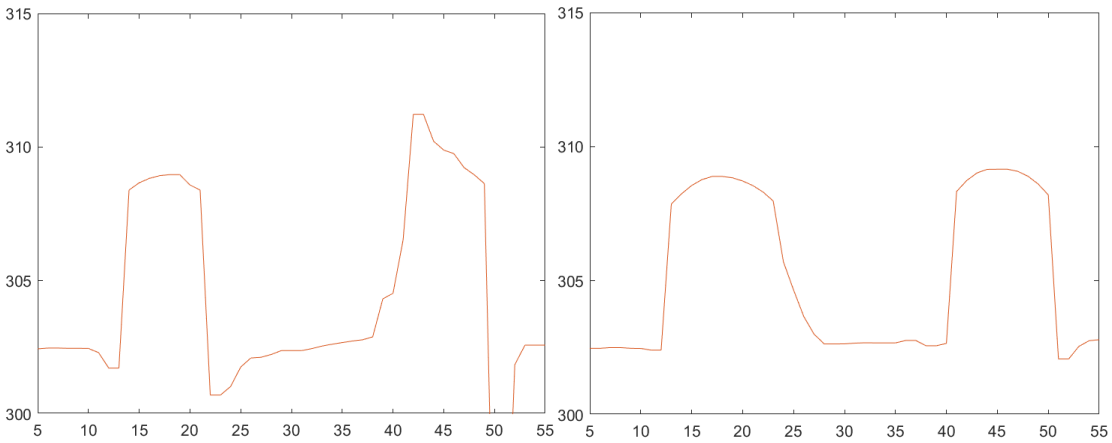

Figure 113 With (left) & without (right) control-9s & 10s